ABSTRACT

Title of Dissertation: EVALUATION OF NCEP GFS CLOUD PROPERTIES USING SATELLITE RETRIEVALS AND GROUND-BASED MEASUREMENTS

Hyelim Yoo, Doctor of Philosophy, 2012

Directed By: Professor Zhanqing Li, Department of Atmospheric and Oceanic Science/Earth System Science Interdisciplinary Center

Cloud properties and their vertical structure are important for meteorological studies due to their impact on both the Earth's radiation budget and adiabatic heating. Examination of bulk cloud properties and vertical distribution simulated by the National Center for Environmental Prediction (NCEP) Global Forecast System (GFS) using various satellite products and ground-based measurements is a main objective of this study. Cloud variables evaluated include the occurrence and fraction of clouds in three layers, cloud optical depth, liquid water path, and ice water path. Cloud vertical structure data are retrieved from both active and passive sensors that are compared with GFS model results. In general, the GFS model captures the spatial patterns of hydrometeors reasonably well and follows the general features seen in satellite measurements, but large discrepancies exist in low-level cloud properties. More boundary layer clouds over the interior continents were generated by the GFS model whereas satellite retrievals showed more low-level clouds over oceans. The GFS model simulations also missed low, shallow

stratocumulus clouds along the west coast of North America, South America, and southwestern Africa and overestimated thick, large-scale clouds associated with the Asian summer monsoon. Although the frequencies of global multi-layer clouds from observations are similar to those from the model, latitudinal variations show large discrepancies in terms of structure and pattern. The modeled cloud optical depth for optically thin or intermediate clouds is less than that from passive sensor and is overestimated for optically thick clouds. The distributions of ice water path (IWP) agree better with satellite observations than do liquid water path (LWP) distributions.

Mistreatment of such stratocumulus clouds in the GFS model leads to an overestimation of upward longwave flux, and an underestimation of upward shortwave flux at the top-of-atmosphere (TOA). With respect to input data bias in cloud fields, the GFS temperature is comparable with satellite retrievals and ground-based measurements, but the GFS relative humidity shows a wet bias at 150 and 850 hPa both from satellite retrievals and ground-based measurements. Discrepancies in cloud fields between observations and the model are attributed to differences in cloud water mixing ratio and mean relative humidity fields, which are major control variables determining the formation of clouds.

To improve the simulation of cloud fields, application of other cloud parameterization scheme to the GFS model is performed. The new scheme generates a large quantity of marine stratocumulus clouds over the eastern tropical oceans as well as low cloud amounts in the other regions. High-level and middle-level clouds generated from the new scheme are more comparable with the satellite retrievals in terms of the spatial distributions and zonally averaged cloud fractions.

An application of a simple linear relationship between de-correlation lengths (Lcf) and latitudes to the GFS model is conducted in order to see how successfully the equation explains the characteristics of cloud vertical structure on the changes in cloud fraction at different vertical levels. The method to solve for Lcf is a combination of Brent (1973) approach and a stochastic cloud generator using data collected from space-borne active sensors. Cloud fractions derived from a simple linear fit are compared to those computed from Lcf values based on observations. The pattern of zonal Lcf values from a simple linear fit is quite different from that of Lcf values based on observations. An offset pattern in subtropical regions is notable. The distribution of median Lcf values calculated from observed clouds do not show much dependence on latitude. This suggests that other physics, such as convection and cloud formation mechanism rather than simply latitude, should be considered when explaining how Lcf behaves. Such findings are expected to help improve the inherent problems of the GFS cloud parameterization scheme and to gain insight into the method used in determining cloud fraction.

EVALUATION OF NCEP GFS CLOUD PROPERTIES USING SATELLITE RETRIEVALS AND GROUND-BASED MEASUREMENTS

By

Hyelim Yoo

Dissertation submitted to the Faculty of the Graduate School of the
University of Maryland, College Park, in partial fulfillment
of the requirements for the degree of
Doctor of Philosophy
2012

Advisory Committee:
Professor Zhanqing Li, Chair/Advisor
Professor Robert Hudson
Professor Eugenia Kalnay
Dr. Yu-Tai Hou
Professor Shunlin Liang, Dean's representative

Acknowledgements

I remember when I saw beautiful clouds in a blue sky. When I was young, a clear sky and white clouds made me smile and comforted. Time after time, I grew up and I stand at the final step of my PhD degree and they become a topic of my doctoral study. Looking back, I have been always with them.

First of all, I would like to thank my advisor, Dr. Zhanqing Li, for his sincere support and encouragement. He has helped me to see science in a full depth and taught me how to research a good scientific topic. Through his wide and insight knowledge of atmospheric science, I can be here and complete my dissertation. I am grateful to Ms. Maureen Cribb for her invaluable help on tracking the writing of my papers for several years. A special thanks goes to the members of my thesis committee, Professors Robert Hudson, Eugenia Kalnay, Shunlin Liang, and Dr. Yu-Tai Hou for their guidance and fruitful comments.

I am grateful to Drs. Shrinivas Moorthi, Brad Ferrier, and Steve Lord from the NOAA/NCEP and to Dr. Howard Barker from Meteorological Service of Canada for their help and valuable comments concerning my work. I would appreciate Dr. Fuzhong Weng at NOAA/NESDIS for his support.

I would like to express my endless love to my parents, Sangchun Yoo and Hyangsun Kim, my brother Yongphil, and parents in law. They support me with warm encouragements and help during my study. The most special person in the world is my husband, Jungbin Mok. He is my joy and happiness. Thanks to his love and faithful support, I can finish my dissertation.

Finally, it is a pleasure to share my life with wonderful people including my friends and University Church family. My time in Maryland has been enriched by happy memories with them during my study.

Table of Contents

List of Tables

List of Figures

Chapter 1: Introduction

1.1. Background

Cloud systems and their interactions with larger scale circulation, radiation, and aerosols are extremely important parts of weather and climate systems. Clouds are also one of the most crucial elements in the hydrology and energy cycles of the Earth, particularly via precipitation processes (Del Genio et al. 2005) and they play an important role in regulating the Earth's radiative energy budget and temperature by reflecting incoming solar radiation and trapping outgoing longwave radiation in the atmosphere.

However, in spite of their significance, accurate representation of clouds has not been achieved in predicting global weather and in estimating climate model capabilities over the past thirty years (Randall et al. 2007). Most significant sources of errors and uncertainties in weather forecast and climate models are come from the treatment of clouds due to the incomplete knowledge of the underlying physical processes (Stephens 2005) and considerable variations of cloud amounts in vertical and horizontal extent (Stowe et al. 1989; Rossow et al. 1989). In addition, the horizontal coverage of clouds and their vertical structure are closely linked together and these affect on atmospheric circulation and the water cycle (Stephens 1990). Representation of cloud processes is one of the central issues in improving global climate and regional weather forecasting models (Stephens 2005).

Clouds are the most difficult parameter to describe their properties among all meteorological variables in any model environment. Firstly, they vary in both spatial

scales from micrometers to tens of thousands of kilometers and temporal scales from a few minutes to weeks. Secondly, they change in three different phases with complicated microphysical properties and have both radiative cooling and warming effects depending on their heights. Shortwave radiation has a cooling effect on surface by clouds which absorb a large quantity of incoming solar radiation. Clouds have both absorbing and emitting effects for longwave radiation and net effect is determined by environmental temperature and location (Klein and Hartmann 1993). Cloud vertical structure is thus important for the Earth's radiative balance as well as for climate studies. Finally, they evolve and vanish rapidly and are strongly coupled with aerosol, water vapor, and atmospheric dynamics.

Among the characteristics of clouds as mentioned above, description of subgrid-scale clouds is the most outstanding and urgent problem to solve in order to make remarkable progress in models for climate studies. Clouds in models are usually parameterized using large-scale atmospheric variables based on statistical or empirical relationships. A large number of different cloud parameterization schemes exist and a sensitivity test for them under different meteorological and environmental conditions has been an active research topic. However, although the sophistication of cloud parameterization schemes has increased the last three decades, there is still more work to be done (Randall et al. 2007). There are severe underestimates of low-level clouds over the eastern tropical oceans and overestimates of high clouds in several models (Ma et al. 1996).

Most models predict condensed cloud water from different sources such as boundary layer processes, detrainment of convection, cloud advection, condensation

and from sinks like precipitation and evaporation. These parameterizations involve some assumptions strongly depending on both the state of the atmosphere and large-scale atmospheric processes. Therefore, the most significant source of errors and uncertainties in simulating clouds in the various models stems from such cloud parameterizations (Houghton et al. 2001).

Evaluation of cloud parameters simulated by numerical climate and weather forecasting models is essential in order to help gain further insights into any fundamental cloud processes to be resolved as well as an enhanced understanding of clouds and their effects on the climate system. This requires a good knowledge of cloud variables such as coverage, thickness, microphysics, which can be observed from both space and on the ground. Satellites can provide the only means of continuous observation of cloud properties on a global scale. In addition, cloud distributions and their spatial and temporal variations have been gained with long-term meteorological satellite programs.

1.2. Problems in the detection of clouds

The International Satellite Cloud Climatology Project (ISCCP) started in operating in 1983 (Rossow and Schiffer 1999) has significantly contributed to the progress in satellite remote sensing. The ISCCP cloud properties are derived from measurements made by several sensors such as the Advanced Very High Resolution Radiometer (AVHRR) onboard the National Oceanic and Atmospheric

Administration (NOAA) polar orbiting satellites, the Geostationary Operational Environmental Satellites (GOES), the Japanese Geostationary Meteorological Satellites (GMS), and the European Meteorological Satellites (METEOSAT). These passive satellite sensors have various channels from visible to infrared, which can be used to derive bulk cloud quantities.

The ISCCP data has been widely used in validating clouds simulated by general circulation models (GCMs) (Webb et al. 2001; Zhang et al. 2005). The evaluations reveal that most GCMs tend to produce less low-level clouds and much less mid-level clouds than the ISCCP product. However, one must consider both their reliabilities as a reference and their respective limitations when comparing model results with satellite retrievals. Total cloud fraction of the ISCCP product is reliable for semi-transparent clouds and multi-layered clouds, but cloud fractions at different vertical levels are not reliable (Chang and Li 2005a, 2005b). The conventional bi-spectral algorithm used in the ISCCP cloud product tends to identify multi-layered clouds as a single mid-level cloud which results in an overestimation of mid-level clouds and an underestimation of low-level clouds. This result can explain partially why most GCMs generate much less mid-level clouds than those of the ISCCP cloud product.

The Moderate Resolution Imaging Spectroradiometer (MODIS) has 36 onboard calibrated channels ranging between 0.415 μm and 14.24 μm (Barnes et al. 1998) and it allows a more reliable detection of clouds and retrieval of cloud properties (King et al. 2003). The MODIS cloud top properties retrieval is based on the combination of a CO_2-slicing technique and an 11-μm brightness temperature

technique (Platnick et al. 2003). The CO_2-slicing technique is known for its effectiveness in determining cloud-top pressures less than 700 hPa (e.g., $p < 700$ hPa) and the 11-μm brightness temperature technique is used for detections of low-level clouds. These techniques allow detections of both high and low clouds more accurately. However, since the MODIS standard algorithm assumes a single-layer cloud as does the ISCCP algorithm, large uncertainties can exist in detecting multi-layered clouds, especially for a combination of thin cirrus over thick water clouds (Warren et al.

1985). The MODIS standard cloud product only gives the top pressure of the highest clouds, but no information about the overlapped low clouds. As a result, passive sensors identify cirrus-over-water clouds as deep convective clouds in most cases (Chang and Li 2005a, 2005b). A poor knowledge about multi-layered clouds in observations has some limitations in validating the global climatology of high, middle, and low-level clouds generated by GCMs. Furthermore, mistreatment of such overlapped clouds can lead to significant errors in estimating heating rates and longwave radiation because deep convective clouds and overlapped clouds have different effects on longwave radiation.

Chang and Li (2005a) developed an algorithm to overcome this major limitation by taking advantage of the multiple channels in identifying multi-layered clouds and retrieving the optical properties of individual cloud layers. Application of this algorithm showed a new global cloud distribution by adding 10 – 20 % more low clouds below high cirrus clouds in the tropical and mid-latitude storm track regions when compared to the other two operational products (i.e., the ISCCP

product and the MODIS standard product) (Chang and Li 2005b).

The A-Train satellite constellation (Stephens et al. 2002) added active remote sensing instruments onboard the CloudSat and the Cloud-Aerosol Lidar and Infrared Pathfinder Satellite Observations (CALIPSO), which are new satellite platforms designed to determine cloud vertical structure and to measure cloud properties. These instruments can probe the profiles of clouds in a more direct manner than passive sensors. The CloudSat and CALIPSO satellites fly in constellation with the passive Aqua platform. Measurements from active and passive satellite instruments create a synergy effect for monitoring clouds in a three-dimensional fashion on a global scale. An unprecedented accuracy of thin cirrus clouds over tropical regions is achieved (Haladay and Stephens 2009) and a better representation of cloud diagnostics is provided (Mace et al. 2009; Chepfer et al. 2010).

The CloudSat and CALIPSO data are used to validate cloud type, height, and amount fields derived from other passive sensors such as the Atmospheric Infrared Sounder (AIRS) (Kahn et al. 2008), the MODIS (Weisz et al. 2007; Holz et al. 2008), and the Multiangle Imaging SpectroRadiometer (MISR), the Ozone Monitoring Instrument (OMI) (Wu et al. 2009). Holz et al. (2008) compared the Cloud-Aerosol Lidar with Orthogonal Polarization (CALIOP) and the MODIS data for cloud detection and cloud-top height measurements. They found that thin cirrus cloud-top heights retrieved from CALIOP are higher in altitude than those retrieved from the MODIS by 2.6 ± 3.9 km. The largest discrepancies occur in the equatorial region for optically thin cirrus clouds with differences greater than 10 km. In addition, the agreement between the MODIS 1 km cloud mask and the CALIOP 1 km cloud mask

is 87 % and 85 % for cloudy and clear sky conditions, respectively.

The importance of marine stratocumulus clouds in the subtropical and the mid-latitude regions is well known because they have a comparable impact on global climate (Klein and Hartmann, 1993). However, the limited capabilities for detecting and measuring such clouds based on passive satellite sensors make it difficult to assess the frequency, amount, and characteristics of low clouds on a global scale. A more detailed characteristic of low clouds can be determined using CloudSat data (Marchand et al. 2008) and microphysical structure changes and evolutions of stratocumulus clouds affected by drizzle are examined globally using CloudSat and CALIPSO data (Leon et al. 2008).

1.3. Problems in the represention of clouds

Climate changes simulated by GCMs substantially differ among different GCMs (Cess et al. 1990). Such differences among models in climate feedback processes mostly come from inadequate representations of cloud fields (Bony et al. 2006). The general spatial patterns of clouds are well produced but the magnitudes and locations of clouds tend to differ more from observations. Although considerable efforts have been made, cloud microphysical and optical properties on a global scale still vary widely from model to model (Randall et al. 2003; Williams and Tselioudis 2007). Most numerical weather forecasting models and many GCMs have large variations in representing different cloud variables which are important

for both radiative transfer calculations and prediction of precipitation and they also do not simulate cloud vertical structure very well on a global scale (Bodas-Salcedo et al. 2008).

Clouds generated by GCMs and their seasonal variations have long been compared with passive satellite retrievals. Weare et al. (1996) compared 24 model simulations against the ISCCP data and found that global means of modeled high clouds are about two to five times greater than satellite retrievals, whereas low-level clouds were underestimated drastically. The fractions of total, low-, mid- and high clouds from 10 GCMs are compared with 2 satellite products (the ISCCP and the Clouds and Earth's Radiant Energy System (CERES) data) (Zhang et al. 2005). They indicated that while the total cloud amounts agree well, large discrepancies exist in cloud vertical structure among the models, and between two satellite products (see Figure 1.1). Furthermore, for cloud detections, the majority of models simulated more than twice as many optically thick clouds than seen from satellite observations and underestimated optically thin clouds.

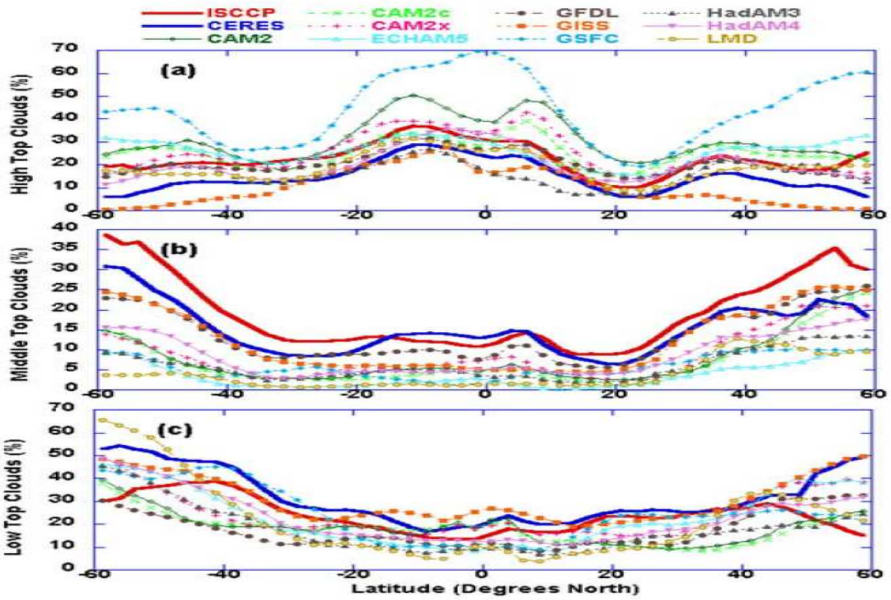

Figure 1.1 Comparisons of cloud fraction for (a) high top clouds, (b) middle top clouds, and (c) low top clouds during winter season (DJF) from both satellite measurements and 10 models (from Zhang et al. 2005).

Other studies primarily focused on specific regions. The mid-latitude cloud fields produced by the European Center for Medium-range Forecasting (ECMWF) model are evaluated against the ISCCP cloud product and the model overestimated cloud optical depth, but it underestimated cloud fraction (Tselioudis and Jakob 2002). Tropical cloud properties and responses to climate perturbations in the three different atmospheric GCMs are evaluated against the ISCCP cloud product in terms of cloud fractions and cloud-top height (Wyant et al. 2006). This study highlighted that there are still large uncertainties in both high and low cloud feedbacks simulated by models.

In addition to GCMs, cloud properties simulated by regional climate models such as the Weather Research and Forecasting (WRF) model have also been

examined with passive satellite retrievals. Otkin and Greenwald (2008) evaluated the WRF model clouds using the MODIS product and found that the model was unable to properly simulate stratocumulus and cumulus clouds.

1.4. Objectives and Outline of the thesis

Diagnosis of the Global Forecast System (GFS) model (2007, 2008, and 2011 versions) cloud properties and cloud parameterization scheme is a main focus of this dissertation. To help understand discrepancies and improve the model cloud performance, this study is divided into the three aspects with regard to cloud biases. The first part of a comprehensive study is to evaluate cloud properties such as cloud fraction (CF), cloud optical depth (COD), liquid water path (LWP), ice water path (IWP), and cloud effective radius (Re) for high, middle and low levels in the atmosphere by comparing with different types of satellite retrievals. A second part involves the impact of clouds on global net radiation and investigating the causes of the discrepancies in cloud fields by attempting to attribute them to both input data and to cloud parameterization schemes used. Finally, cloud overlapping issue is included to gain a better understanding of cloud vertical structure. A maximum-random overlap assumption made in the GFS model is diagnosed and a test of exponential random overlap assumption is performed. Cloud vertical structure on a global scale and cloud sub-grid variability are still arguably the most outstanding problems to be resolved in order to figure out how much cloud overlapping

contribute to the differences in cloud variables. Therefore, this study is expanded to investigate cloud vertical distribution and internal structure of cloud layers as well as cloud horizontal distribution.

This study makes extensive use of global satellite products from the A-Train sensors and local ground-based measurements from the Department of Energy's Atmospheric Radiation Measurement (ARM) Climate Research Facility (ACRF) site in Oklahoma. The satellite products provide global information pertaining to the cloud distributions and reveal any regional biases associated with weather regimes. The ground-based measurements can be used to help understand any fundamental physics describing various key processes. The following cloud products are employed; data from the MODIS, AIRS, CloudSat, CALIPSO, the merged CloudSat-CALIPSO products, and the ground-based measurements operated at mid-latitude.

It is obvious that satellite remote sensing is crucial to help validate and reduce any systematic errors in generating clouds in weather forecasting and climate models. However, a use of ground-based measurements is also necessary to investigate cloud properties which cannot be resolved solely from satellite retrievals. Below are specific tasks in this study:

1) Passive remote sensing data such as MODIS and AIRS measurements are used to evaluate cloud properties simulated by the GFS model on a global scale. The significantly advanced MODIS sensor provides a wealth of unprecedented information for monitoring clouds at high spatial resolution. The MODIS cloud products (MOD06/MYD06) contain cloud-top pressure, cloud-top temperature,

cloud phase, cloud optical depth, and effective particle radius at 1 km and 5 km. The sounding data having high spectral resolution from AIRS sensor provide important information about weather and climate processes. The AIRS sensor is designed to measure atmospheric water vapor and temperature profiles on a global scale. It accompanies two multichannel microwave instruments, the Advanced Microwave Sounding Unit (AMSU-A) and the Humidity Sounder for Brazil (HSB). The temperature and moisture profiles retrieved from a combination of infrared and microwave measurements show a certain degree of accuracy.

2) Active remote sensing data from CloudSat and CALIPSO are used to diagnose the frequent occurrence of overlapped clouds and cloud overlapping assumptions. Measurements from CloudSat and CALIPSO provide more reliable and comprehensive information pertaining to the vertical structure of clouds. The lidar is sensitive to very thin cirrus clouds, while the radar is able to detect lower, more optically opaque cirrus and can penetrate through much of deep convective clouds. The combined lidar-radar product can detect the majority of multi-layered clouds thus they are used to examine the occurrence of cloud layers as simulated by the GFS model. The cloud amount at different cloud categories (i.e., high, middle, and low) in most models usually depends on how layers of clouds are overlapped. The GFS model uses a maximum-random overlap assumption for adjacent and non-adjacent layers. Results from CloudSat/CALIPSO active sensors are utilized to identify the most suitable cloud overlapping scheme for the GFS model.

3) The Department of Energy's ARM Program has produced continuous and high quality field measurements in order to provide a long-term dataset for

evaluating and improving the parameterizations used in weather forecasting models. Such more reliable and more extensive observational dataset will help understand various atmospheric physical processes and find out the causes for any GFS model problems. Furthermore, this research investigates the most suitable set of meteorological conditions leading to cloud formation in the GFS model through comparisons with observational data.

The PhD dissertation is organized as follows. Chapter 2 examines the distributions of cloud properties generated by the GFS model by comparing with satellite retrievals and includes discussions regarding the soundness of the GFS model cloud representations. Chapter 3 assesses the atmospheric meteorological variables used in the GFS cloud parameterization against both satellite retrievals and ground-based measurements. Also, suggestions are discussed concerning where the improvements can be made in the cloud parameterization scheme. Description of other cloud parameterization schemes and the results of the application to the GFS model are contained in Chapter 4. An evaluation of the cloud overlapping assumption used in the GFS model and a test of exponential random overlap assumption are performed in Chapter 5. Finally, Chapter 6 presents the main findings and a summary of this work and discusses some additional studies to perform for the usefulness of the GFS model.

Chapter 2: Diagnosis of the GFS Cloud Properties Using Multiple Satellite Products

2.1. Introduction

Climate sensitivity simulated by general circulation models (GCMs) differs considerably among different GCMs (Cess et al. 1990) and it strongly depends on radiative feedbacks associated with clouds (Bony et al. 2004). Weare et al. (1996) compared 24 model simulations of cloud amounts against the International Satellite Cloud Climatology Project (ISCCP) data. They found that global means of modeled high cloud amounts are about two to five times greater than that from satellite retrievals, whereas low-level cloud amounts were underestimated drastically. Zhang et al. (2005) compared the fraction of total, low-, mid- and high clouds from 10 GCMs and 2 satellite products (ISCCP and the Clouds and Earth's Radiant Energy System (CERES)). While the total cloud amounts agree well, large discrepancies exist in cloud vertical structure among the models, and between satellite products.

For clouds, knowledge about the vertical structure of cloud layers is important because 42 % of all cloud observations are classified as multi-layered clouds from radiosonde data (Poore et al. 1995; Wang et al. 2000). Estimation of cloud layers from radiosonde is sound but also subject to numerous errors: detection algorithm, limited number of stations and, more seriously, the vast majority of the stations only report values at standard and representative levels. Using high vertical resolution (~50 m) radiosonde observations, a recent study by Zhang et al. (2011) showed that radiosonde-based estimates of cloud boundaries match very well with

ground-based estimates retrieved by cloud radar and lidar (Clothiaux et al. 2000). Unfortunately, only a handful of stations can provide such data.

For GCM evaluations, space-borne passive sensors have been employed to detect global clouds by virtue of their global coverage and long records. However, differentiating clouds at different layers has been a challenging task for passive remote sensing such as from the Advanced Very High Resolution Radiometer (AVHRR) (Baum et al. 1995; Ou et al. 1996) and the High resolution Infrared Radiation Sounder (HIRS) (Jin et al. 1996). Due to the inherent limitation in information generated from only a few spectral bands, there usually exist large uncertainties in detecting multi-layered clouds. This problem is lessened with the advent of instruments measuring radiances from a large number of spectral channels, as demonstrated using the Moderate Resolution Imaging Spectroradiometer (MODIS) Airborne Simulator (Baum and Spinhirne 2000).

Taking advantage of MODIS channels, Chang and Li (2005a) developed an algorithm that can identify single and cirrus-over-water dual-layer clouds. Applying their algorithm to global MODIS data, they obtained global multi-layer cloud distributions (Chang and Li 2005b). Thanks to the addition of a second layer of low clouds, their estimate of total low clouds over the globe is larger than all previous estimates based on passive sensors, but matches closely with space-borne lidar-based retrievals (see below). The ability of lidar to see through thin clouds aloft is reproduced by the algorithm of Chang and Li (2005a) using a combination of passive channels.

Active remote sensing can provide a better alternative to examine cloud

vertical structure and their optical properties, as demonstrated by the CloudSat and the Cloud-Aerosol Lidar and Infrared Pathfinder Satellite Observations (CALIPSO) sensors which are a part of the A-Train satellite constellation. The 94-GHz radar onboard the CloudSat can penetrate through most cloud layers (Stephens et al. 2002). From CloudSat-CALIPSO merged data, Mace et al. (2009) obtained the first global view of multi-layer clouds from active sensors. An unprecedented accuracy in estimating the amount of thin cirrus clouds over tropical regions was also achieved (Haladay and Stephens 2009). By simulating space-borne CloudSat radar signals, Bodas-Salcedo et al. (2008) evaluated clouds simulated by the U.K. Meteorological Office's global forecasting model.

Using datasets capable of detecting multi-layer clouds and their optical properties, we can evaluate cloud properties forecasted by the National Centers for Environmental Prediction (NCEP) Global Forecast System (GFS) model. Currently, many GCMs and weather forecasting models do not simulate cloud vertical structure very well on a global scale (Bodas-Salcedo et al. 2008). The general spatial patterns of clouds are well-produced but the magnitudes and locations tend to differ more from observations. To improve the prediction accuracy of weather forecast models, the cloud vertical distribution generated by models should be properly estimated.

In this Chapter, we examine the prediction ability of the GFS model in generating clouds at different levels so that the representation of cloud processes might be objectively improved. Furthermore, the comparisons provide a general guidance for improving the capabilities of the GFS model in producing clouds by revealing model deficiencies in terms of both model output (clouds) and input

(temperature, humidity, etc.). This Chapter is focused on the comparison of clouds from the GFS model and multiple satellite observations, while Chapter 3 investigates the causes of the discrepancies in cloud fields.

Section 2.2 describes the various datasets used in this study and the methodology and Section 2.3 introduces a brief description of the GFS model. The geographical distributions of different cloud parameters, analysis of the results, and comparisons of model output with several satellite retrievals are presented in Section 2.4. A summary is given in Section 2.5.

2.2. Satellite retrievals

2.2.1. MODIS data

Data collected from the MODIS onboard the Terra (overpass time, 10:30 local time) satellite platform is used to extract cloud properties. The MODIS instrument has 36 onboard calibrated channels/bands (0.415-14.24 μm) (Barnes et al. 1998). Two sets of MODIS-based cloud products are employed here: the official operational product generated by NASA which is based on the algorithm developed originally by Platnick et al. (2003) with some subsequent revisions and a newly generated research product based upon the algorithm of Chang and Li (2005b). The two products are hereafter referred to as ***MODIS-EOS*** and ***MODIS-CL***, respectively. Both datasets cover the period of January and July 2007. The MODIS provides daily data covering the globe, data used in this study are every day of a particular month.

The MODIS Level 2B cloud product, MOD06 (version Collection 5.1), used

here includes the following variables at two spatial resolutions (1 km and 5 km): cloud-top pressure, cloud-top temperature, cloud phase, cloud water path, cloud fraction, effective particle radius, and cloud optical depth (COD). Among these variables, cloud water path, effective particle radius, and COD are derived at a 1-km resolution and averaged over 1ºx1º latitude-longitude grid boxes; monthly means are calculated for each grid box. All cloud variables based on satellite retrievals, except for COD, are classified as high, middle, or low according to cloud-top pressure. A mid-level cloud is identified when the cloud-top pressure falls between 350 and 642 hPa which is the criterion used in identifying such clouds in the GFS model. For each cloud category, cloud fraction is calculated as the number of cloudy pixels in a grid box divided by the total number of pixels in that grid box. Like most passive cloud retrieval algorithms, the MODIS algorithm was based on the assumption of single-layer clouds in the retrieval of cloud properties. As such, the retrieved cloud top represents the top of the highest cloud regardless of the presence of any lower cloud layers.

The algorithm of Chang and Li (2005a) (hereafter the C-L algorithm) alleviates the problem because it can detect and retrieve cloud parameters for single-layer clouds and for thin-over-thick dual-layer clouds. Due to the frequent occurrence of such overlapped clouds, the C-L algorithm generates substantially more low clouds than the MODIS algorithm. The total amount of low clouds over oceans and over land retrieved from the C-L algorithm (MODIS product) is 34% (22%) and 28% (16%), respectively (Chang and Li 2005b). In addition to detecting more low clouds, the COD of the topmost layer and lower cloud in multi-layer

clouds are differentiated using the C-L algorithm.

2.2.2. CloudSat-CALIPSO merged data

The CloudSat and CALIPSO satellites were launched in April 2006, carrying a 94-GHz cloud profiling radar (CPR) (Im et al. 2006) and a two-wavelength polarization sensitive lidar (Winker et al. 2007). Three sensors, including the MODIS, are members of the A-Train afternoon constellation (Stephens et al. 2002), flying in tight orbital formation so that all instruments probe the atmosphere within a few seconds of each other, rendering synergistic, simultaneous and independent information pertaining to cloud vertical structure. The lidar is capable of resolving very thin cirrus layers below 15 km to thicker cirrus clouds between 12 and 13 km while the radar is able to detect lower, more optically opaque cirrus clouds and can penetrate through much of deep convective clouds. Merged lidar-radar data offers the best compromise between the strengths and weaknesses of the two instrument retrieval methods (Mace et al. 2009). This combined dataset is called CloudSat-CALIPSO merged data (hereafter referred to as C-C satellites) which provides more detailed and more reliable cloud vertical structure information.

This study uses the Level 2B Geoprof-lidar product (CloudSat CPR + CALIPSO Lidar Cloud mask) and the Level 2B TAU (cloud optical depth from CloudSat) product for every day in January and July 2007. Up to a maximum of five different cloud layers can be output from C-C satellites and each layer has its

individual cloud-top altitude and cloud-base altitude. These data are averaged over 2º latitudinal bands for plotting purpose from which zonally-averaged cloud layers are computed.

While the two active sensors provide the most direct and accurate measurement of cloud vertical structure, their horizontal coverage is much smaller than the wide swath (~2700 km) of the MODIS imaging sensor which provides nearly global wall-to-wall coverage, except for data gaps at low latitudes. Both CloudSat and CALIPSO view the Earth in the nadir direction with footprints of 1.4 km and 1.1 km, respectively. It is therefore necessary to use products from both passive and active sensors to complement each other's weaknesses/strengths. Because of the low spatial sampling rate, monthly mean values were computed for $3^{o}x6^{o}$ lat/long grids for mapping in order to reduce the number of empty grids, as done in other studies using products of C-C satellites (Sassen and Wang 2008; Mace et al. 2009). We note that as a result of this averaging, C-C plotting results appear more smoothly than those plots generated from other products.

2.3. GFS model description

The GFS model is a global weather prediction model run by NOAA. The GFS model has 64 vertical sigma-pressure hybrid layers and a T382 (about 35 km) horizontal resolution. GFS model grid 003 data are used in this study with a 1ºx1º latitude-longitude resolution. Output fields for a one day forecast generated at 3-hour intervals (i.e. at 03, 06, 09, 12, 15, 18, 21, 24 Z), starting from the control time

of 00Z, are used. In other words, the forecasting data used here are from 00Z to 24Z for each day. Cloud properties output in each grid box are used for comparison with satellite retrievals over the domain covering 60ºS-60ºN during January and July 2007. At high latitudes, the presence of bright snow and/or ice-covered surfaces leads to low accuracy in retrievals from passive sensors (Li and Leighton 1991), so data from these regions are not considered in this study. The GFS model fields were interpolated to satellite overpass times in order to match satellite retrievals. The GFS model outputs include cloud cover, cloud-top pressure and height, and cloud-base pressure and height at high, middle and low levels of the atmosphere. High, middle, and low categories are defined with respect to cloud layer top pressure: less than 350 hPa, between 350 hPa and 642 hPa, and greater than 642 hPa, respectively.

2.3.1. GFS Cloud Fraction

The cloud fraction in a given grid box of the GFS model is computed using the parameterization scheme of Xu and Randall (1996):

$$C = \max[R^{0.25}(1 - \exp\{-\frac{2000\times(q_c - q_{c\min})}{\min[\max([(1-R)\times q^*]^{0.25}, 0.0001), 1.0]}\}), 0.0], \qquad (2.1)$$

where R is the relative humidity, q* is the saturation specific humidity, q_c is the cloud water mixing ratio, and q_{cmin} is a minimum threshold value of q_c. Depending on the ambient temperature, the saturation specific humidity is calculated with

respect to the liquid or ice phase. Clouds in the GFS model are assumed to be maximum-randomly overlapped (http://www.emc.ncep.noaa.gov/officenotes).

2.3.2. GFS Cloud Optical Depth (COD), Effective Radius (Re), Liquid and Ice Water Path (LWP and IWP)

The GFS model posts parameters for 21 vertically different layers. From the surface (1000 hPa) to the 900-hPa level, the vertical resolution is 25 hPa; less than 900 hPa, there are 16 levels at a 50-hPa resolution. Cloud phase is determined by the mean temperature (Tc) of a cloud layer which is defined as the average of temperatures at the top and bottom of a cloud layer. If Tc is less than 258.16 K, the cloud layer is an ice cloud; otherwise, it is a water cloud.

Two methods have been used to parameterize cloud properties in the GFS model. The first method makes use of a diagnostic cloud scheme, in which cloud properties are determined based on model-predicted temperature, pressure, and boundary layer circulation from Harshvardhan et al. (1989). The diagnostic scheme is now replaced with a prognostic scheme that uses cloud water condensate information instead (http://www.nws.noaa.gov/om/tpb/484.htm).

For water clouds (i.e., R_{ew}), a fixed value of 10 μm for Re is assumed over oceans and Re values over land depend on temperature. Over land, Re is defined as:

$$R_{ew} = -0.25 \times Tc + 73.29. \quad (2.2)$$

Its value ranges from 5 μm to a maximum of 8.7 μm for Tc of 258.16 K, below which cloud is treated as an ice cloud.

Liquid Water Path (LWP) is calculated using the following equation:

$$LWP = q \times \rho \times \Delta z, \tag{2.3}$$

where q is the cloud water mixing ratio in units of kg/kg, ρ is the density in kg/m^3 (assumed to be constant), and Δz is the geopotential height thickness in units of m.

LWP and Re information is used to calculate total column COD in the GFS model (Chou et al. 1998):

$$\tau_w = LWP(a_1 + (a_2 / R_{ew})), \tag{2.4}$$

where LWP is given in units of g/m^2, and the coefficients a_1 and a_2 are given in Chou et al. (1998).

For ice clouds, Re is calculated as empirical functions of ice water concentration and environmental temperature (Heymsfield and McFarquhar 1996):

$$\begin{aligned} R_{ei} &= (1250 / 9.917)\, IWC^{0.109} && (Tc < 223.16\ K), \\ R_{ei} &= (1250 / 9.337)\, IWC^{0.080} && (223.16\ K < Tc < 233.16\ K), \\ R_{ei} &= (1250 / 9.208)\, IWC^{0.055} && (233.16\ K < Tc < 243.16\ K), \\ R_{ei} &= (1250 / 9.387)\, IWC^{0.031} && (243.16\ K < Tc < 258.16\ K), \end{aligned} \tag{2.5}$$

where IWC is calculated as:

$$IWC = 1.371 \times 10\text{^}(-14.0 + 0.04962 \times Tc). \tag{2.6}$$

Ice Water Path (IWP) calculations are made in a similar manner. The COD for an ice cloud, τ_i, is computed as:

$$\tau_i = IWP(a_3 + (a_4 / R_{ei})), \tag{2.7}$$

where IWP is the cloud ice water path in units of g/m^2, and the coefficients a_3 and a_4 are given in the GFS documentation. A total column COD in a particular grid box is obtained by summing water and ice CODs.

2.4. Results

2.4.1. Comparison of the two MODIS cloud products

Figure 2.1 shows comparisons of the joint histograms of cloud-top pressure and COD from MODIS-EOS, MODIS-CL, and the GFS model. The GFS results only show deep convective clouds at high levels and mostly underestimate optically thin low clouds. Also, a distinct bimodal distribution of cloud-top pressure as presented in two satellite products is not clearly seen in the model results. The MODIS-CL results reveal frequent occurrences of two dominant cloud types: optically thin cirrus clouds at high altitudes and optically thicker boundary layer clouds at lower levels. A general similar pattern is seen in the MODIS-EOS product, but more optically thick high clouds and less optically thick low clouds are evident. MODIS-CL retrievals have more optically thin high clouds and less optically thick high clouds when compared to MODIS-EOS products (see Fig 2.1) because the former can differentiate overlapped thin cirrus over thick water clouds. However, the total amount of high clouds in the MODIS-CL retrievals is the same as that retrieved from the MODIS-EOS algorithm (Chang and Li 2005b). The presence of overlapped cirrus over low clouds is the major cause for the differences which is further rooted to the assumption of single-layer cloud in the MODIS retrieval, leading to the general underestimation of low cloud amounts. In other words, many low clouds are missed, because they are beneath the upper cirrus clouds that were not separated from single-layer clouds. Cirrus-over-water dual-layer clouds are

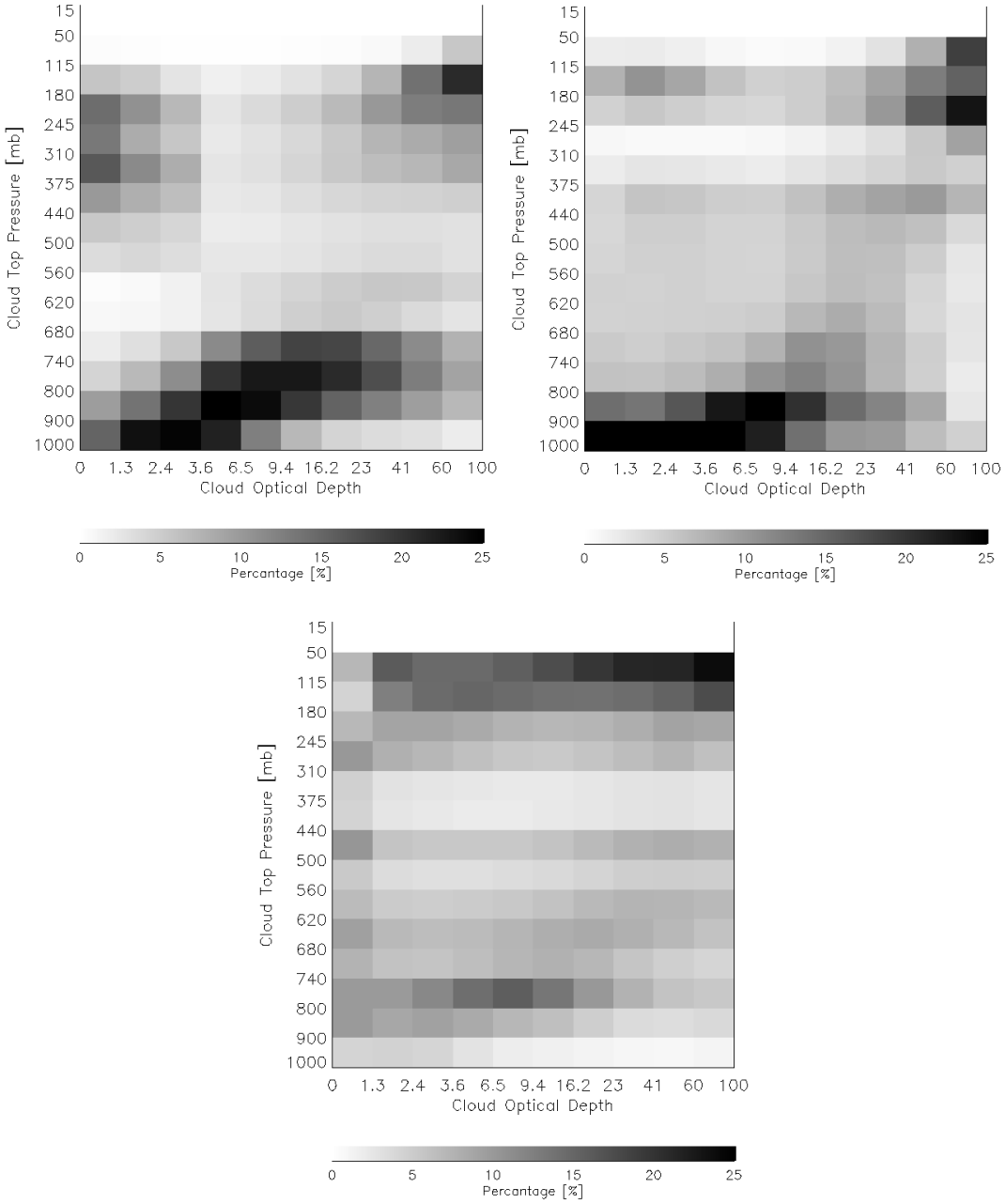

Figure 2.1. Joint histograms of cloud top pressure and cloud optical depth derived from near-global retrievals by applying the C-L algorithm (top left panel), the MODIS-EOS products (top right panel), and the GFS model (bottom center panel) in July 2007.

Table 2.1. Comparison of cloud layer statistics from GLAS (Wylie et al. 2007) and the C-L algorithm (Chang and Li 2005b).

	From GLAS	From MODIS-CL
Global Cloud Cover	70 %	71 %
Single Layer Cloud	43 %	44 %
Multiple Layer Cloud	27 %	27 %

identified as deep convective clouds for most cases based on passive sensors. Mistreatment of such overlapped clouds can lead to significant errors in estimating heating rates and longwave radiation because deep convective clouds and overlapped clouds have different effects on longwave radiation.

Thanks to the identification of both single and dual-layer clouds through exploitation of more MODIS channels, the C-L algorithm can identify such overlapped clouds except for those with uppermost cloud layers that are too thick (COD greater than ~ 4). It is worth noting that the overall cloud-layer statistics of the MODIS-CL agree well with those from a previous study using space-borne lidar measurements from the Geoscience Laser Altimeter System (GLAS) (Wylie et al. 2007). Coincidently, the frequency of multilayer clouds from both instruments is 27 % (see Table 2.1).

2.4.2. Multi-layer Cloud Occurrence Frequencies

Clouds in different vertical layers dictate the adiabatic heating rates and radiation balance of the atmospheric column. Mistreatment of cloud layers as single-layer cloud can lead to substantial errors in cloud amounts in different model layers, which could feedback to erroneous dynamics. Table 2.2 summarizes the global frequencies of occurrence of single-layer and multi-layer clouds from C-C satellites, MODIS-CL, and GFS model results. The frequency of single-layer, dual-layer, and multi-layer (three or more layers) clouds from C-C satellites in January (July) is 67.50 % (67.89 %), 26.58 % (25.98 %), and 5.92 % (6.13 %), respectively. The frequency of single-layer and dual-layer clouds from the MODIS-CL for the two months is 84.41 % (82.86 %) and 15.59 % (17.14 %), respectively. Frequencies of single-layer, dual-layer and multi-layer clouds from the GFS model for the two months are 68.94 % (67.11 %), 27.12 % (28.40 %), and 3.94 % (4.49 %), respectively. Overall, the GFS model produced sound frequencies of single-layer and multi-layer clouds. The MODIS-CL results are consistent with those in January and July of 2001 obtained earlier by Chang and Li (2005b) for which the frequencies of cirrus overlapping lower clouds over ocean and land is 25 % (23 %) and 32 % (23 %) in January (July), respectively (Chang and Li 2005b). The differences in the frequencies of occurrence of dual-layer clouds from C-C satellites and the MODIS-CL are attributed chiefly to the retrieval of the topmost cloud layer. Cirrus clouds with CODs greater than 1.5 are classified as a single layer of cloud in the C-L algorithm. This explains why the occurrence frequencies of single-layer clouds from the MODIS-CL are greater than those from the C-C satellites. The GFS model

results are comparable with C-C satellites results as far as the identification of multi-layer cloud scenes is concerned.

Figure 2.2 shows the latitudinal variations of the occurrence frequencies of zonal-mean single-layer and dual-layer cloud configurations obtained from C-C satellites and GFS model output. The patterns for single-layer cloud from observation and modeling are similar except for slight differences in their magnitudes. The C-C satellites show that dual-layer clouds occur most frequently over the inter-tropical convergence zone (ITCZ) and relatively less frequently at middle or high latitudes, relative to the GFS model results. Overall, from January (left plot in Figure 2.2) to July (right plot in Figure 2.2), the patterns shift with the movement of the Sun. The frequencies of occurrence of multi-layer clouds from the C-C satellites have an oscillation that peaks around 0º ~ 10ºN with a value near 40 % and reaches a minimum of 15 % at around 20ºN. The GFS model results show a maximum value of 35 % at around 45ºS and a minimum value of 20 % at about 10ºS and 20ºN in January.

Figure 2.3 presents the latitudinal variations of the occurrence frequency of cloud layer thickness from the C-C satellites and the GFS model. Both exhibit maxima in cloud layer thickness associated with deep convective clouds in the Tropics and mid-latitude continental clouds while minima occur over subtropical subsidence regions related to marine stratus and cumulus clouds. The GFS model generally overestimates cloud layer thickness, particularly for deep convective clouds in the tropical regions and mid-latitude storm track regions. The GFS model also tends to miss those very thin clouds (cloud layer thicknesses less than 2 km)

that are captured in the C-C satellites. Some possible causes for the different distributions of cloud layers may be either systematic biases in the prognostic cloud scheme used in the GFS model or incorrect input variables. Another possible cause of these discrepancies could be uncertainties in cloud overlapping. Investigation of potential model errors is a subject of Chapter 3.

Table 2.2. Global occurrence frequencies of single-layer clouds, dual-layer clouds, and clouds with 3 or more layers from the C-C satellites, the MODIS-CL retrievals, and GFS model results in January and July 2007.

Number of layers	January			July		
	C-C	C-L	GFS	C-C	C-L	GFS
Single layer	67.50 %	84.41 %	68.94 %	67.89 %	82.86 %	67.11 %
Dual layers	26.58 %	15.59 %	27.12 %	25.98 %	17.14 %	28.40 %
Three or more layers	5.92 %	-	3.94 %	6.13 %	-	4.49 %

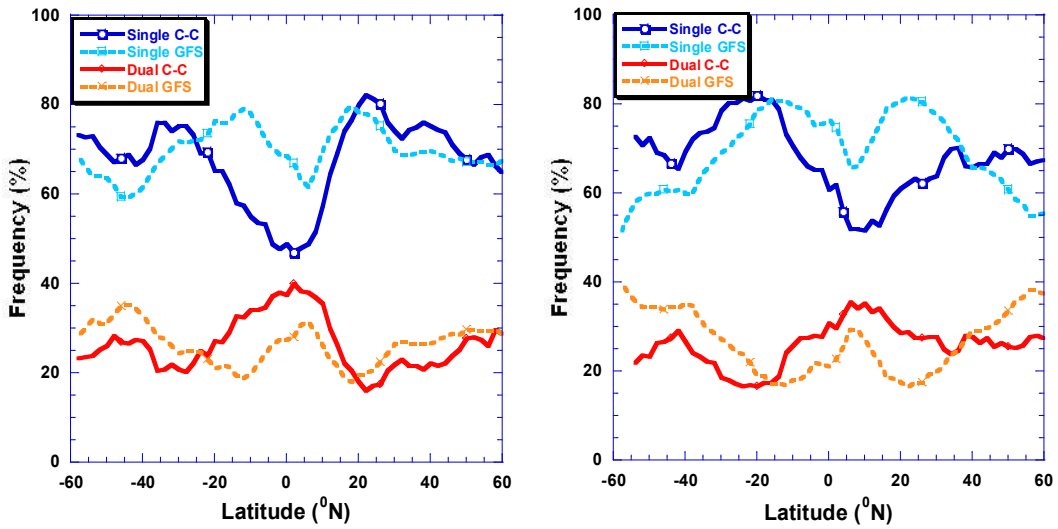

Figure 2.2. Latitudinal variations of the frequencies of cloud occurrence from the C-C satellites and the GFS model for single and dual-layer clouds in January (left plot) and July (right plot) of 2007. The blue solid (dashed) lines and red solid (dashed) lines represent single-layer and dual-layer clouds from the C-C satellites (the GFS), respectively.

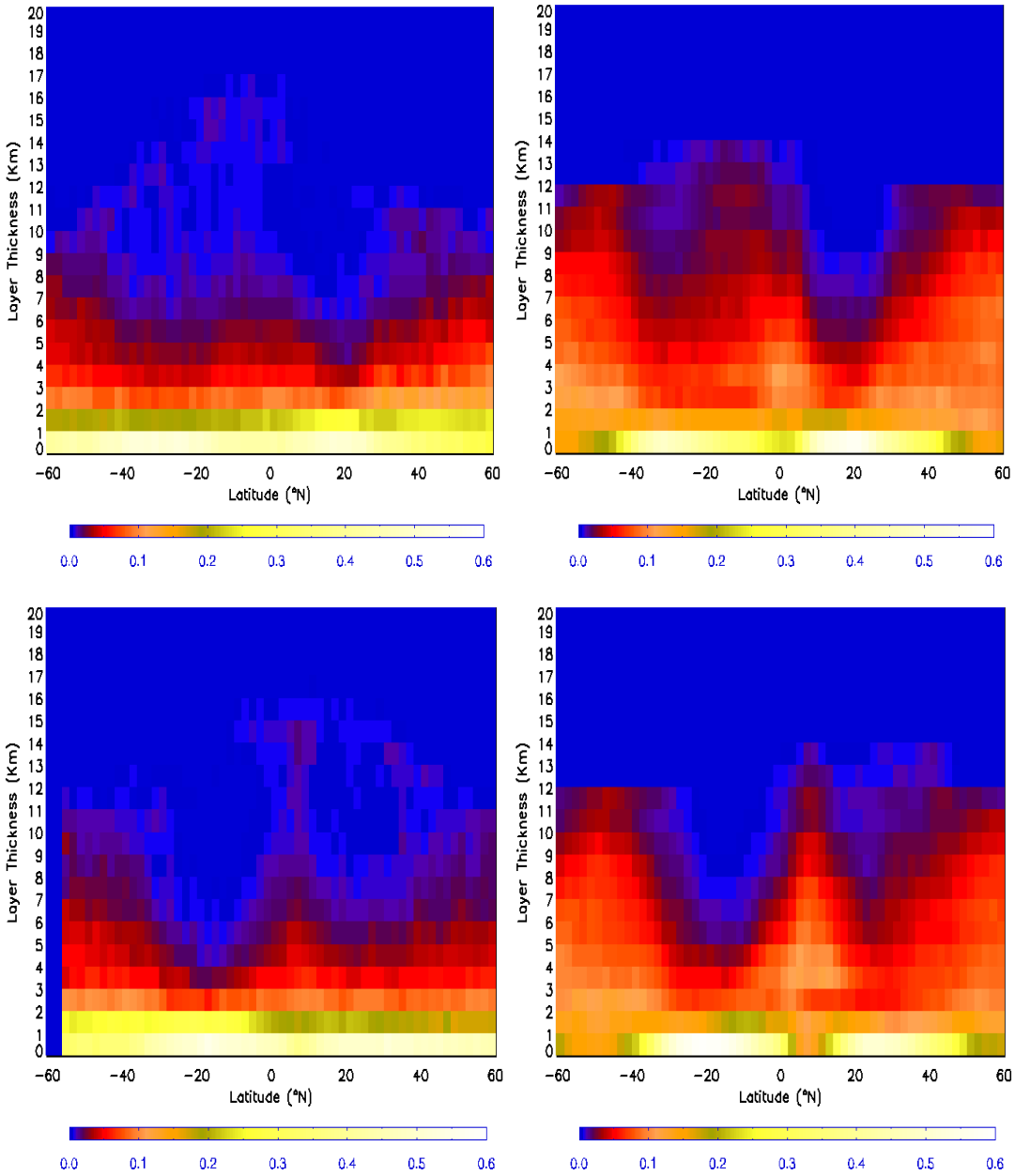

Figure 2.3. The latitudinal and vertical distributions of the frequency of occurrence (denoted by the different colors) of cloud layer thickness from the C-C satellites (left plots) and the GFS model (right plots), averaged over 2º latitudinal bands for January (top panels), and July (bottom panels) 2007.

2.4.3. Cloud Fraction

Several typical cloud types are present in the lowest part of the atmosphere, such as stratus, shallow cumulus, and stratocumulus (Kuettner 1971; Agee 1984). At high levels, clouds are more associated with synoptic weather systems, like mid-latitude fronts, cyclones, tropical storms, and anvils (Starr and Cox 1985; Sheu et al. 1997). In the middle of the atmosphere (~500-600 hPa), minimal cloud amounts were found in the tropical region from the TOGA COARE (Zuidema 1998) and from the global satellite remote sensing product of Chang and Li (2005b), as well as from the analysis of ARM ground-based measurements (Xi et al. 2010).

Figures 2.4, 2.5 show the distributions of high, middle, and low-level cloud fractions from the C-C satellites, MODIS-CL, and the GFS model in January and July 2007. In general, the GFS model generates more clouds at all levels than does the C-L algorithm during the two months, except for low-level clouds (see Table 2.3). Middle-level cloud fractions from the GFS model are most comparable with the two satellite retrievals, as shown in Figures 2.4 and 2.5, but large discrepancies exist in low-level clouds. In particular, more boundary layer clouds are generated by the GFS model over the interior continents at high latitudes whereas satellite retrievals show more marine stratus clouds over oceans. GFS model simulations also miss low-level shallow stratus clouds along the west coast of North America, South America, and southwestern Africa and overestimate thick, large-scale clouds associated with the Asian summer monsoon.

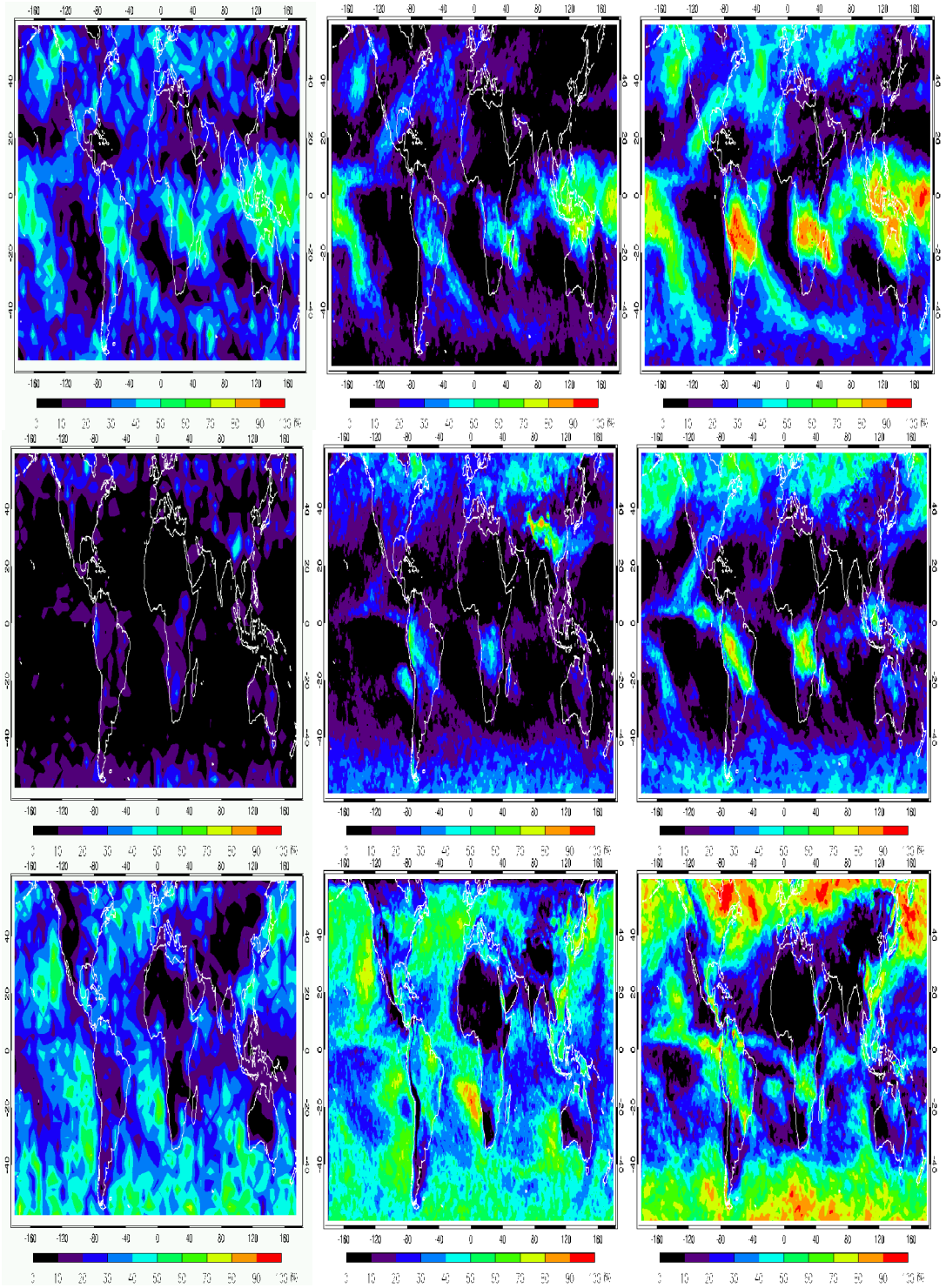

Figure 2.4. Geographic distributions of monthly mean cloud fractions from the C-C satellites (left panels), the MODIS-CL (middle panels), and the GFS model (right panels) in January 2007. Top, middle, and bottom plots denote high, middle, and low clouds, respectively.

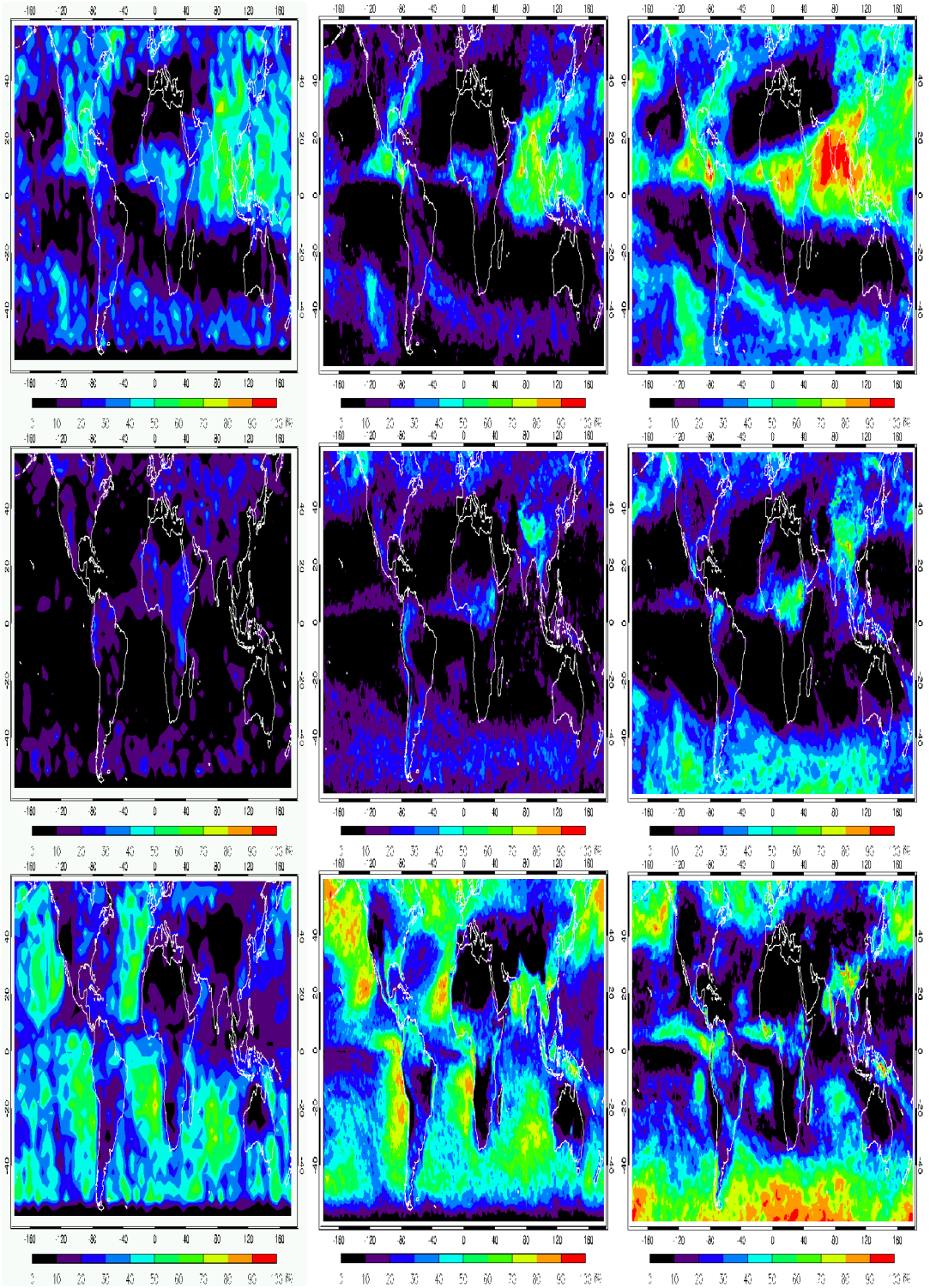

Figure 2.5. Same as Figure 2.4 except for July 2007.

The global mean mid-level cloud fraction simulated by the GFS model in January was 22.79 %, which is 6 % more than the magnitude of that retrieved by the C-L algorithm (17.05 %). In comparison, the global mean value of mid-level clouds from ISCCP is 18.0 %, which includes the inevitable misclassification of overlapped cirrus over low water clouds as single-layer mid-level clouds (Jin et al. 1996). It should be emphasized that mid-level clouds in the ISCCP are defined between 440 hPa and 680 hPa while those in the GFS are between 350 hPa and 642 hPa. The mid-level cloud fraction retrieved from the C-L algorithm using ISCCP criterion is about 9-10 %. We can thus affirm that the GFS overestimates mid-level clouds. The global mean cloud fraction of low-level clouds from the GFS model was 39.24 %, which is similar to that from the C-L algorithm in January (38.98 %) although the spatial patterns differ (see Table 2.3).

To examine the global distribution patterns of clouds, three separate geographical regions are defined in order to identify areas of the largest differences in cloud fraction: tropical (20ºS ~ 20ºN), mid-latitude (20ºN ~ 40ºN, 20ºS ~ 40ºS), and high latitude (40ºN ~ 60ºN, 40ºS ~ 60ºS). Differences were calculated by subtracting GFS results from C-L algorithm retrievals; the numbers in Table 2.4 are zonally-averaged cloud fractions over 2º latitudinal bins. The GFS model cloud fractions at high latitudes for all levels are greater than those from satellite retrievals. In particular, the GFS model simulates too much boundary layer clouds at high latitudes. At mid-latitudes (the Tropics), the GFS-forecasted high cloud fractions in January are greater than those retrieved from satellite by 10.87 % (14.10 %) and 2.01 % (7.25 %) for mid-level clouds, but low cloud fractions are less by 9.40 %

(7.91 %).

Figure 2.6 illustrates the latitudinal variations of zonal-mean cloud fractions corresponding to the three cloud vertical categories (i.e., high, middle, and low). Two features stand out. First, GFS model results vary in the same manner as satellite retrievals in terms of spatial features and locations except for low-level clouds. Second, modeled zonally-averaged high and mid-level cloud amounts are generally overestimated over nearly all latitudinal bands. Variations of high-level clouds from both the C-L algorithm and the GFS model show the jump in cloud amount in the Tropics from January to July due to deep convective clouds and the decrease in high-level cloud amount in subtropical regions in the Southern Hemisphere. For mid-level clouds, the GFS model captures the July reduction in cloud amount in the mid-latitudes but overestimates cloud amounts at high latitudes. Low cloud fractions generated by the GFS model diverge remarkably from satellite retrievals. Note that the C-L algorithm results in July show a sharp decrease in cloud fractions at around 55ºS. This is because the C-L algorithm uses solar zenith angle (SZA) information for detecting clouds. When the SZA is larger than a specific threshold value (e.g., 80º), no retrievals are made. Simulations of cloud from the GFS model do not explicitly involve sunlight information, so clouds can be seen over that particular region.

Table 2.3. Global monthly mean high-, mid-, and low-level cloud fractions obtained from the C-L algorithm and the GFS model during January and July 2007.

	C-L algorithm		GFS	
	January	July	January	July
High	16.45 %	16.36 %	30.61 %	32.90 %
Mid	17.05 %	13.61 %	22.79 %	19.46 %
Low	38.98 %	37.11 %	39.24 %	31.15 %

Table 2.4. Zonally-averaged cloud fraction (and differences) from the MODIS-CL and the GFS model in January and July 2007. Differences are calculated as C-L algorithm results minus GFS model results.

	January			July		
	40 º ~ 60 º -40 º ~ -60 º	20 º ~ 40 º -20 º ~ -40 º	-20 º ~ 20 º	40 º ~ 60 º -40 º ~ -60 º	20 º ~ 40 º -20 º ~ -40 º	-20 º ~ 20 º
High	12.52/30.36	13.96/24.83	23.84/37.95	13.82/34.30	14.16/24.58	21.46/40.60
Diff	-17.83	-10.87	-14.10	-20.48	-10.42	-19.14
Mid	27.37/35.84	13.28/15.30	10.20/17.45	20.82/32.49	11.17/14.78	8.72/10.92
Diff	-8.47	-2.01	-7.25	-11.67	-3.62	-2.20
Low	43.31/61.52	38.12/28.72	35.24/27.33	39.94/51.23	37.19/21.99	34.04/20.14
Diff	-18.21	9.40	7.91	-11.28	15.20	13.90

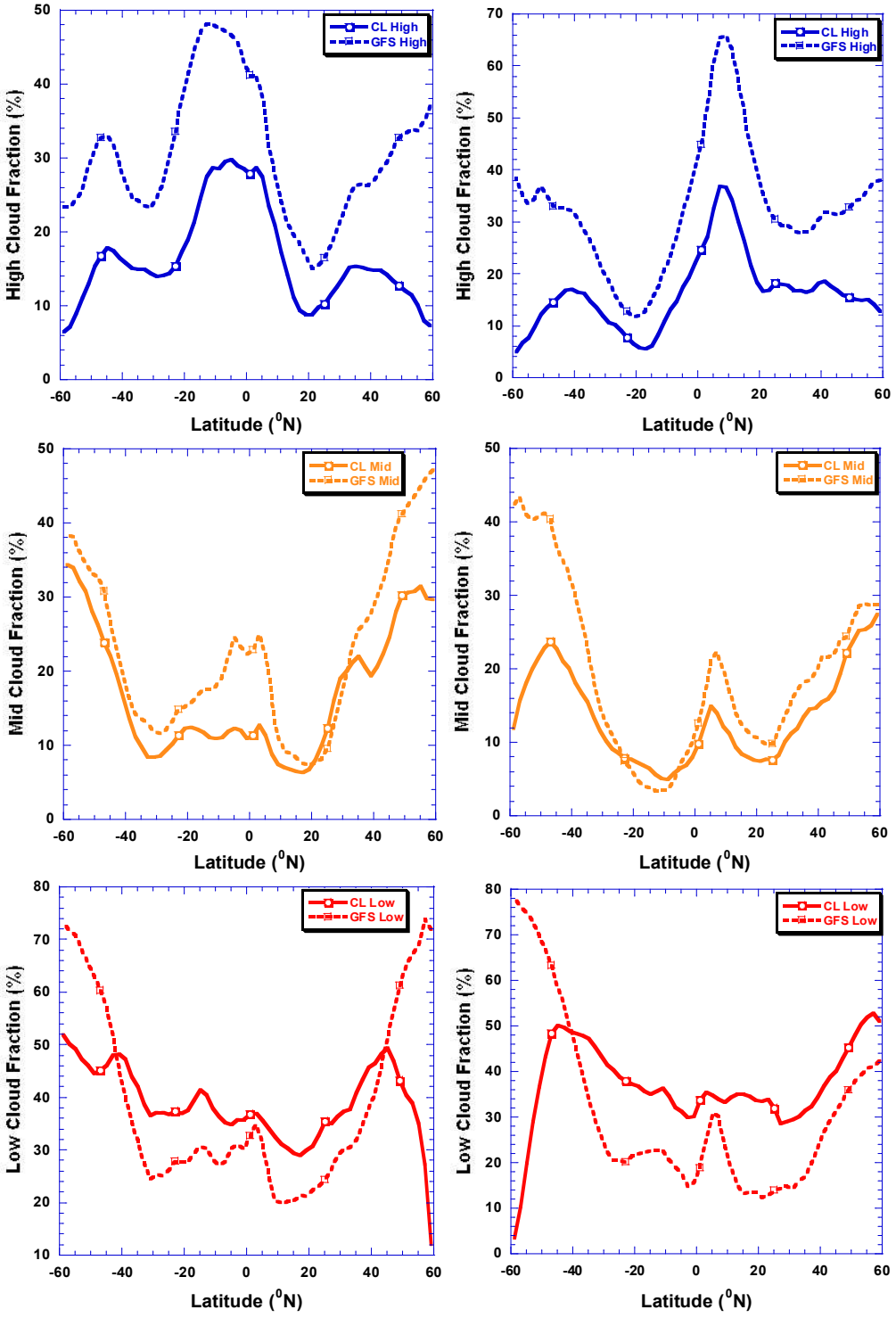

Figure 2.6. Latitudinal variations of cloud fraction for high clouds (top plots), middle clouds (middle plots), and low clouds (bottom plots) in January (left) and July (right) 2007. Solid lines and dashed lines represent results from the C-L algorithm and the GFS model, respectively.

2.4.4. Liquid Water Path and Ice Water Path

Cloud LWP/IWPs are estimated from both MODIS measurements and the GFS model during the daytime. The modeled LWP is based on the cloud water mixing ratio at each level and the observed LWP is retrieved from the C-L algorithm using the MODIS data. The MODIS-CL LWP/IWPs are calculated using cloud optical depth and a fixed effective radius of 10 μm (30 μm) for water (ice) clouds and they are more reliable than those from the MODIS-EOS products because the C-L algorithm retrievals include overlapped low clouds beneath high clouds. The LWP retrieved by the MODIS is more reliable than that from the AVHRR because retrievals are made using information from more wavelengths (1.6, 2.1, and 3.7 μm as opposed to 3.7 μm only) which contains certain information about the vertical distribution of cloud particle size (Chang and Li 2002; Chang and Li 2003), from which LWP can be better estimated (Chen et al. 2007).

The spatial distributions of modeled and satellite-retrieved LWPs for January and July 2007 are shown in Figures 2.7 and 2.8. The LWP of high-level clouds simulated from the GFS is substantially smaller than that retrieved from satellite measurements in both January and July. Mid-level GFS and MODIS-CL LWPs in January showed quite different distribution patterns. The GFS-modeled LWP was more generated over South America, the southern parts of Africa, and the ITCZ, but it was mostly missed over the eastern coastal area of North America and the East Asia region (100º - 180ºE, 20º - 40ºN) relative to the satellite retrievals. The low-level LWP from MODIS-CL retrievals was significantly greater than that simulated by the GFS model, particularly over ocean areas and at high latitudes in both hemispheres.

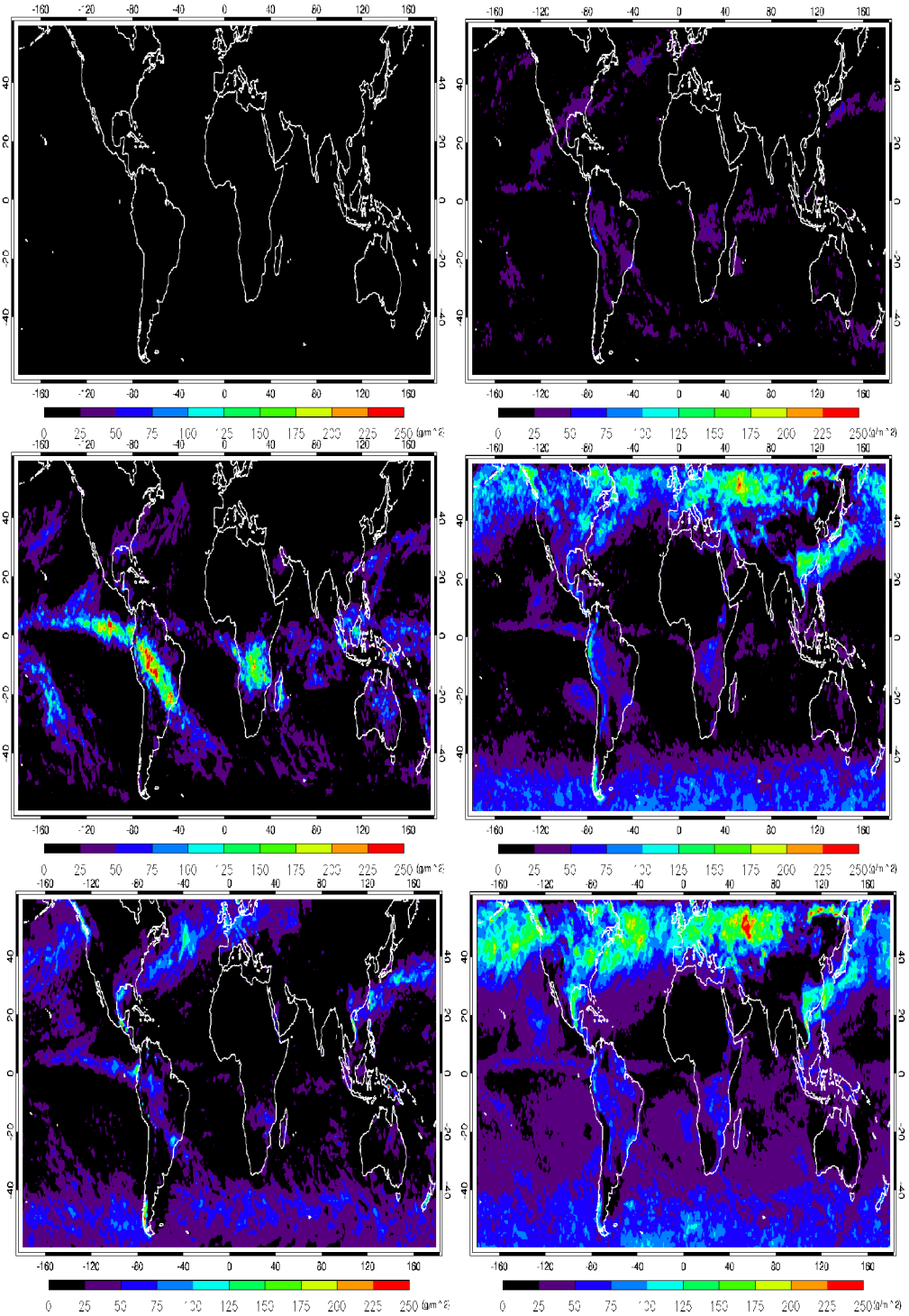

Figure 2.7. LWP from the GFS-model (left plots) and MODIS-CL (right plots) LWP in January 2007. Upper, middle, and bottom sets of figures represent high, mid, and low level LWPs, respectively. Units are in g/m^2.

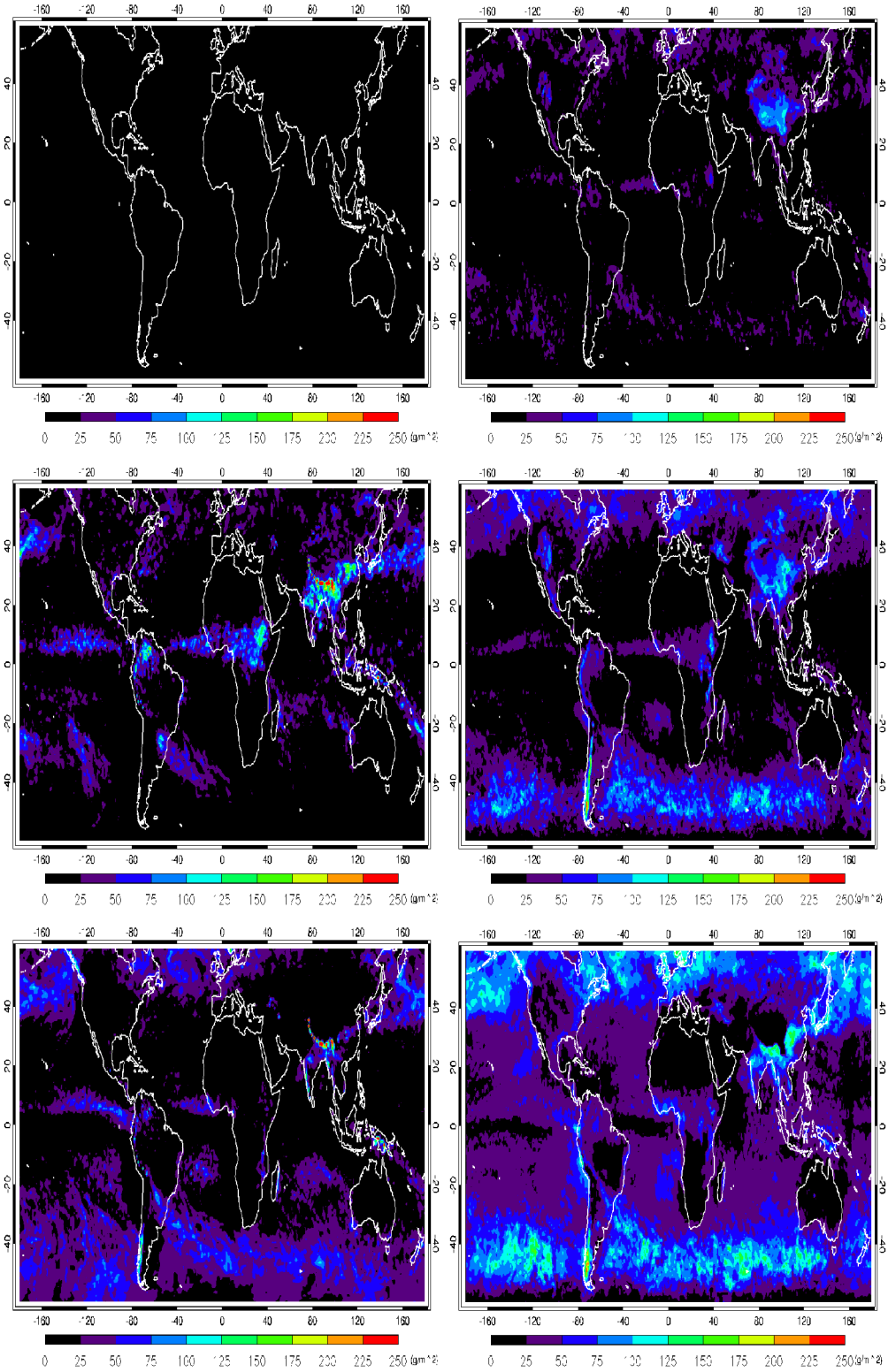

Figure 2.8. Same as Figure 2.7 except for July 2007.

These features are also evident in July. High and mid-level distributions of monthly mean LWP in July are similar (except for magnitude), but large discrepancies in low-level LWPs are evident over oceans and particularly at high latitudes in the both hemispheres.

Figures 2.9 and 2.10 show near-global distributions of monthly mean IWP obtained from both MODIS-CL retrievals and the GFS model in January and July 2007. In general, the GFS model produces more IWPs in the Tropics but agrees in spatial distribution with the satellite product. GFS simulations of high-level IWP are smaller than MODIS-CL IWP retrievals over the North Atlantic Ocean, the northeastern Pacific Ocean, and the East Asia region during January and over the Southern Ocean during July. The spatial distributions of mid- and low-level IWP from both model and satellite are generally comparable, although the mid-level IWP generated by the GFS is somewhat underestimated beyond 40ºN during January. Except in high-latitude regions, very little low-level IWP is seen from both model and observation.

On a global scale, underestimation of the modeled low-level LWP over oceans leads to significant errors in the low cloud fraction. Cloud fraction and LWP/IWP generated by the GFS model strongly depend on the cloud water mixing ratio variable. The cloud water mixing ratio is the sole predictor of LWP/IWP and the primary predictor of cloud fraction. Underestimation of low-level LWP and cloud fraction means that the GFS model has difficulty in simulating cloud water mixing ratio in the lower atmosphere. We will show possible causes for the discrepancies in terms of input variables and parameterization scheme used in the

GFS model in Chapter 3.

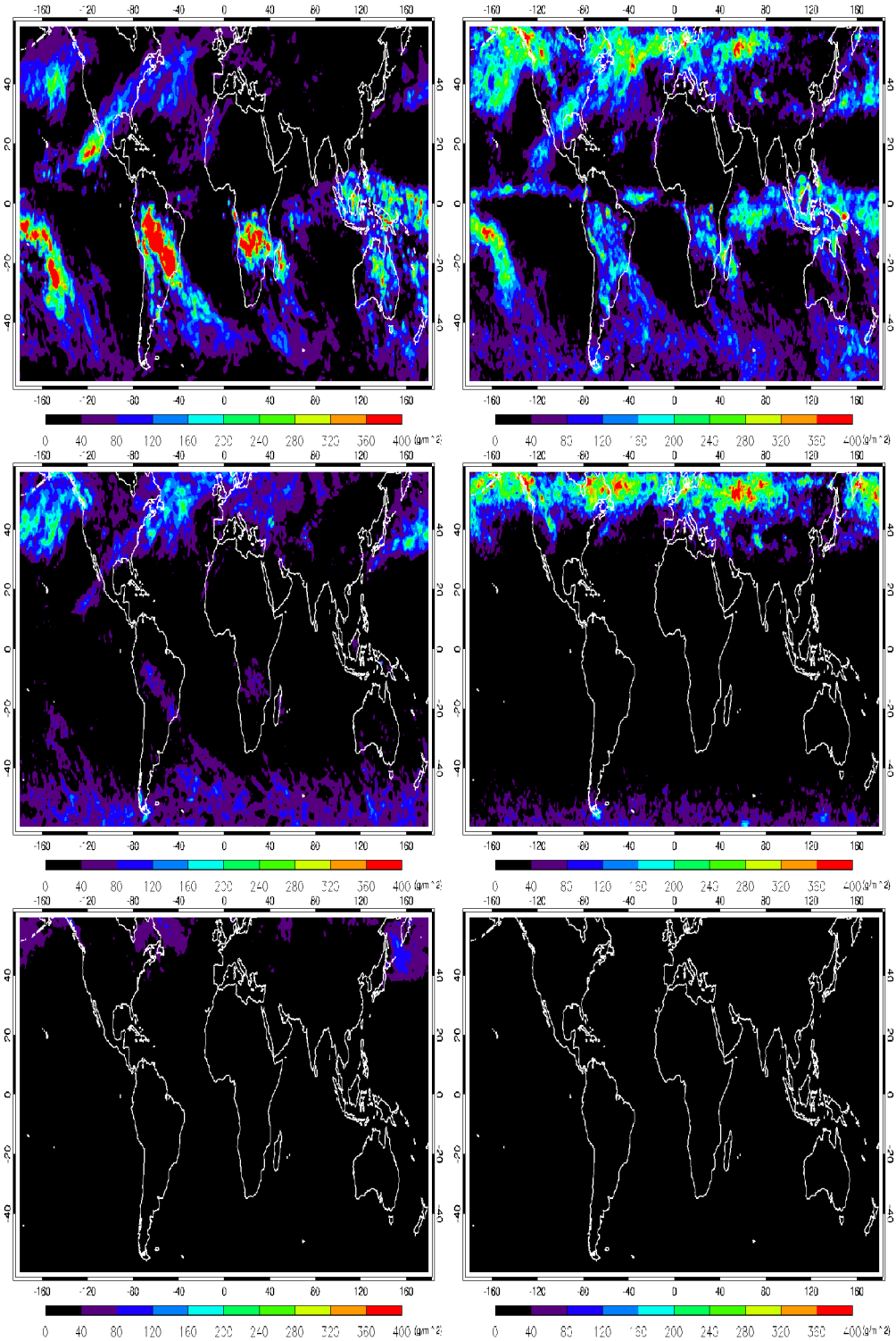

Figure 2.9. IWP from the GFS model (left plots) and MODIS-CL (right plots) in January 2007. Upper, middle, and bottom sets of figures represent high-, mid-, and low-level IWPs, respectively. Units are in g/m^2.

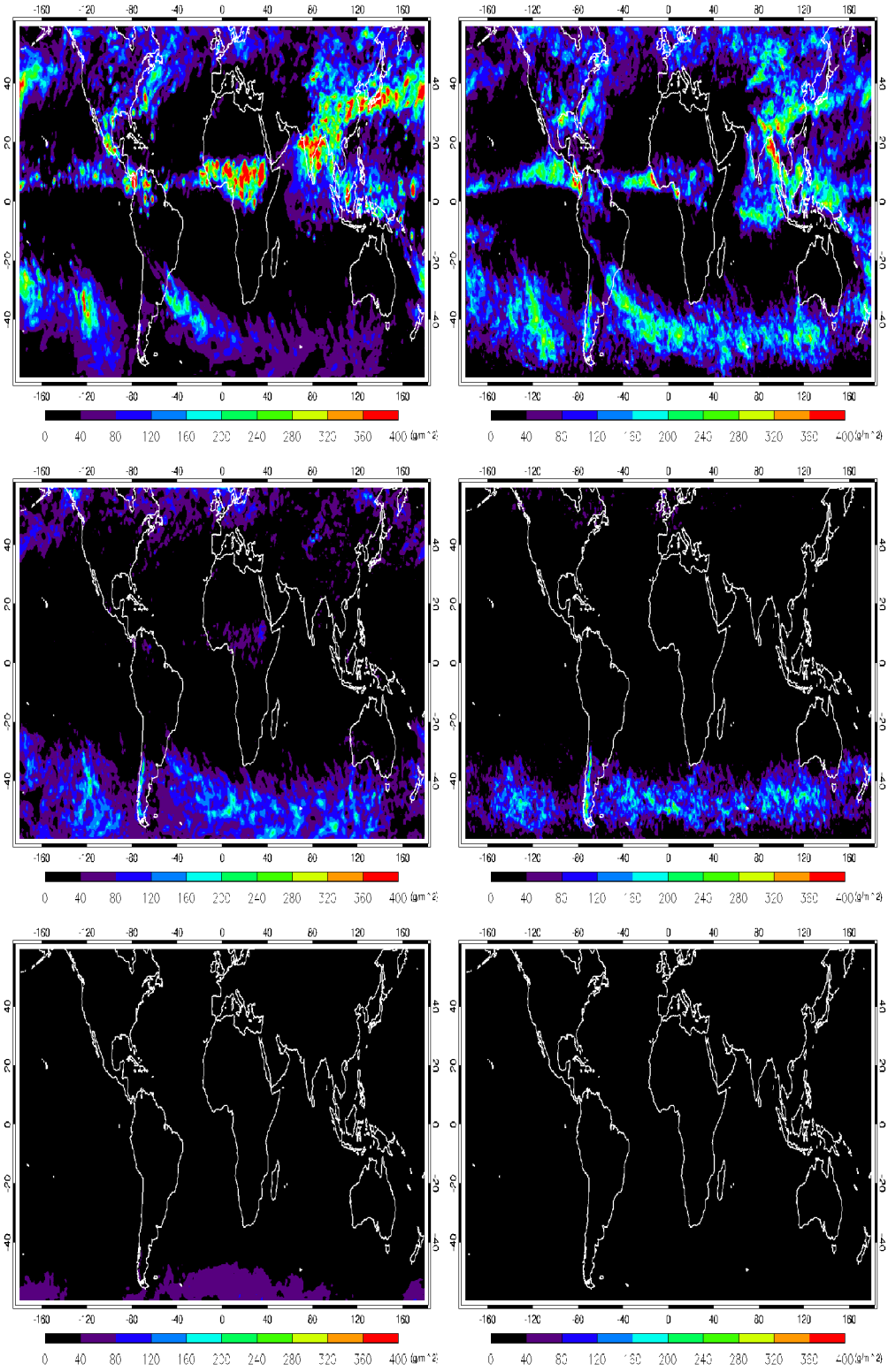

Figure 2.10. Same as Figure 2.9 except for July 2007.

2.4.5. Cloud Optical Depth

Global distributions of COD obtained from different sources are shown in Figures 2.11 and 2.12. The upper plots in Figure 2.11 represent retrievals from the same instrument but using different algorithms (the C-L algorithm on the left and the MODIS algorithm on the right); patterns are similar between two retrievals but magnitude of COD from the MODIS-CL is larger than that from MODIS-EOS retrievals on a global scale. This is a result of the recovery of low clouds with overlapped high clouds. Note that the C-L algorithm can only detect dual-layer clouds if the top clouds are optically thin (optical depth ~4), beyond which it cannot retrieve the second cloud layer. The two MODIS-based CODs are generally prevalent in mid-latitude storm-track regions during January. The GFS model can simulate the general pattern of observed CODs but the magnitudes are too small over those regions. Overestimation of CODs is seen over South America, the southern portion of Africa; CODs are underestimated over the mid-latitude storm-track regions.

Regarding CloudSat, Kahn et al. (2008) reported that thin cirrus cloud retrievals from the radar-only scheme had some differences with retrievals from the combined radar-lidar scheme. Optically thin clouds are undetected when using the radar-only cloud scheme because of the existence of small ice particles. Also, low clouds below 1 km are difficult to detect with the radar-only scheme due to ground clutter issues. This shows that CloudSat is not as sensitive to thin cirrus and boundary layer clouds. So CloudSat retrievals of COD are underestimated over most areas of the globe. The lidar is more sensitive than the radar to small hydrometeors, such as small ice crystals and water droplets, but is not capable of detecting clouds

at lower levels of the atmosphere because it cannot penetrate through clouds all the way to the surface. Lidar COD retrievals range from 0 to 5 only and the C-C satellites does not provide COD retrievals. Therefore, more reliable active sensor datasets such as the C-C satellites retrievals are required in the future so that more accurate verification of COD retrievals can be performed.

Figure 2.12 shows the latitudinal variations of monthly mean COD distributions from MODIS-EOS, the MODIS-CL, CloudSat, and the GFS during January (left plot) and July (right plot). Averages were taken over 2^{o} latitudinal bins. The C-L algorithm results are more than results from the MODIS algorithm in most areas for the two months. The GFS model significantly underestimates COD beyond 20ºS and 10ºN in January. Within this region, COD retrievals from the GFS model are around 2-3 times less than retrievals from the MODIS. Two peaks in both of the MODIS products are seen near 50ºS and 10ºN in July, corresponding to clouds from storm tracks in the Southern Hemisphere and convective clouds in the ITCZ. Zonally-averaged CODs generated by the GFS model in July are less than satellite retrievals of COD in the entire Southern Hemisphere. Zonally-averaged CODs from CloudSat retrievals are generally much smaller than the other satellite-based retrievals/model results during January and July. In brief, the GFS model overestimated COD for optically thick clouds, such as deep convective clouds, and underestimated COD for optically thin or intermediate clouds over the storm track regions of the world.

Systematic forecast errors exist in radiation fields due to poorly simulated cloud properties in the boundary layer. A previous study using a single column

model implemented the GFS physical processes reported that modeled downwelling shortwave fluxes were significantly overestimated while sensible heat fluxes were underestimated at the surface (Yang et al. 2006). Thus, it is necessary to quantify cloud parameters such as effective droplet radius and cloud optical depth in order to determine radiative quantities. These parameters potentially impact longwave/shortwave cloud forcing and diabatic heating through scattering and absorption processes. An evaluation of radiation and moisture budgets generated by the GFS will be addressed in Chapter 3.

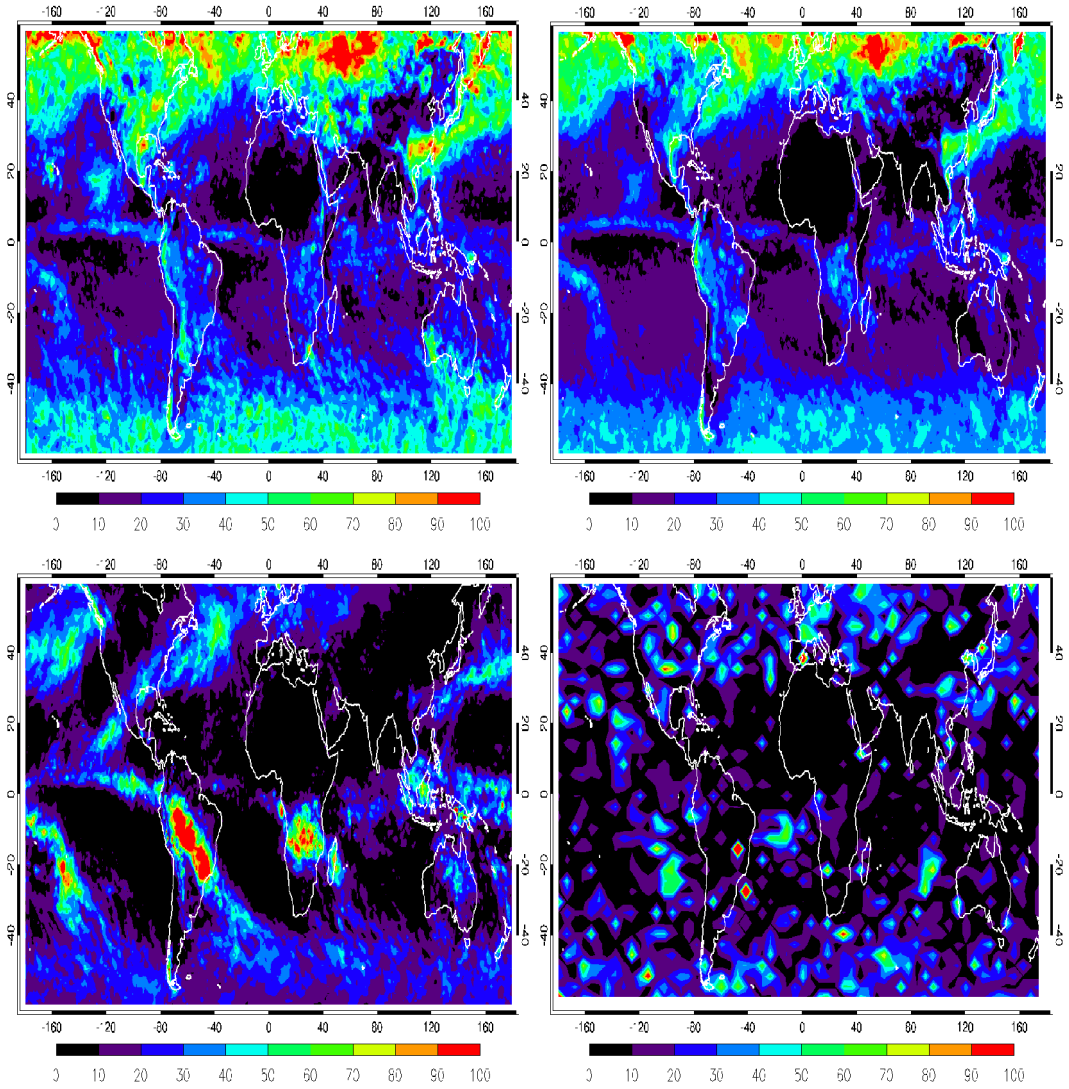

Figure 2.11. Total COD from (clockwise, starting from the upper left plot) the MODIS-CL, MODIS-EOS, CloudSat, and the GFS model during January 2007.

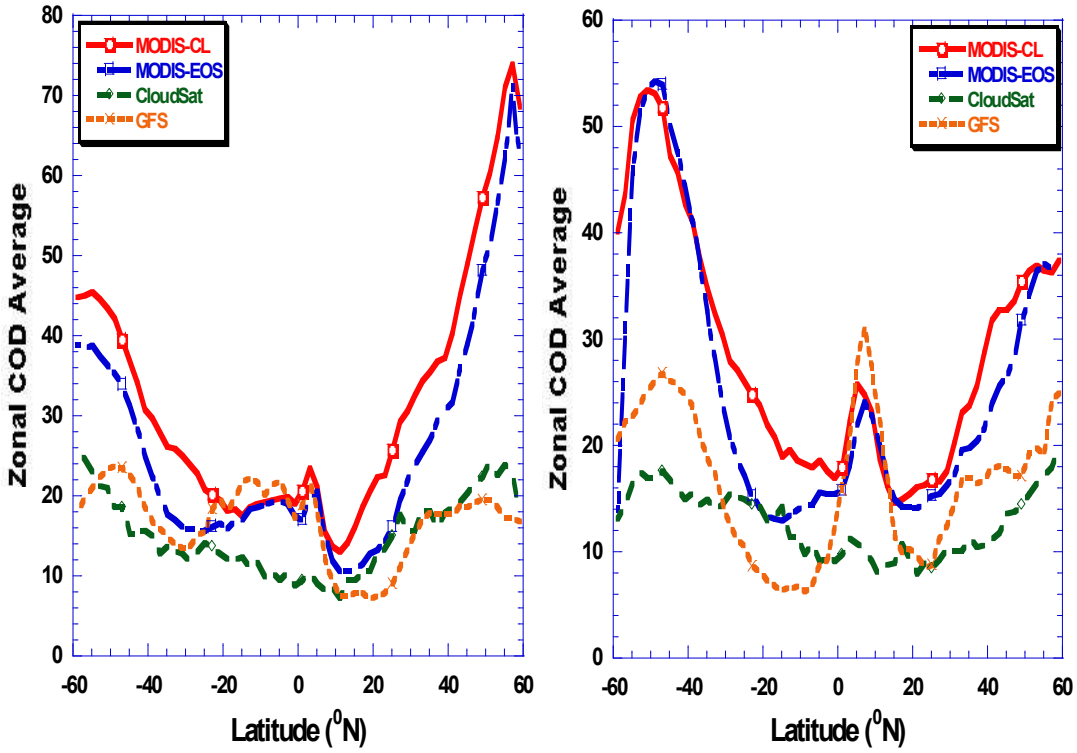

Figure 2.12. Latitudinal variations of COD in January (left plot) and July (right plot) 2007. The solid red lines, dash-dotted blue lines, dashed green lines, and dotted orange lines represent results from MODIS-CL, the MODIS-EOS, CloudSat, and the GFS model, respectively.

2.4.6. The top & base height and its thickness of the lowest cloud layer

Cloud fractions generated from the GFS model are comparable with the two satellite retrievals for high and middle clouds, but huge discrepancies in the low-level cloud amounts are most remarkable (see Figs. 2.4-5). Thus, this section puts more focus on properties of the lowest cloud (hereafter referred to as LC) layer. Figure 2.13 displays comparisons of zonal-mean top and base height occurrence

frequencies of the LC layer from both the C-C satellites and the GFS model during July 2007. The model does a good job for capturing the general feature seen from the satellite retrievals except for slight differences in its altitude. The results obtained from the C-C satellites show that top heights of the LC occur frequently at 1-2 km in the Southern Hemisphere and base heights of the LC have the most frequent occurrence at 0-1 km. Overall, the GFS model produces somewhat higher top and base heights of the LC relative to the C-C satellites. The most frequent occurrences of top and base heights of the LC in the GFS model results occur at 3-6 km and at 0-2 km, respectively.

Figure 2.14 shows the latitudinal variations of the occurrence frequencies of the LC thicknesses obtained from the C-C satellites and the GFS model output. A thickness of the LC in this study is defined as the top height of the LC minus the base height of the LC. The GFS model results show a cosine function-like shape having an axis at 10º N. This pattern is much broader and thicker than those retrieved by the C-C satellites.

Figure 2.15 compares top height occurrence frequencies of the LC corresponding to the base height of the LC derived from the C-C satellites (right panel) and the GFS results (left panel). It is obvious that the thicknesses of the LC from the GFS model are much thicker than those from the C-C satellites approximately 4 km if we add a reference line to the axes. This outcome is consistent with the above results. Underestimation of stratocumulus clouds in the GFS model may be attributed to the discrepancies in these comparisons.

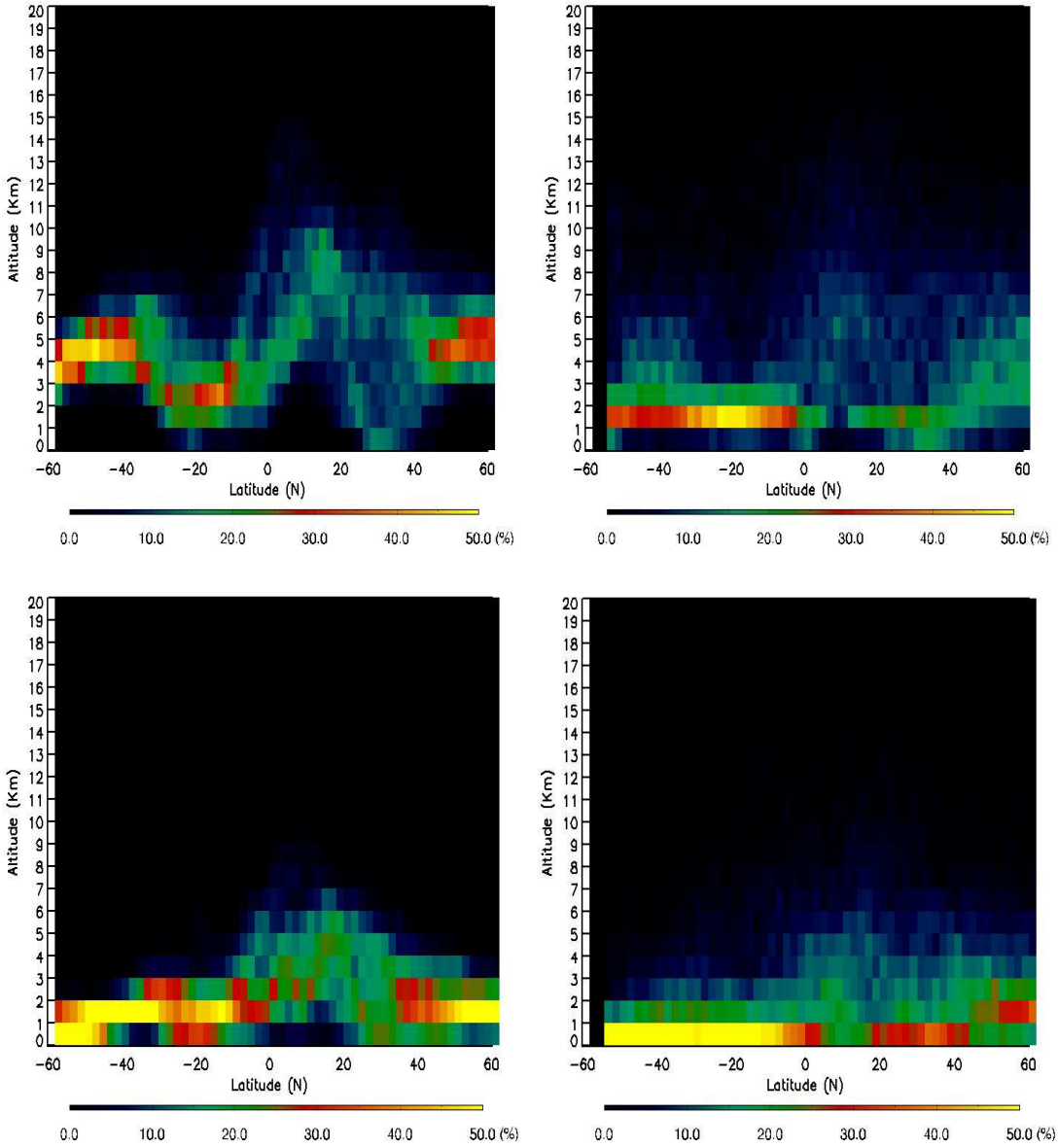

Figure 2.13. Latitudinal variations of zonal-mean occurrence frequency of the LC; for top height from the GFS (top left), the C-C satellites (top right) and for base height from the GFS (bottom left), the C-C satellites (bottom right) in July 2007.

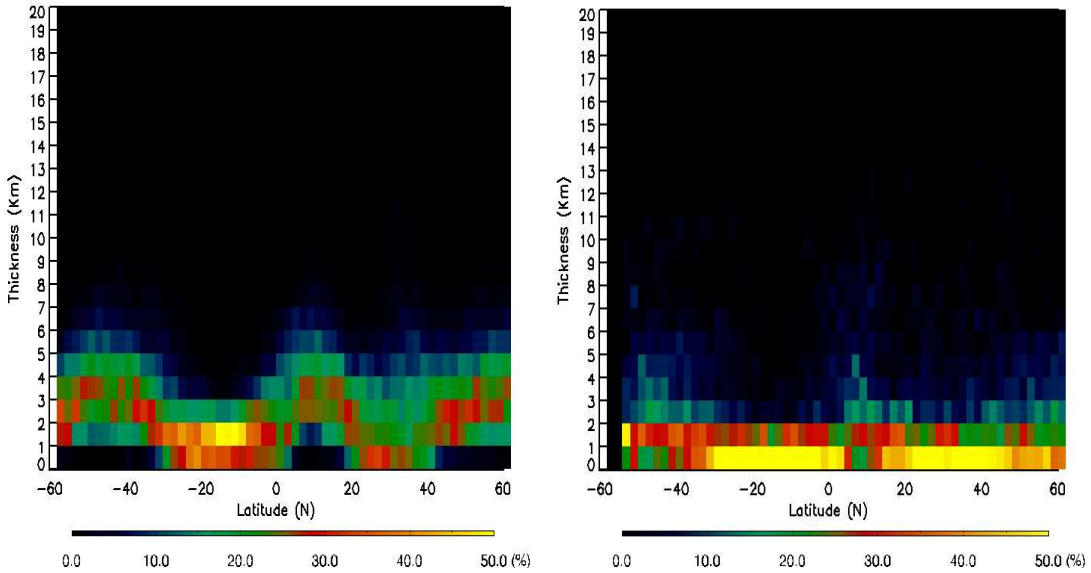

Figure 2.14. Latitudinal variations of the occurrence frequencies of the LC thickness from the GFS (left) and the C-C satellites (right) in July 2007.

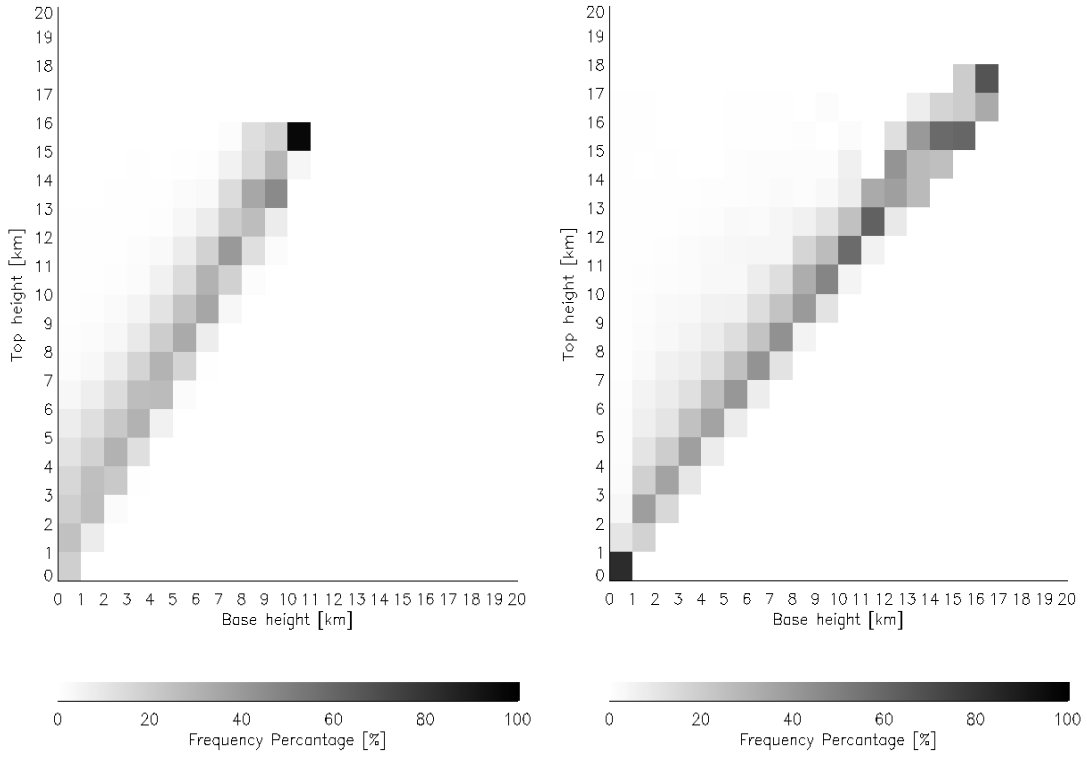

Figure 2.15. Top height occurrence frequencies of the LC corresponding to the base height of the LC from the GFS model (left), the C-C satellites (right) in July 2007.

2.5. Summary

Clouds and their interactions with large-scale atmospheric circulation are crucial parts of weather and climate systems. So far, we have a poor understanding of how well clouds are simulated by weather forecast and climate models due to limited reliable observations, especially concerning the vertical distribution of clouds. However, the advent of advanced remote sensing techniques in the recent decade allows us to assess and improve cloud fields in terms of both horizontal and vertical variations.

In this Chapter, we employed multiple global satellite products from the A-Train constellation to evaluate clouds generated by the NCEP GFS model. Cloud properties simulated by the GFS model are compared with satellite retrievals from CloudSat, CloudSat-CALIPSO merged data, MODIS-EOS and a new MODIS-based research product developed by Chang and Li (2005a, b). Extensive cloud variables are assessed including the frequencies of cloud layers occurrence, cloud fraction and thickness, cloud optical depth, liquid water path, and ice water path. In particular, an evaluation of the GFS cloud vertical structure on a global scale is the main focus of this chapter.

The GFS model captures well the spatial distributions of hydrometeors, which bear a reasonable resemblance to those seen from satellite retrievals, although large differences exist in the magnitudes. The GFS model generates more high-level and mid-level clouds, but less low-level clouds than do satellite retrievals. More boundary layer clouds over the interior of continents at high latitudes were generated

by the GFS model whereas satellite retrievals showed more low clouds over oceans. In other words, the GFS model tends to miss low-level marine stratocumulus clouds and overestimate interior continental low-level clouds. GFS-modeled CODs are less than those from MODIS retrievals in high-latitude regions of both hemispheres and are overestimated over South America and the southern African region during January 2007. The GFS model overproduces optically thick clouds in deep convective cloud regimes and the southeastern Asian summer monsoon region during July. CODs for optically thin or intermediate clouds are underestimated. GFS-modeled IWP distributions agree better with satellite retrievals than do LWP distributions.

These comparisons provide useful guidance toward diagnosing the source of possible errors, especially with regard to systematic biases that help identify major flaws in either cloud parameterization schemes or input variables, or both. More thorough and rigorous investigations into the causes of discrepancies are shown in Chapter 3 by means of model radiation fields, analysis of various input variables used in cloud parameterization schemes, and further validation of these variables. More independent satellite products such as atmospheric profiles of temperature and moisture from microwave radiometers and ground-based measurements will also be employed to help understand the discrepancies.

Chapter 3: Causes of the Discrepancies in Cloud Fields

3.1. Introduction

Clouds play an important role in regulating the Earth's radiative energy budget and temperature and they are also one of the most critical factors in the hydrology cycle of the Earth (Del Genio et al. 2005). Despite their significance, an accurate representation of clouds in global climate and weather models has not yet been achieved due to the incomplete knowledge of the underlying physical processes (Stephens 2005) and the considerable variations in cloud amount in both vertical and horizontal directions (Stowe et al. 1989; Rossow et al. 1989). Cloud representations in models are the critical source of uncertainty in projections of future climate change (Wielicki et al. 1995; Houghton et al. 2001). A more accurate representation of cloud behavior is required in order to generate realistic simulations of the Earth's climate change. As more observational data have become available, the impact of clouds on weather and climate can be better assessed and various cloud parameterization schemes can be tested. Among the diverse set of ground-based and space-borne instruments, satellites are the only platforms that can provide continuous observations of cloud properties on global scales.

Many general circulation models (GCMs) have difficulty in representing low cloud distributions, especially over the eastern tropical oceans (Ma et al. 1996; Hannay et al. 2009). This is also seen in a fully coupled climate system model (Dai and Trenberth 2004; Mechoso et al. 1995) and regional climate models (Xie et al. 2007). Such findings require substantial improvements in simulating low cloud

amount. Otkin and Greenwald (2008) evaluated cloud properties simulated by the Weather Research and Forecasting (WRF) model using the Moderate Resolution Imaging Spectroradiometer (MODIS) cloud product and found that the model was unable to properly simulate stratocumulus and cumulus clouds. This inability of climate models to simulate marine stratocumulus cloud decks is one of the most significant sources of errors and uncertainties in the tropical cloud feedback (Bony and Dufresre 2005; Randall et al. 2007). Similarly, a long-existing problem in the global forecast system (GFS) model is an underestimation of such stratocumulus clouds over the subtropical eastern oceans (Sun et al. 2010). Marine stratocumulus and low clouds over the oceans are known to have a radiative cooling effect on the global energy budget by reflecting incoming solar irradiances (Hartmann et al. 1992). Additionally, these clouds can impact the cloud microphysical structure and diurnal cycle by causing light precipitation (Nicholls 1987). Under-prediction of such clouds results in positive sea surface temperature biases over the coast of Peru in ocean-atmosphere coupled models (de Szoeke et al. 2006).

Many satellite products based on retrievals from passive sensors have suffered from certain fundamental limitations in detecting and measuring low clouds due to the presence of overlying high clouds (Chang and Li 2005a, 2005b). Observations from ships (Warren et al. 1985), airborne lidar measurements (Platt et al. 1994; Clothiaux et al. 2000), and a surface-based radar (Mace and Benson-Troth 2002) reported the frequent occurrence of multi-layer clouds.

Thanks to space-borne active sensors (Stephens et al. 2002; Mace et al. 2009) and an advanced cloud retrieval algorithm (Chang and Li 2005a, hereafter referred

to as the C-L algorithm), a great deal of more accurate knowledge about low cloud distributions and their temporal and spatial variations has been gained. Application of the C-L algorithm using MODIS data led to a new global-scale low cloud distribution with daily coverage. The C-L algorithm can detect the presence of low clouds below high clouds and retrieve their optical properties.

In this Chapter, investigating the causes of the discrepancies in cloud fields is mainly discussed. It is attempted to 1) diagnose the status of the GFS model in simulating marine stratocumulus cloud fractions over the eastern tropical oceans; 2) analyze input data globally and regionally; 3) explore and test another cloud parameterization scheme. Cloud fractions are obtained by applying the C-L algorithm and are retrieved from space-borne active sensors in order to validate low clouds generated by the GFS model. Simulated temperature and relative humidity (RH) profiles are examined against retrievals from the Atmospheric InfraRed Sounder (AIRS) sensor and ground-based measurements. The evaluation of atmospheric environmental variables makes it possible to ascertain whether discrepancies in low cloud distributions between the model and observations come from misrepresented input parameters or from deficiencies in the model cloud parameterization scheme. Another cloud parameterization scheme based on a diagnostic approach is applied to the GFS model and resulting cloud fields are also compared to those generated by the original version of the GFS model. This is done to test the soundness of the original GFS cloud parameterization and to improve the representation of cloud processes through application of more concrete relationships between input variables.

The study in Chapter 3 is organized as follows. Section 3.2 describes the dataset used in this research. The comparison of GFS-generated vertical profiles of temperature and relative humidity fields with observations is presented in section 3.3. Section 3.4 shows results from the application of another cloud parameterization scheme to the GFS model. Finally, section 3.5 presents the main findings and a summary of this work.

3.2. Data and Methodology

In terms of observational data, atmospheric environmental variables are obtained from both the AIRS sensor onboard the Aqua satellite and a ground-based instrument. Cloud fraction is retrieved from the C-L algorithm using MODIS data also acquired from MODIS of the Terra/Aqua satellite platforms and is obtained from space-borne active sensors. These datasets provide an invaluable opportunity for monitoring clouds, changes in atmospheric temperature on a global scale and for assessing the accuracy of weather forecast models. All data used in this study are for every day for July 2008. For section 3.4, data for January and July 2007 are used to compare those with the results from section 2.3.3.

3.2.1. AIRS Atmospheric Variables

The AIRS sensor launched in May 2002 is the first high spectrally-resolving infrared sounder with near-global coverage on a daily basis (Aumann et al. 2003). It

flies on the Aqua satellite in a Sun-synchronous orbit 705.3km above the Earth's surface, descending at 01:30 local time and ascending at 13:30 local time. The AIRS measures outgoing radiances using 2378 infrared channels ranging from 15.38 μm to 3.74 μm. Its spatial resolution is 13.5 km at nadir and the sensor is accompanied by two microwave sounders: the Advanced Microwave Sounding Unit-A (AMSU-A) and the Humidity Sounder for Brazil (HSB). These microwave instruments are used to correct for cloud contamination in AIRS footprints. However, the HSB sensor suddenly stopped working right after launch due to an electrical failure. Here, calibrated AMSU-A brightness temperatures (Pagano et al. 2003) are utilized to derive atmospheric environmental profiles and cloud liquid water for microwave retrievals (Rosenkranz 2003; Susskind et al. 2003).

The AIRS sensor is dedicated to providing highly accurate and spectrally-resolved radiances to the operational numerical weather forecasting and climate research communities. It can measure temperature, water vapor, ozone profiles, and the presence of additional minor gases such as CH_4, CO, as well as other atmospheric properties (Chahine et al. 2006). Based on previous studies (Tobin et al. 2006; Walden et al. 2006), AIRS Level 2 data have an accuracy of ~1K root mean square (RMS) error in 1-km layers for temperature and ~ 20% RMS error for water vapor concentrations in 2-km layers as compared to radiosonde data. Others have demonstrated the invaluable contribution of AIRS data toward understanding maritime tropical Atlantic conditions (Nalli et al. 2006), describing a wide range of atmospheric phenomena (Divakarla et al. 2006), and assessing reanalysis data from the European Center for Medium-range Forecasting (ECMWF) (Susskind et al.

2006).

There are three different AIRS products: retrieval products using AIRS infrared (IR) data only (AIRS2STD), a combination of AMSU-A and HSB data (AIRH2STD**),** and a combination of AIRS IR and AMSU-A data without HSB data **(**AIRX2STD**)**. This study uses AIRS Level 2 version 5 standard daily products (e.g., AIRX2STD) that include AMSU-A retrievals because IR-only AIRS retrieval uncertainties increase rapidly when cloud fractions exceed 80 % (Tobin et al. 2006).

3.2.2. MODIS Cloud Products

MODIS is the principal instrument onboard the polar-orbiting Terra and Aqua satellites and has 36 calibrated spectral channels ranging from 0.415 μm to 14.24 μm (Barnes et al. 1998). This sensor detects clouds and allows making reliable retrievals of cloud properties (King et al. 2003; Ackerman et al. 1998; Menzel et al. 2002), such as cloud particle thermodynamic phase, cloud optical depth, cloud top pressure and temperature, and effective particle radius, using the MODIS CO_2 slicing method (Platnick et al. 2003).

The International Satellite Cloud Climatology Project (ISCCP) (Rossow and Schiffer 1999) dataset has been widely used to evaluate GCMs in generating clouds (Webb et al. 2001; Zhang et al. 2005). Evaluations reveal that GCMs tend to produce less low-level clouds and much less mid-level clouds than the ISCCP product. However, these findings are attributed to mistreating overlapped cirrus and low clouds as single-layer middle clouds in the ISCCP product (Chang and Li 2005b).

Therefore, use of ISCCP data as a reference is not reliable for the assessment of simulated cloud amounts at different vertical levels.

Taking advantage of the multiple channels of the MODIS allows for the detection of both single and multi-layered clouds. However, there is a lack of cloud profile observations originating from some limitations in passive sensors and inadequate satellite retrieval methods. To overcome this major limitation in the use of MODIS data, Chang and Li (2005a) developed a new retrieval algorithm, which showed more low clouds in the Tropics (up to 10% more) and in the mid-to-high latitudes (up to 20% more around 55^{o}S) in comparison with MODIS algorithm products (Chang and Li 2005b). This study using the C-L algorithm will compare low-level cloud fractions generated by the GFS model with output retrieved from both the active remote sensing and MODIS algorithms over the eastern tropical oceans in July 2008. MODIS data from the Aqua satellite (version Collection 5.1), and excluding data collected when the solar zenith angle is greater than 80°, is processed in this study.

3.2.3. ARM Measurements at SGP site

The Atmospheric Radiation Measurement (ARM) program's ground-based products are used to assess the existence of systematic errors in the temperature and relative humidity fields used in the GFS model's cloud diagnostic scheme. The Southern Great Plains (SGP) site in north-central Oklahoma is the first field measurement site established by the Department of Energy's ARM program. The site

is well-equipped with a large set of instruments useful for weather and climate research. Data from the site are widely employed to improve the prediction accuracy of weather forecast models and parameterization schemes (Lazarus et al. 1999; Xi et al. 2010) and to estimate cloud optical and macrophysical properties at different levels (Wang and Sassen 2004; Dupont et al. 2011).

Atmospheric Emitted Radiance Interferometer (AERI) observations of temperature and water vapor profiles are used in this study. AERI measurements provide atmospheric temperature and water vapor profiles with a high temporal resolution (about every 8 minutes). GFS model outputs at a specific grid point and spatially matched satellite retrievals are compared with AERI data.

3.2.4. CERES TOA Fluxes

The Clouds and the Earth's Radiant Energy System (CERES) instrument provides highly accurate radiative fluxes with coincident cloud and aerosol properties on a global scale (Wielicki et al. 1995; Loeb et al. 2007). This sensor is onboard both Terra and Aqua satellites; only CERES data from the Aqua satellite is analyzed here. This study uses the Single Scanner Footprint (SSF) product which contains longwave/shortwave fluxes at the top-of-the-atmosphere (TOA) and at the surface for clear and all-sky conditions on a daily basis. Outgoing longwave, shortwave, and net fluxes at the TOA are compared with the GFS model output.

3.2.5. CloudSat and CALIPSO merged data

Data collected by CloudSat and Cloud-Aerosol Lidar and Infrared Pathfinder Satellite Observation (CALIPSO) satellites during July 2008 are examined to compare low cloud fraction with both cloud retrievals based on passive sensors and cloud results simulated by the GFS model over the eastern tropical oceans. The CloudSat and CALIPSO satellites were launched in April 2006, carrying a 94-GHz cloud profiling radar (CPR) and dual-wavelength lidar in order to provide more accurate cloud vertical structure. This study uses the merged products (i.e., CloudSat CPR + CALIPSO lidar cloud mask, hereafter referred to as the C-C satellites) to obtain low cloud fraction. The combined dataset provides more reliable cloud information pertaining to multi-layered clouds such as optically thin high clouds over lower thick clouds (Mace et al. 2009).

3.2.6. GFS Cloud Parameterization Scheme

The GFS model is the operational medium-range global forecast model run by the National Centers for Environmental Prediction (NCEP). This version uses a T382 spectral triangular truncation with a horizontal resolution of 35 km and 64 vertical layers. This study uses forecasting data generated every 3 hours from 00Z to 24Z on each day. Cloud fraction is calculated based on a prognostic cloud scheme which involves the combination of model-predicted temperature, relative humidity, and three-dimensional cloud water mixing ratios. Cloud fraction in a given grid box in the GFS cloud scheme is computed using the approach of Xu and Randall (1996).

Unlike other cloud parameterizations including probability distribution functions (PDFs), the Xu and Randall methodology depends only on the relative humidity, the saturation specific humidity, and the cloud mixing ratio. Some detailed explanations with regard to an equation for cloud fraction are already provided in the previous section (see section 2.3.1). In this Chapter, GFS data cover the period of January and July 2007 and for July 2008.

3.3. Results

3.3.1. Global Radiation Budget at the TOA

Clouds are important in determining the radiative heating and cooling of atmospheric system on a global scale. Figure 3.1 compares global distributions of low-level cloud fraction from the C-L algorithm based on MODIS data and the GFS model. The simulated low clouds agree with the satellite retrievals in terms of the location of cloud layers. While the distribution of low clouds observed by satellite shows extensive marine stratocumulus clouds over the eastern tropical Pacific and Atlantic, such clouds are not well simulated in the GFS model. These results are consistent with previous studies which reported an underestimation of marine stratocumulus clouds over those regions in coupled GCMs (Giese and Carton 1994; Stockdale et al. 1994).

A comparison for global distributions of monthly mean upward shortwave (SW), longwave (LW), and net radiation at the TOA is shown in Figure 3.2. Net

radiation at the TOA is defined as the net balance between solar radiation and terrestrial radiation. Note that incoming terrestrial radiation at the TOA is assumed to be zero for both datasets. The basic pattern for both upward SW and LW radiation at the TOA is very similar between observation and model on a global scale, but disagreements exist over the eastern Pacific and Atlantic regions. The GFS model simulates less upward SW radiation and more outgoing LW radiation than that measured by CERES due to the underestimation of marine stratocumulus clouds. This is evident when we see the SW, LW, and net radiation differences between CERES and GFS in Figure 3.3. Positive biases in the SW radiation differences are dominant over oceans, especially in marine stratocumulus cloud decks. The net radiation differences show a positive bias tendency in the Southern Hemisphere, but a negative bias tendency in the Northern Hemisphere. Table 3.1 summarizes global monthly mean upward SW, LW, and net radiation under all-sky conditions from both CERES and GFS model. The mean value of SW, LW, and net radiation for CERES (GFS) for July 2008 is 90.91 W/m^2 (81.13 W/m^2), 247.62 W/m^2 (252.53 W/m^2), and -2.21 W/m^2 (13.35 W/m^2), respectively.

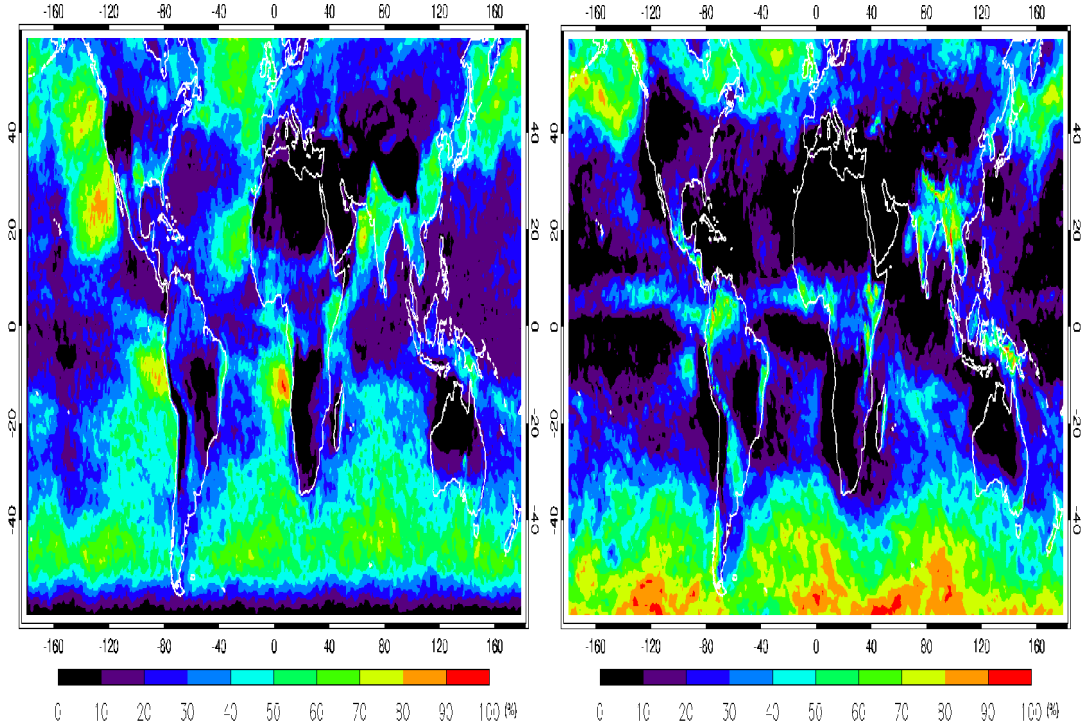

Figure 3.1. Low cloud fraction from the C-L algorithm (left plot) and the GFS model (right plot) during July 2008.

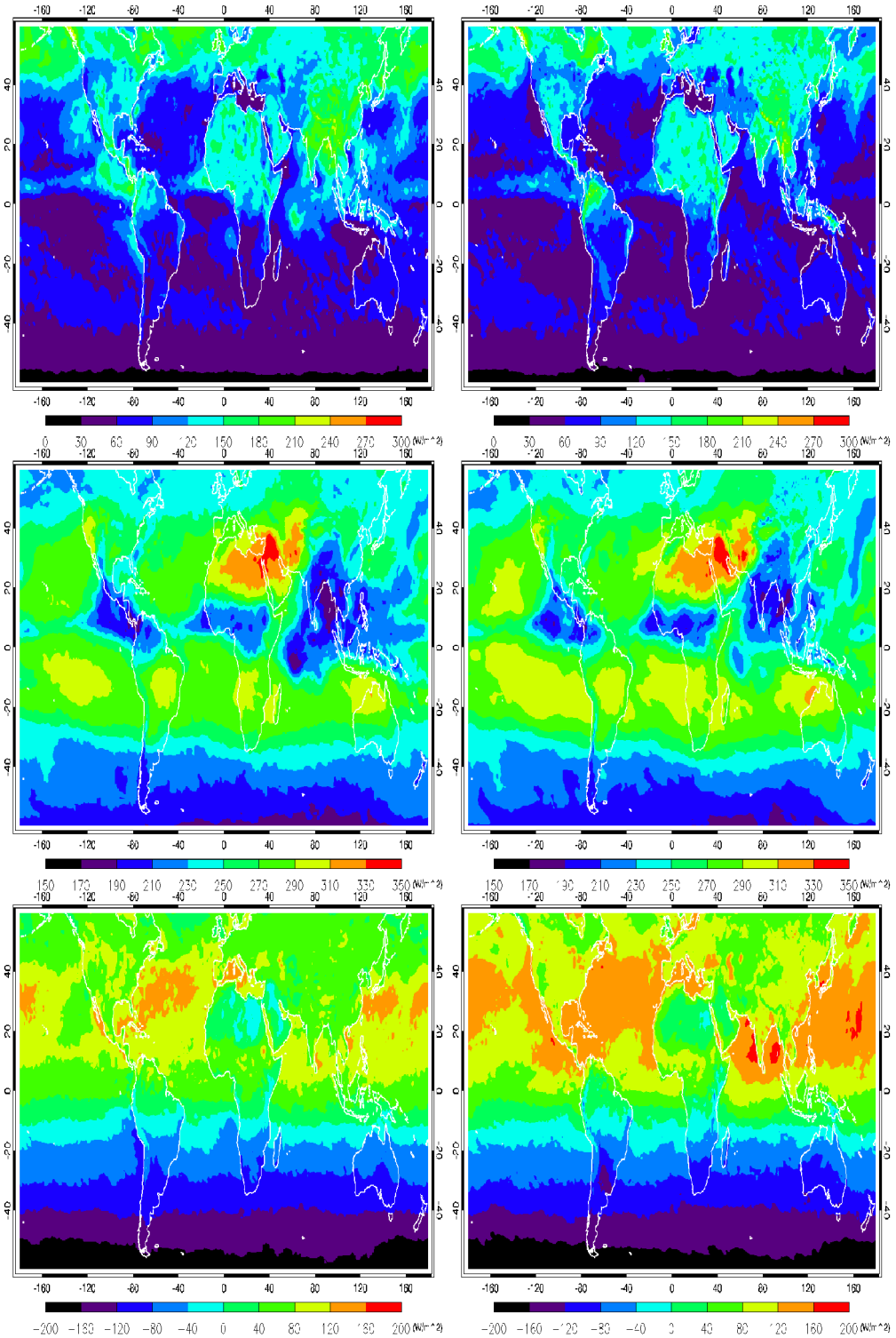

Figure 3.2. Global distributions of the outgoing SW radiation (top plots), LW radiation (middle plots), and net radiation (bottom plots) at the TOA from the CERES (left) and GFS (right) during July 2008.

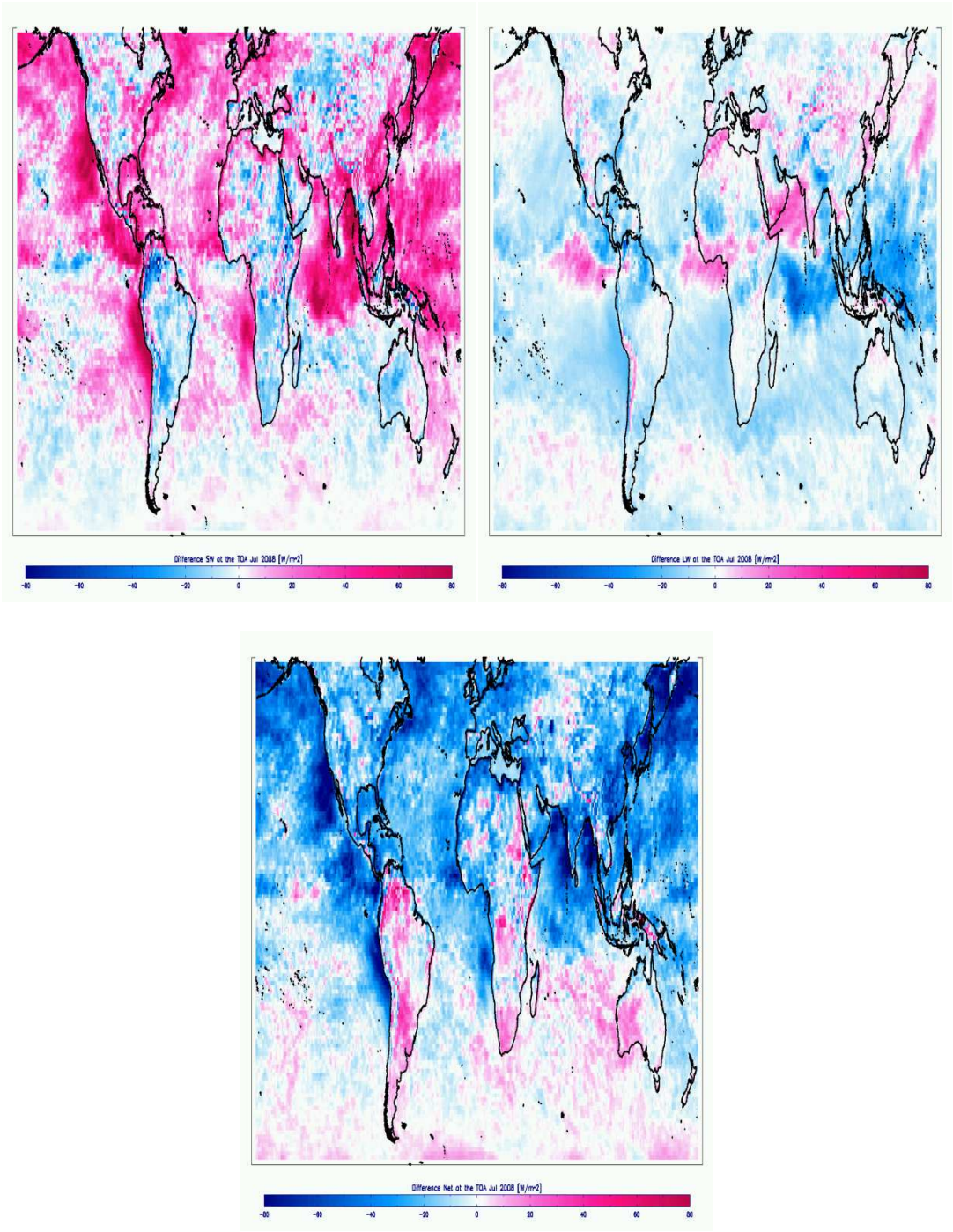

Figure 3.3. Global distributions of the differences between the CERES and the GFS for outgoing SW radiation (top left plot), LW radiation (top right plot), and net radiation (bottom center plot) at the TOA during July 2008.

Table 3.1. Global monthly mean SW, LW, and net fluxes at the TOA obtained from the CERES and the GFS model during July 2008.

	CERES	GFS
SW Flux	90.91 W/m^2	81.13 W/m^2
LW Flux	247.62 W/m^2	252.53 W/m^2
Net Flux	-2.21 W/m^2	13.35 W/m^2

Net radiations at the TOA from CERES and the GFS model have opposite signs, emphasizing the impact of marine stratocumulus clouds on the global net radiation. It is broadly recognized that marine stratocumulus clouds play a key role in regulating sea surface temperature over the eastern tropical regions by interacting with both SW and LW radiations (Philander et al. 1996; Ma et al. 1996). Such clouds scatter incident radiation for wavelength shorter than 0.9μm with a reflectivity of 0.66 and absorb radiation for wavelength longer than 0.9μm with an absorptivity of 0.3 (Katayama 1972).

To investigate the causes of the discrepancies in marine stratocumulus cloud decks between the GFS model and observations, four areas along the west coast of America and Africa are selected. Figure 3.4 shows the four marine stratocumulus cloud regions investigated in this study. These domains are located in the subtropics and are characterized by a strong limited mixing between boundary layer and free atmosphere. The geographic boundaries of each region are a bit arbitrary and different from those analyzed by Klein and Hartmann (1993). The individual regions are defined as: Californian (10° - 40°N, 160° - 110°W), Peruvian (0° - 30°S, 110° - 75°W), Namibian (0° - 30°S, 30°W - 10°E), and Canarian (10° - 40°N, 60° - 20°W).

Regional mean radiation fields are summarized in Table 3.2. Simulated SW (LW) fluxes at the TOA are all less than (greater than) those observed from space with differences ranging from 10.67 W/m^2 to 24.77 W/m^2 (3.92 W/m^2 to 9.82 W/m^2) due to the underestimation of marine stratocumulus clouds.

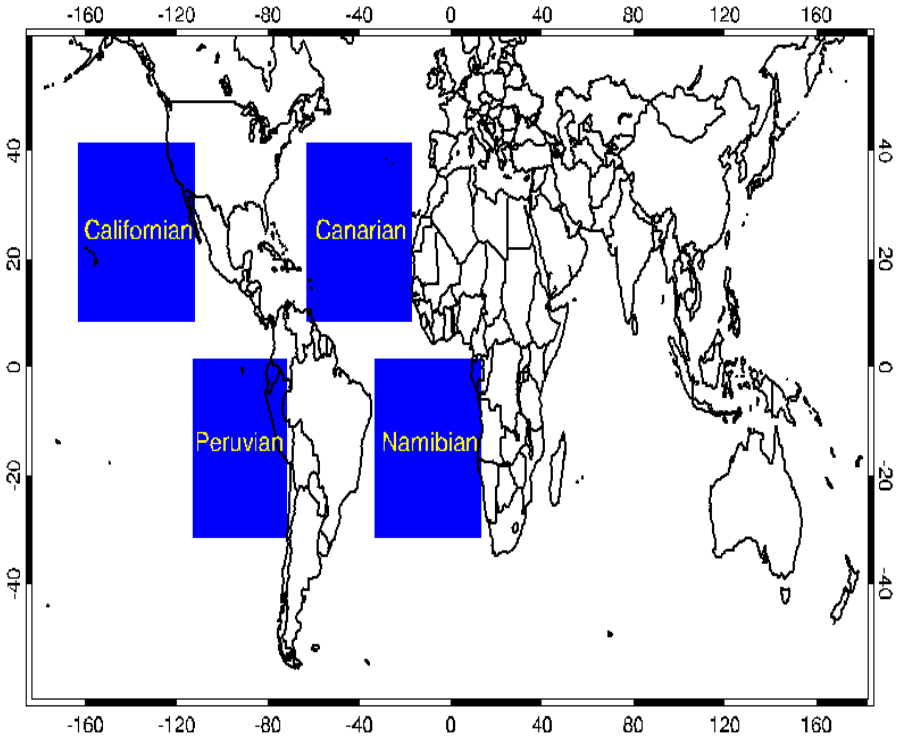

Figure 3.4. Four geophysical locations of marine stratus clouds occurrence regions: Californian (10° - 40°N, 160° - 110°W), Peruvian (0° - 30°S, 110° - 75°W), Namibian (0° - 30°S, 30°W - 10°E), and Canarian (10° - 40°N, 60° - 20°W).

Table 3.2. Regional mean SW and LW fluxes under all-sky conditions at the TOA from the CERES and the GFS over the selected regions in July 2008.

	CERES		GFS	
	SW	LW	SW	LW
Californian	99.15 W/m^2	273.22 W/m^2	74.38 W/m^2	280.04 W/m^2
Peruvian	79.08 W/m^2	274.99 W/m^2	56.94 W/m^2	284.81 W/m^2
Namibian	62.02 W/m^2	278.46 W/m^2	51.07 W/m^2	286.04 W/m^2
Canarian	74.46 W/m^2	272.47 W/m^2	63.79 W/m^2	276.39 W/m^2

3.3.2. Global Analysis of the modeled temperature and relative humidity

As mentioned earlier, the GFS modeled clouds agreed well with observations in some regions while they were poorly simulated in other places. Discrepancies in cloud vertical structure/amounts between observations and the GFS model can be attributed to differences in relative humidity, temperature, and cloud mixing ratio fields, which are major three control variables determining the formation of clouds in the model environment (see eq. 2.3.1). Thus, it is needed to examine ambient atmospheric temperature and relative humidity (RH) profiles under clear/cloudy conditions in order to find out some clues or suggestions on the improvement of cloud simulations. If meteorological variables in the model are close to the observed ones, we can consider that the disagreements in cloud comparisons between the model and observations stem from the errors in the cloud parameterization scheme. Otherwise, a large discrepancy in cloud fields can be attributed mainly to the simulated atmospheric profiles which consequently produce different cloud distributions against observations.

Figure 3.5 illustrates global temperature RMS differences under clear and cloudy conditions for "land" and "ocean" categories. The AIRS temperature measurements from microwave (MW) only retrievals are regarded as a truth since they are in good agreement with the radiosondes (Divakarla et al. 2006). The clear/cloudy conditions are defined as the agreement of cloud fractions from both AIRS and GFS model. The GFS forecasted temperature RMS difference against the AIRS retrievals is less than 2.5 K for clear conditions over oceans whereas it shows somewhat worse RMS difference at $p < 600$ hPa under cloudy conditions. The temperature RMS difference over land is similar to that of ocean category at $p < 600$ hPa, but it becomes larger approaching the surface. One thing is noted that the temperature RMS differences under clear conditions over both oceans and land are smaller than the RMS differences computed under cloudy conditions, while the results at $p > 600$ hPa are opposite. Two plausible causes can be pointed out. Firstly, the GFS model has systematically difficulty in simulating temperature profiles in the lower troposphere. Another cause is associated with cloud contamination in AIRS retrievals. Here, we used the temperature measurements from MW only retrievals, but the accuracy of the temperature profile retrievals for AIRS usually decreases under overcast cloud scenes (Tobin et al. 2006).

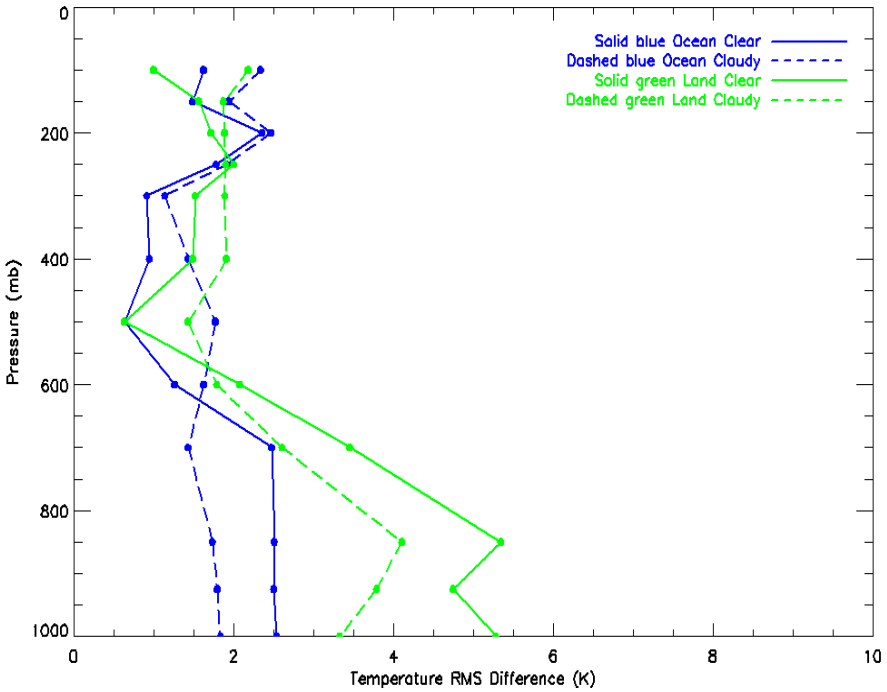

Figure 3.5. The temperature RMS difference for "land" and "ocean" categories: clear conditions over oceans, solid blue; cloudy conditions over oceans, dashed blue; clear conditions over land, solid green; cloudy conditions over land, dashed green, respectively.

Figures 3.6-8 describe comparisons of the monthly mean RH between satellite observations and the GFS model results during July 2008. All AIRS data are gridded into a 1º x 1º latitude/longitude projection, selecting only for the ascending orbits. In order to better describe RH field, RH products are analyzed into two parts; output RH with respect to liquid and with respect to ice phase, respectively. The GFS model defines a separation temperature at T > 273.15 K with respect to liquid phase and at T < 253.15 K for ice phase. Temperature for a blending phase is determined using a linear combination of the two. The AIRS data with AMSU-A retrievals have a separation temperature as 273.15 K (Rosenkranz 2006).

The GFS RH output with respect to ice at 150 hPa is substantially larger than

that retrieved from satellite. The GFS RH at 500 hPa is underestimated over the middle parts of Africa and America as well as Asia regions, but overestimated in the southern ocean as seen in Figure 3.6. Such underestimation of RH in the GFS model over those regions is found in Figure 3.7. The GFS model simulates RH output with respect to liquid phase at 500 hPa while satellite observations indicate those ones as ice phase. The combined GFS RH results (e.g., liquid and ice phase) at 150 hPa in Figure 3.8 are significantly greater than those from satellite retrievals and they are slightly overestimated at 1000 hPa, particularly over oceans in both hemispheres. These findings support some parts of a previous study, which notes that several models tend to generate too much moisture in the upper troposphere over the tropical and extra-tropical regions relative to the AIRS observations by 25 %-100 % (Pierce et al. 2006). The discrepancies between observation and model might be come from some possibilities; firstly, there can be a contamination from undetected low clouds resulting in drier conditions at $p > 800$ hPa in the AIRS observations. Secondly, the GFS model is systematically likely to overestimate RH values in the upper troposphere with respect to ice phase as well as slightly in the lower troposphere. The patterns of the RH distribution are well correlated with high–level cloud fractions, but not correlated with low-level clouds, suggesting a weak contribution of RH variable in low-level cloud formations. This cannot fully explain why the biased cloud fractions occur over the eastern tropical oceans in the GFS model.

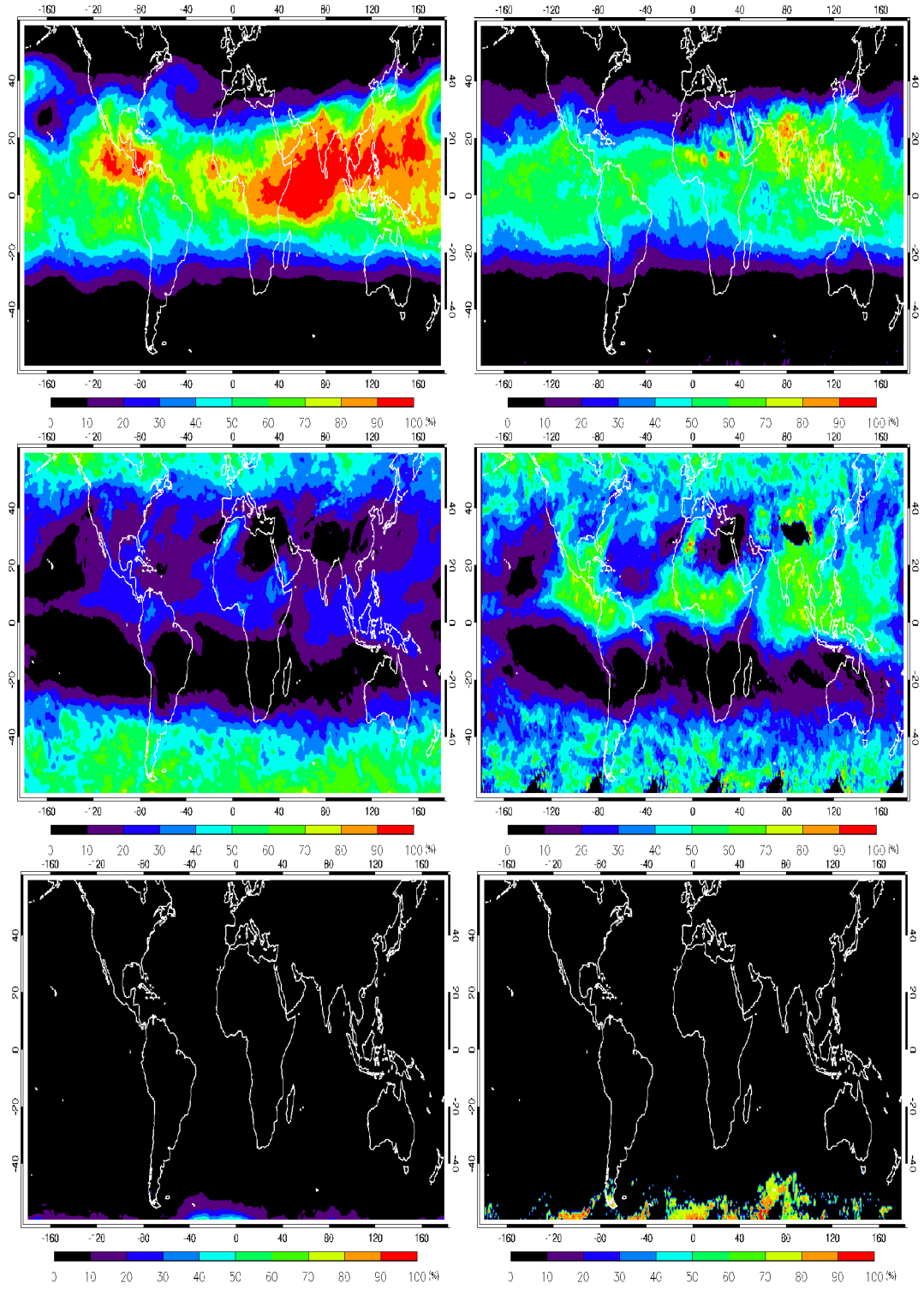

Figure 3.6. Comparisons of relative humidity with respect to ice for the AIRS retrievals (right panels) and the GFS model (left panels) at 150 hPa (upper), 500 hPa (middle), and 1000 hPa (bottom) during July 2008.

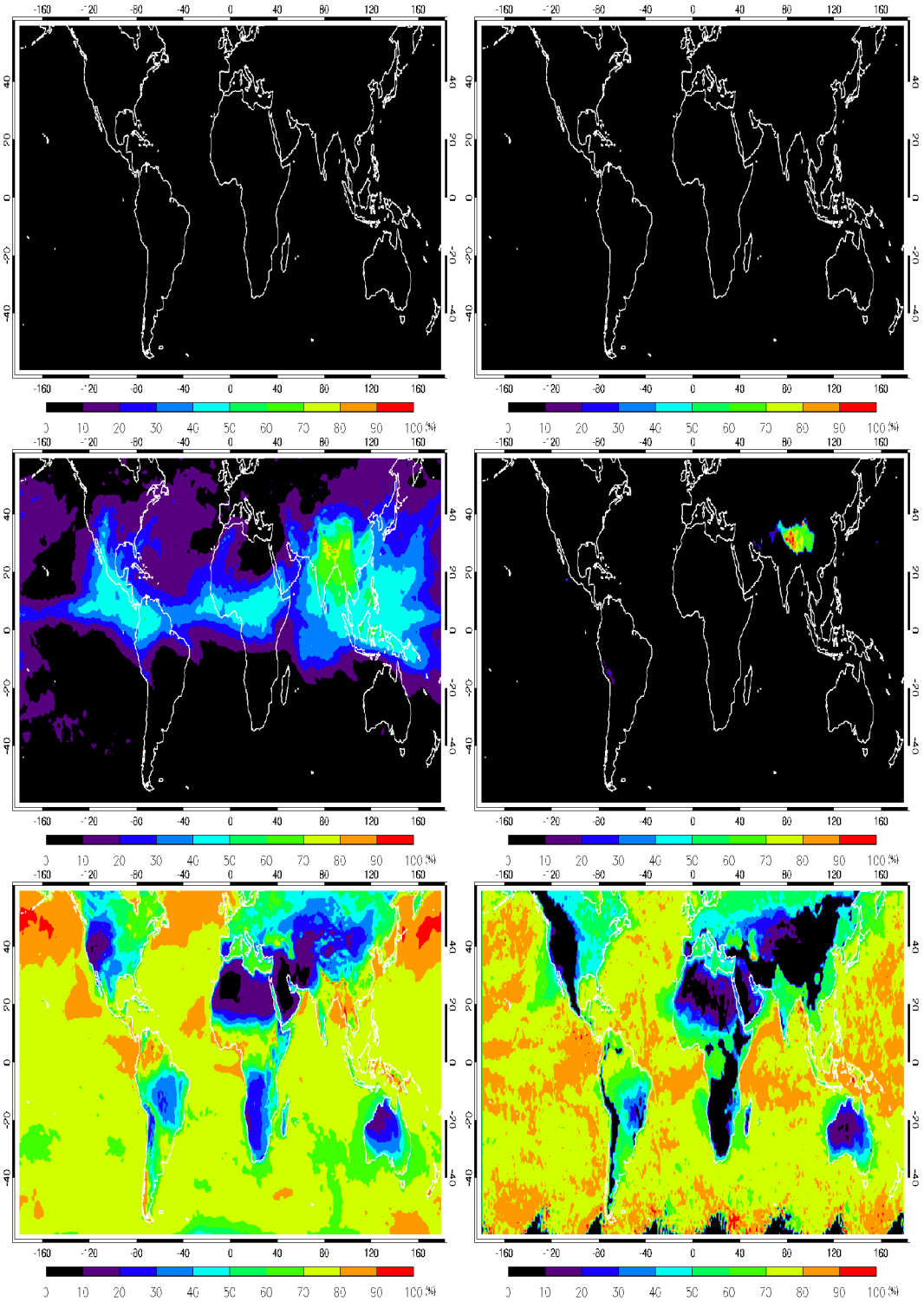

Figure 3.7. Same as in Figure 3.6 except for relative humidity with respect to liquid.

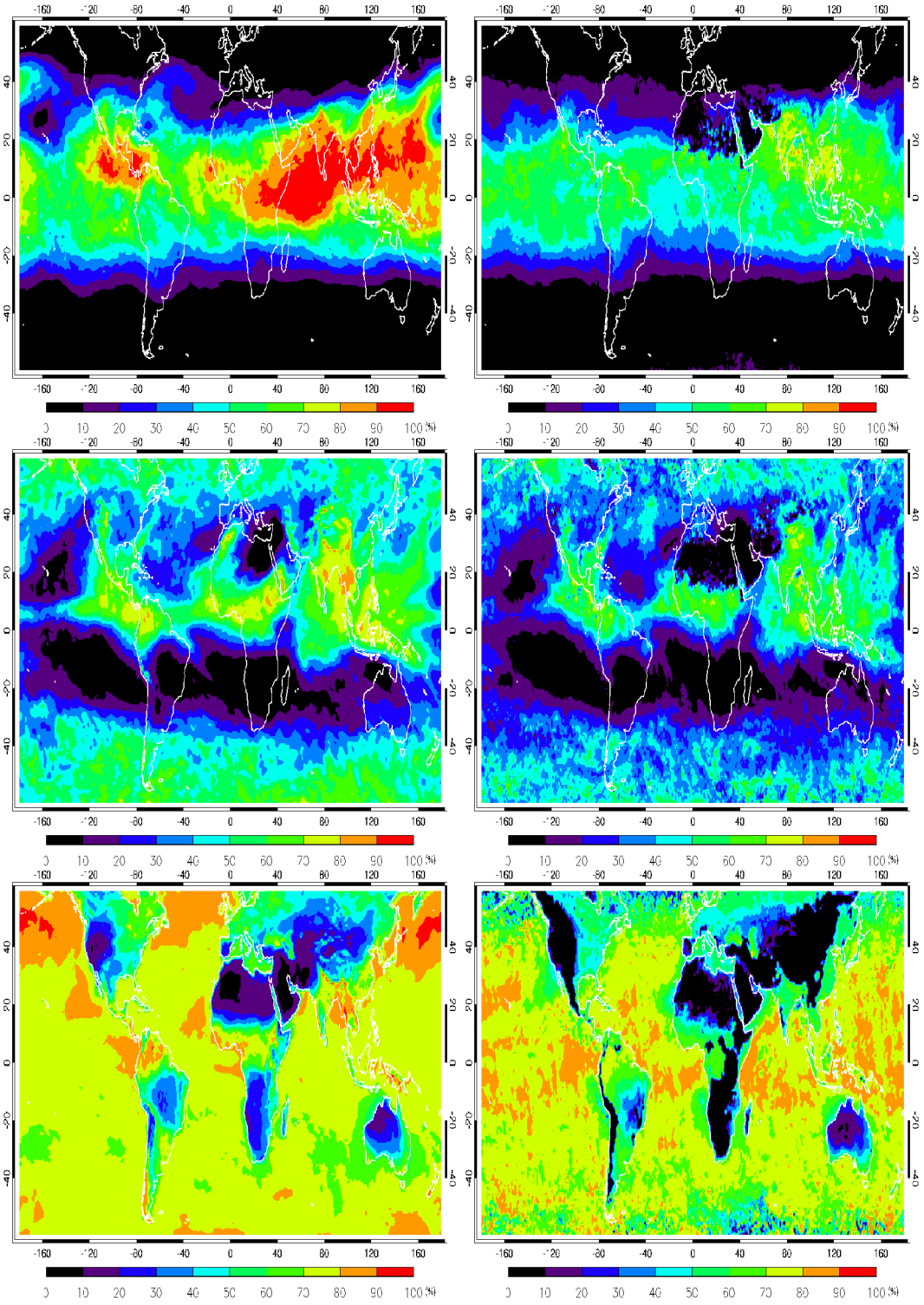

Figure 3.8. Comparisons of relative humidity field for the AIRS retrievals (right panels) and the GFS model (left panels) at 150 hPa (upper), 500 hPa (middle), and 1000 hPa (bottom) during July 2008.

3.3.3. Regional Analysis of the GFS cloud fraction, temperature, and relative humidity fields

This subsection aims to analyze whether the discrepancies in low cloud fields come from incorrect input variables or parameterization schemes used in the model. First, input variables used in cloud parameterization scheme are examined for a global scale by comparing satellite retrievals. Similar evaluation is conducted over the selected regions as mentioned in the previous section by adding ground-based measurements. Figure 3.9 presents a comparison of zonal mean low cloud fractions derived from both satellite retrievals and the GFS model over each region. Note that two satellite results are generated from the application of different algorithms to the same MODIS data. The low cloud fraction derived from the C-L algorithm is much greater than that retrieved from the MODIS algorithm in all regions as a result of the recovery of a large quantity of low clouds beneath high clouds. This comparison illustrates how the same satellite data might result in considerable discrepancies in low-level cloud detection depending on which algorithm was used in cloud retrievals. Another satellite result in Fig. 3.9 is retrieved from the C-C satellites. It mostly lies between the results of the C-L algorithm and the MODIS products but it is more similar with the retrievals of the C-L algorithm. The low cloud fraction simulated by the GFS model is substantially smaller than three satellite retrievals over all regions. These results are consistent with those from a previous study, which reported that the Xu and Randall cloud parameterization scheme underestimated cloud fractions when compared to observations from the Atlantic Stratocumulus Transition Experiment (ASTEX) (Lazarus et al. 1999).

The GFS model temperature and RH profiles over the selected four regions are compared with AIRS retrievals at different vertical levels. Figure 3.10 displays the zonally averaged temperature profiles from both AIRS observations (using the AIRS MW only algorithm) and the GFS model. Except at 1000 hPa and 925 hPa in the Californian region, the agreement is remarkable. Figure 3.11 shows the latitudinal variations of zonal-mean RH corresponding to four vertical levels in the atmosphere. The agreement between profiles from the GFS model and observations is generally worse than that for temperature. The GFS model overestimates RH values (especially at 850 hPa) in most cases with differences up to 100 % of the satellite estimates in the four regions. This suggests that the vertical mixing of heat and moisture in the GFS model does not describe the realistic moisture accumulation in cloud layers, especially in marine stratocumulus cloud decks. Although the RH values simulated by the GFS model are mostly larger than the satellite retrievals, simulated cloud fractions are severely underestimated over the four regions. Other possible causes of this bias might reside in the choice of coefficients in the Eq. 2.1 or in an unrealistic simulation of vertical diffusion in marine stratocumulus cloud regimes.

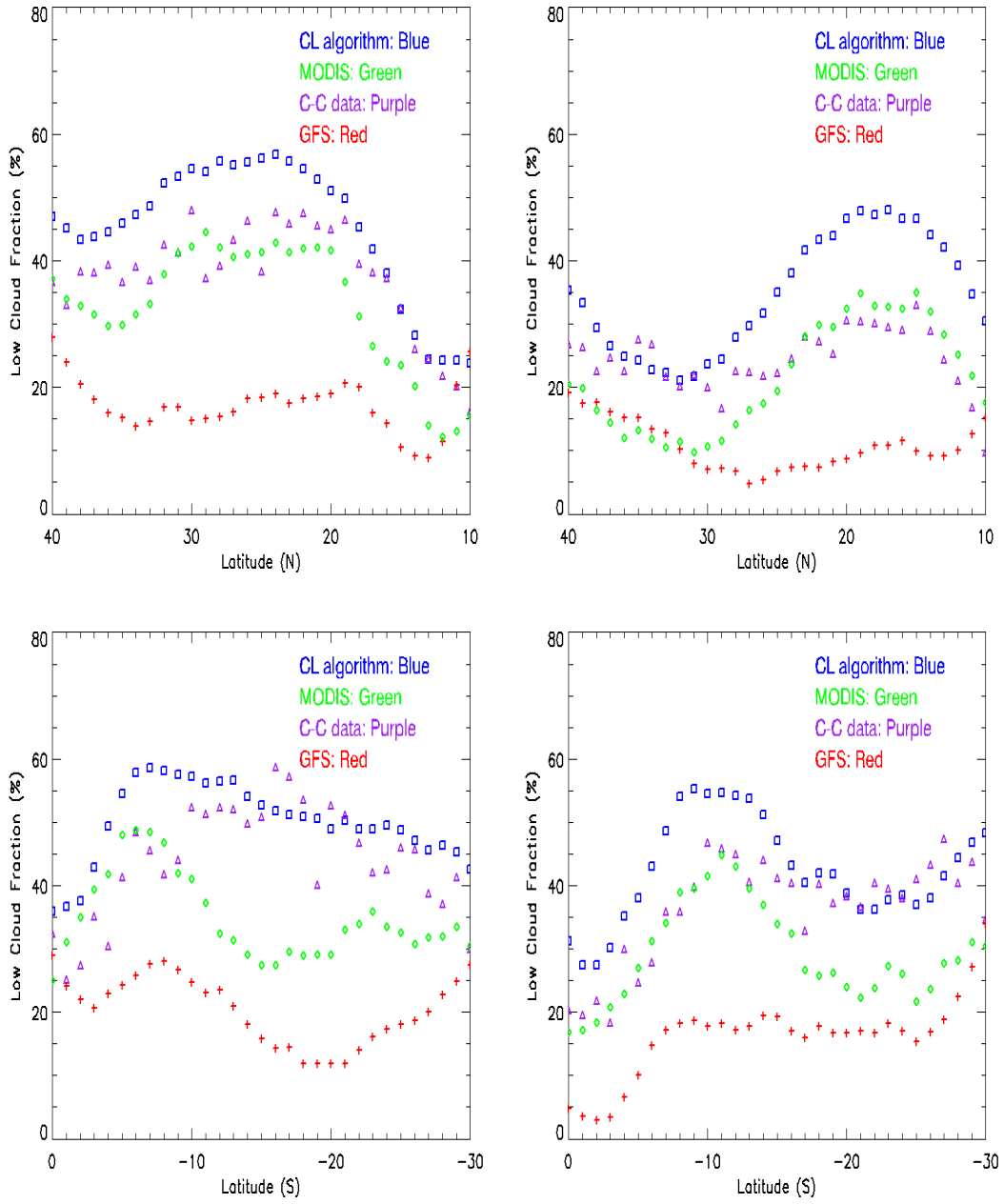

Figure 3.9. Comparisons of the zonal-mean low cloud fractions derived from sa tellite observations and the GFS model for (clockwise, starting from the upper left plot) Californian, Canarian, Namibian, and Peruvian regions during July 2008. The blue square symbols, the green diamond symbols, the purple triangle symbols, and the red plus symbols represent the CL algorithm, the MODIS algorithm, the C-C data, and the GFS simulations, respectively.

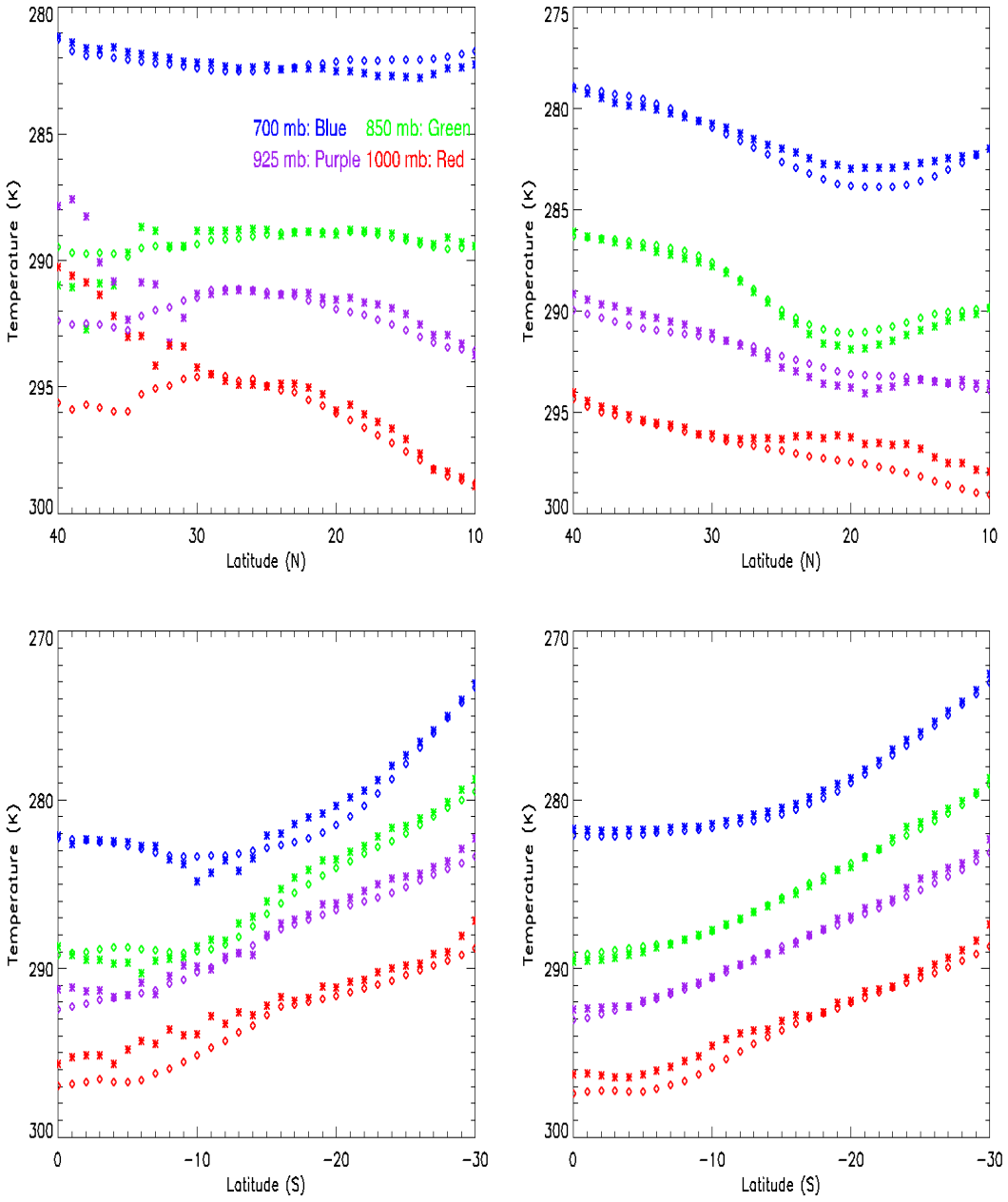

Figure 3.10. Comparisons of zonal-mean temperature profiles derived from AIRS observations (asterisk symbols) and the GFS model (diamond symbols) for the four regions during July 2008. The blue, green, purple, and red colors represent results at 700 hPa, 850 hPa, 925 hPa, and 1000 hPa, respectively.

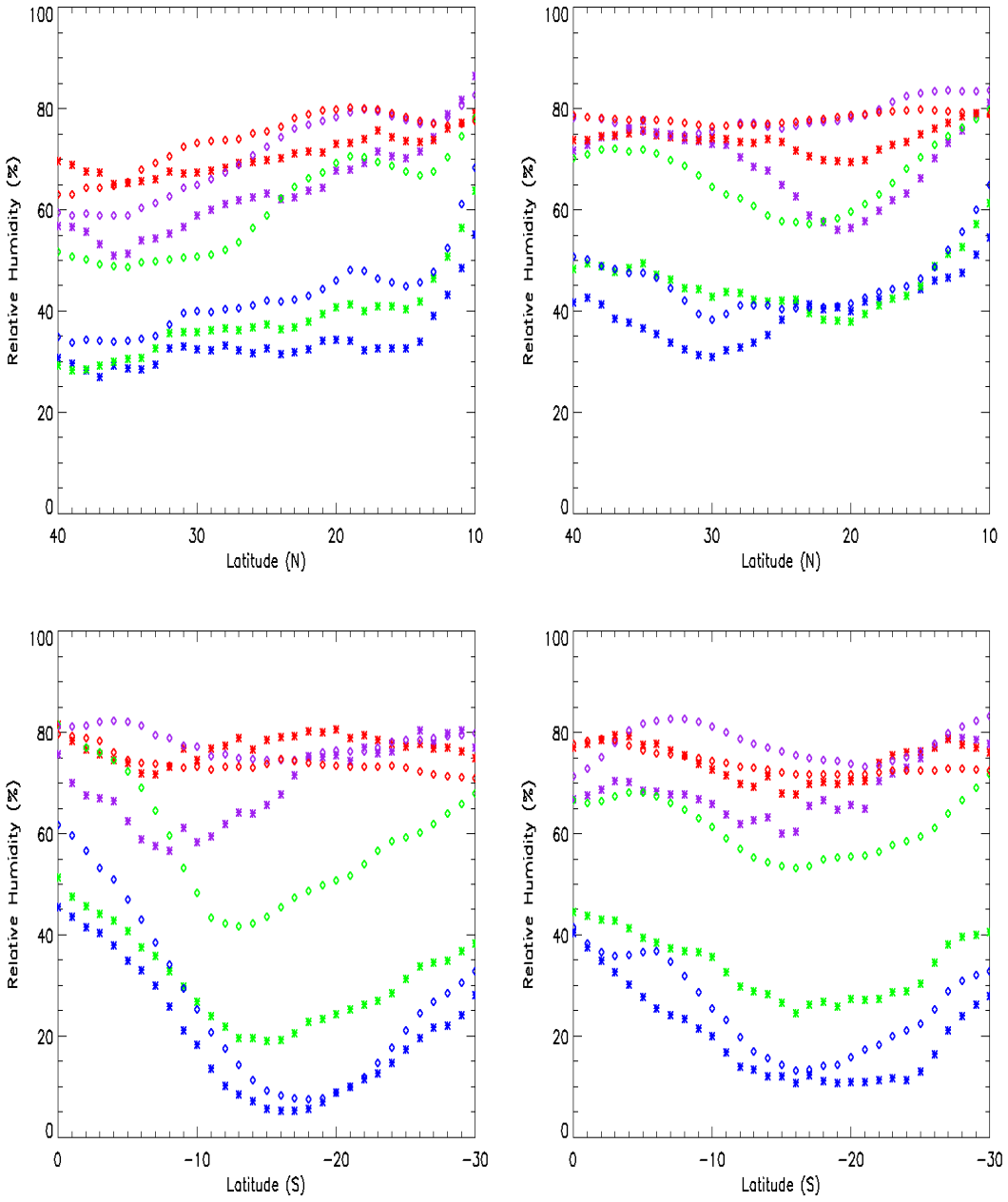

Figure 3.11. Same as Figure 3.10 except for relative humidity profiles.

3.3.4. Comparison of temperature and relative humidity profiles with ground-based measurements

Satellite measurements provide useful atmospheric information on a global scale and are generally more reliable than model simulations, but they also have shortcomings such as retrieval uncertainties and limitations. Therefore, a comparison with ground-based measurements is also needed. Since there are temporal and spatial differences between satellite measurements and surface-based observations, a careful approach is required. We only deal with a small area (i.e., a 1°x1° grid box) centered on the SGP site and determine the specific time scales that can be represented by the satellite overpass time. Figure 3.12 shows RH and temperature biases of the model and the satellite retrievals at the SGP site. The AERI measurement is taken as a reference and differences are calculated as the AERI data minus individual products. In general, the satellite-derived RH values have a better agreement with the ground-based measurements than those of the GFS model. The AIRS measurements have a RH bias within 10 % at all vertical levels, while the GFS-generated RH has a significant negative bias both in the upper and lower troposphere. This reinforces the finding of a wet bias in the modeled RH field, as noted in a comparison with satellite data (cf. Section 3.3.2-3). With respect to temperature, both AIRS and GFS profiles have a positive bias in the upper troposphere and smaller biases in the middle troposphere. However, these biases grow large and negative closer to the surface in a similar way (see Figure 3.12).

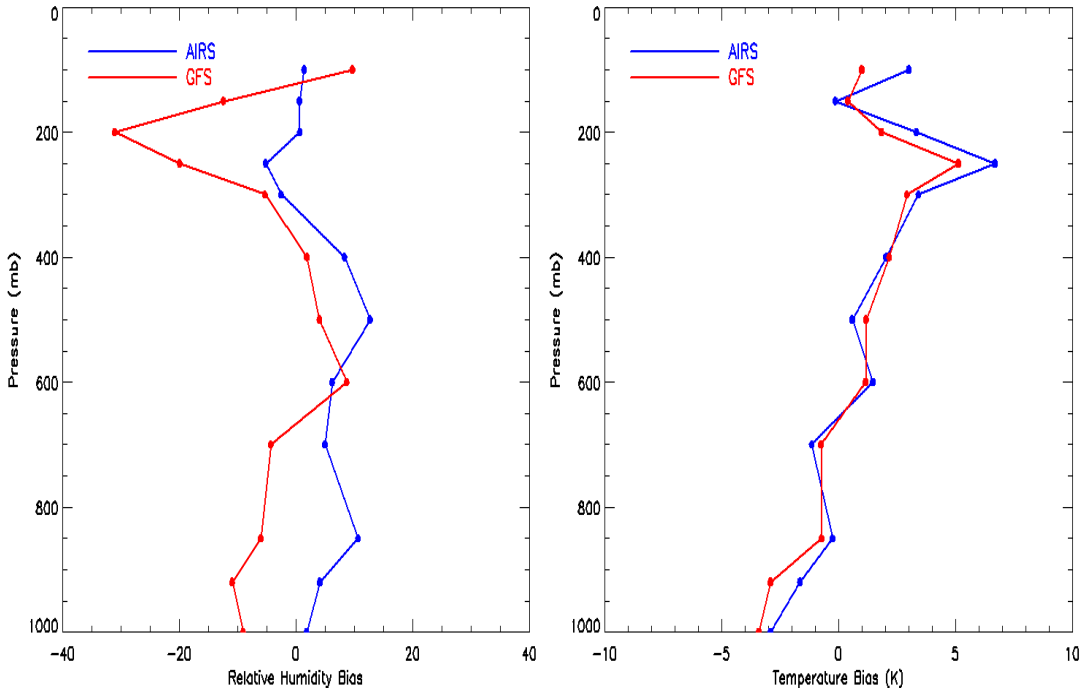

Figure 3.12. Relative humidity (left panel) and temperature (right panel) biases during July 2008: AERI versus AIRS, blue line; AERI versus GFS, red line.

Although the GFS model output has a relatively coarse spatial resolution compared with satellite observations, it shows a reasonable agreement with ground-based measurements. This may be due to the use of global radiosondes information in the model analysis data (Divakarla et al. 2006).

Left plot in Figure 3.13 shows comparisons of three different cloud fraction products: the GFS original output, the GFS cloud product with AERI measurements as input, and combined millimeter wavelength cloud radar (MMCR)-micropulse lidar (MPL) observations. The MMCR generates continuous cloud profiles from radar reflectivity and the MPL is sensitive to optically thin clouds so combined radar-lidar measurements are a suitable tool to estimate cloud fraction (Xi et al.

2010). The GFS model largely underestimates low cloud fraction against the result of the combined measurements at the SGP site and this finding is consistent with a previous study (Yang et al. 2006). The GFS cloud product using AERI temperature and RH measurements is generated to examine the soundness of the 2008 version of the GFS model cloud parameterization scheme. Cloud fractions generated by the GFS model using AERI measurements as input are smaller than those generated by the original GFS model because observed RH values are generally less than simulated RH values. The results from both did not show an improvement on formulating more realistic low clouds. It is worth noting that condensed water vapor was not adequately generated near the surface even though the GFS model slightly overestimated the absolute amount of water vapor in the lower troposphere (see right plot in Figure 3.13). This means that the cloud mixing ratio as a primary predictor of cloudiness is not well represented near the surface in the 2008 version of the GFS model cloud parameterization scheme. Such problem is attributed to the shallow convection scheme which uses an unrealistic turbulent diffusion and to planetary boundary layer scheme which is optimized to dry boundary layers. Especially, the shallow convective scheme makes cloud condensate water vapor to be destroyed by increasing vertical diffusion in the cloud layers. The combined effects of the improper schemes on cloud simulations result in a systematic underestimation of low clouds (Han and Pan 2011). Therefore, the parameterization scheme rather than GFS input variables seems to primarily contribute to discrepancies found in cloud fields. Consideration of other processes is required in order to fully describe and understand physical processes taking place in modeled cloud systems.

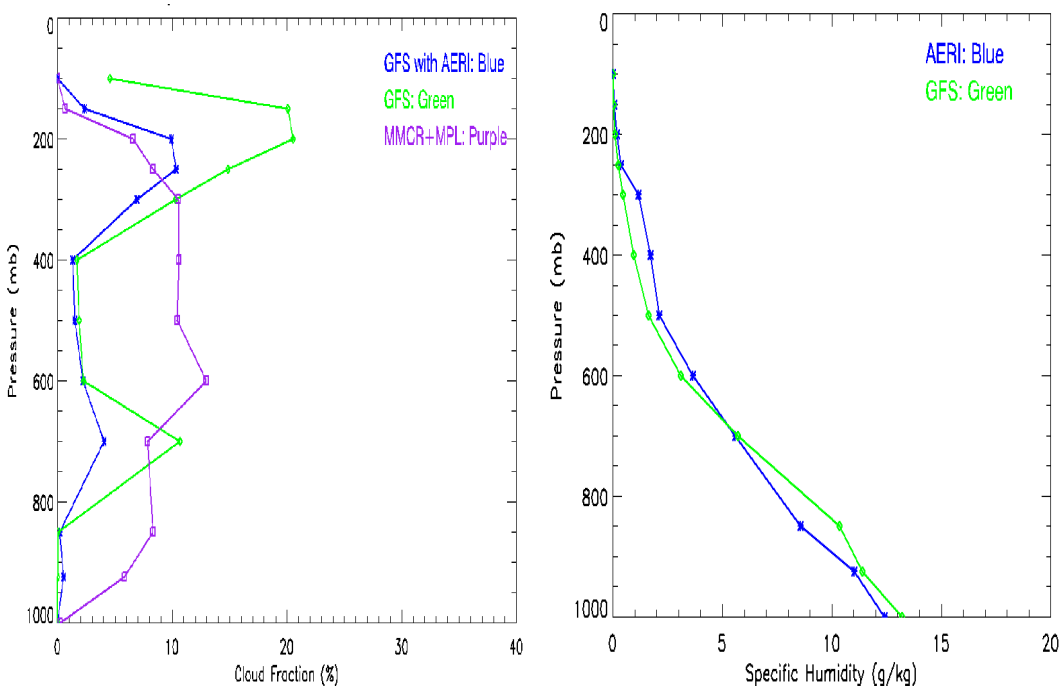

Figure 3.13. Left panel: Comparison of cloud fractions at the SGP site from three different products-the GFS original output (green line), the GFS cloud product using AERI measurements as input (blue line), and the combined radar-lidar product (purple line). Right panel: Comparison of specific humidity from AERI (blue line) and the GFS model (green line) at the SGP site.

3.4. Application of Other Cloud Parameterization Scheme to the GFS model

3.4.1. Introduction

In previous Chapters 2-3.3, we address the problem of representing cloud fields in the GFS model. Model-generated cloud fields are diagnostically represented by connecting with atmospheric properties such as relative humidity and cloud water mixing ratio. This diagnostic cloud scheme is simple and successful in reproducing the gross features of global cloudiness but it has a limitation to generate stratocumulus clouds, in particular, over the eastern Pacific and Atlantic Oceans.

The cloud water mixing ratio of the GFS model is a primary predictor of cloud fraction. Such variable is determined by three-dimensional advection, convective processes through cloud-top detrainment, grid-scale condensation, the rate of conversion of cloud mixing ratio to precipitation, the evaporation rate of cloud condensate, and the horizontal and vertical diffusion. Thus, the cloud parameterization scheme of the GFS model strongly depends on how well other parts of the model can simulate cloud water mixing ratios. However, this variable is not adequately represented in the lower atmosphere, particularly in regions where marine stratocumulus clouds are common. This finding indicates that significant changes to the convection and vertical diffusion schemes in the GFS cloud scheme are necessary in order to simulate more realistic cloudiness in low-level clouds.

This section introduces two diagnostic cloud parameterization schemes: a cloud prediction scheme for the ECMWF model (Slingo 1987) and a modification of Slingo (1987) (Gordon 1992). Gordon (1992) implemented the modified version of

Slingo (1987) into the Geophysical Fluid Dynamics Laboratory (GFDL)-EP (where EP denotes experimental prediction) spectral atmospheric general circulation model (AGCM). The method used in the GFDL-EP AGCM closely resembles the study of Slingo (1987) but it is evolved from that one by modifying the power law relationship between relative humidity and threshold relative humidity and by modifying the parameterization of marine stratocumulus clouds. The scheme implemented by Gordon (1992) was an earlier version of the GFDL AGCM and a variant of the cloud scheme of Tiedtke (1993) was incorporated for predicting cloud liquid water and fraction. Currently, the GFDL AGCM operates the new cloud scheme which includes an addition of the air mass-based droplet number concentration as a third prognostic variable as well as the treatment of the prognostic variables such as cloud liquid water and fraction (Ming et al. 2005; Ming et al. 2007).

The Gordon (1992) scheme consists of three components, i.e., (i) the diagnostic cloud fraction; (ii) the treatment of cloud optical depth; and (iii) anchoring of the cloud radiative properties to the cloud optical depth. It has its roots in an empirical scheme of Slingo (1987), but some details of the two schemes are different. Relative humidity in both schemes is still a primary predictor but auxiliary predictors such as vertical motion, lapse rate, static stability, and convective activity are added. Major differences are briefly summarized between Gordon (1992) and Slingo (1987) as follows: 1) in the Gordon, high, middle, and low cloud fraction vary linearly instead of quadratically; 2) a value of threshold relative humidity is reduced from 0.8 to 0.7; 3) shallow convective cloud amount is computed separately.

An approach conducted in this section is based on the method used in the GFDL-EP model and is hereafter referred to as the SG scheme. The SG scheme does not exactly follow either Slingo (1987) or Gordon (1992), rather this employs some of cloud respects from both. Most of the equations for computing cloud fraction in the SG scheme are based upon the empirical equations of Slingo (1987) and Gordon (1992).

The SG scheme is similar to the GFS cloud parameterization scheme in that cloudiness is determined by an empirical formulation, but a link with convective activity is also included. The areal cloud fraction in the SG scheme depends more on thermodynamical and dynamical model variables. This part carries out an application of the SG cloud scheme to the GFS model and figures out whether the SG scheme can overcome the shortcomings of the current cloud parameterization scheme used in the GFS model.

3.4.2. Description of the SG Cloud Parameterization Scheme

The height criterion of high, middle, and low clouds can vary with latitudes and seasons in reality but we use a fixed boundary of high clouds with having pressure (p) less than 350 hPa. Relative humidity is the sole predictor of cloud fraction for high and middle clouds and the primary predictor for low clouds. The optimal relative humidity-cloud fraction relationship and a default value of relative

humidity are sensitive to the cumulus parameterization scheme (Gordon 1992). A value of relative humidity threshold (hereafter referred to as RHc) and a linear relationship worked well as 70 % in Gordon (1992). In contrast, a quadratic relationship and the value of 80 % are better suited to the relaxed Arakawa-Schubert (RAS) cumulus parameterization employed in the GFDL-EP model because RAS generates a moister troposphere than that produced by Gordon (1992). Therefore, the default coefficients for RHc in the SG scheme are 80 % and 84 % for p < 750 hPa and p ≥ 750 hPa, respectively.

The high cloud fraction, Nh, is given by

$$\mathrm{Nh} = \begin{bmatrix} 0.0 \\ (RH - RHc)^2 / (1.0 - RHc)^2 \\ 1.0 \end{bmatrix}, \qquad \text{if} \begin{bmatrix} RH < RHc \\ RHc \le RH \le 1.0 \\ RH > 1.0 \end{bmatrix}. \qquad (3.1)$$

Anvil and super anvil cirrus clouds are treated the same as other high clouds in terms of cloud fraction in the SG scheme. This approach was also used in the cloud scheme of Gordon (1992), which recognizes anvil and super anvil cirrus clouds as special categories of high clouds only in terms of cloud optical properties.

Similarly, the middle cloud fraction, Nm, is given by

$$\mathrm{Nm} = \begin{bmatrix} 0.0 \\ (RHe - RHc)^2 / (1.0 - RHc)^2 \\ 1.0 \end{bmatrix}, \qquad \text{if} \begin{bmatrix} RHe < RHc \\ RHc \le RHe \le 1.0 \\ RHe > 1.0 \end{bmatrix}, \qquad (3.2)$$

where RHe is defined as RH*(1.0 – N_{cnv}) and N_{cnv} is the convective cloud fraction which is provided by the GFS model. RHe is scaled after adjusting for the convective cloud amount.

Unlike other cloud parameterizations including probability distribution functions (PDFs), the cloud fraction calculation of Xu and Randall (1996) depends only on the relative humidity, the saturation specific humidity, and the cloud mixing ratios. Note that cloud fraction of the Xu and Randall (1996) is determined by one equation whereas the SG cloud scheme has different equations in calculating cloud fraction for different types of low clouds. Low clouds in the SG scheme are broken down into three types: synoptic subclass of low stratiform clouds, marine stratocumulus clouds, and shallow convective clouds. Cloud fraction for synoptic subclass of low stratiform clouds is expressed as a product of two linear functions:

$$\mathrm{Nsl} = \mathrm{A(RHe)} * \mathrm{B}(\omega), \tag{3.3}$$

where the A and B functions depend only on the environmental relative humidity (RHe) and pressure vertical velocity (ω), respectively. Specifically,

$$\mathrm{A(RHe)} = \begin{bmatrix} 0.0 \\ (RHe - RHc)^2 / (1.0 - RHc)^2 \\ 1.0 \end{bmatrix}, \text{ if } \begin{bmatrix} RHe < RHc \\ RHc \le RHe \le 1.0 \\ RHe > 1.0 \end{bmatrix}, \tag{3.4}$$

As mentioned earlier, the default coefficients for RHc are 0.80, 0.84 for p < 750 hPa

and p ≥ 750 hPa, where p is the pressure. The other linear function is expressed as

$$B(\omega) = \begin{bmatrix} 1 \\ (\omega - \omega_0)/(\omega_1 - \omega_0) \\ 0 \end{bmatrix}, \quad \text{if} \begin{bmatrix} \omega < \omega_1 \\ \omega_1 \le \omega \le \omega_0 \\ \omega > \omega_0 \end{bmatrix}, \tag{3.5}$$

where $\omega_1 = 0$ and $\omega_0 = 3.6$ hPa/h (Slingo 1987). Synoptic subclass of low stratiform clouds are generated by strong vertical ascent in the atmosphere and are dissipated when there is strong vertical descent.

The parameterization of marine stratocumulus and stratus clouds in the SG scheme resembles the formulation of Gordon (1992) and Slingo (1987). This scheme showed an improved performance associated with simulations of subtropical marine stratocumulus clouds. Note that RH in Eq. (3.6) is the relative humidity at the base of the highest contiguous inversion layer. Existence of a low-level inversion is ignored in the GFS model, however, consideration of the low level inversion contributes to enhance generation of stratocumulus clouds in the Southeast Pacific region by eliminating background diffusion (Sun et al. 2010). Similarly, the marine stratocumulus cloud parameterization is a product of two functions:

$$\text{Nmcl} = S\left(-\frac{\partial\theta}{\partial p}\right) * B(\text{RH}), \tag{3.6}$$

where θ is the potential temperature and $\partial\theta/\partial p$ is the lapse rate (K/hPa). The first

term in the product on the right-hand side of the equation is defined as

$$S\left(-\frac{\partial\theta}{\partial p}\right)=\begin{bmatrix}1.0\\ \alpha\left(-\frac{\partial\theta}{\partial p}\right)+\beta\\ 0.0\end{bmatrix},\qquad \text{if}\begin{bmatrix}\left(-\frac{\partial\theta}{\partial p}\right)>0.10\\ 0.05\le\left(-\frac{\partial\theta}{\partial p}\right)\le 0.10\\ \left(-\frac{\partial\theta}{\partial p}\right)<0.05\end{bmatrix}, \tag{3.7}$$

where α is 20 hPa/K and β is -1.0. The stratification criteria for marine stratocumulus clouds in the SG scheme is less stringent than that in the study of Gordon (1992), where α is 6.67 hPa/K and β is -0.667. The second term in the product on the right-hand side of Eq. (3.6) is expressed as

$$B(RH)=\begin{bmatrix}1\\ (RH-RH_{\min})/(RH_{\max}-RH_{\min})\\ 0\end{bmatrix},\ \text{if}\begin{bmatrix}RH>RH_{\max}\\ RH_{\min}\le RH\le RH_{\max}\\ RH<RH_{\min}\end{bmatrix}, \tag{3.8}$$

where the default values for RH_{min} and RH_{max} are 0.60 and 0.80, respectively (Gordon 1992).

For shallow convective clouds, Nshl, the following equation is applied.

$$\text{Nshl} = 0.2*A_{max}(\text{RHe}). \tag{3.9}$$

The A function is from Eq. (3.3) and A_{max}(RHe) is the maximum value of RHe.

In summary, the low cloud fraction is determined by applying the maximum overlapping assumption,

$$Nlow = Max[Nsl, Nmcl, Nshl]. \quad (3.10)$$

It is worth pointing out that all GFS results are generated using the GFS model's original atmospheric fields rather than running the GFS model with the SG cloud scheme.

3.4.3. Results

3.4.3.1. Application of the SG scheme to the GFS model

Figures 3.14-15 show how the three cloud fraction products (the product generated from the C-L algorithm, the original GFS cloud fraction product, and the product generated from the application of the SG cloud parameterization scheme to the GFS model) compare. In general, the newly generated GFS cloud fractions at different vertical levels are much more comparable with those retrieved by the C-L algorithm. In particular, a comparison of the low cloud fraction is remarkable. For high clouds during January 2007, the original GFS cloud product shows a severe overestimation of high cloud fraction over the eastern Pacific, South America, South Africa, and large-scale clouds associated with convection over the Tropics. However,

the high cloud fraction calculated from the SG scheme is quite similar with the magnitude of that retrieved by the C-L algorithm. Such results are also seen in middle-level clouds. The newly generated GFS cloud products have less cloud amounts when compared to the original GFS products for both high and middle clouds. The most significant improvement in cloud fraction fields occurs in low-level clouds. The original GFS cloud simulations tend to miss marine stratocumulus cloud regimes over the subtropical oceans, especially along the west coast of North America, South America, and southern Africa (see Section 2.4.3). Misrepresentation of such marine stratocumulus clouds made large discrepancies with observations in low-level clouds. A systematic underestimation of stratocumulus clouds is one of the long existing problems in the GFS model. Now, the SG scheme generates such clouds well and produces the reasonable magnitudes of cloud fraction. The global distribution patterns of clouds in the new GFS cloud products show a better agreement and the magnitudes of cloud fraction at all levels are matched well with satellite retrievals. These results are also found during July.

It is worthy to note that cloud fractions using the SG scheme are calculated based on a coarser resolution than those simulated by the original GFS scheme. In other words, cloud fractions from the original GFS scheme are obtained from 64 vertical layers whereas the new GFS cloud products are calculated from 21 vertical levels. Also, two products have a different cloud overlapping assumption. A maximum-random overlap is assumed in the original GFS scheme, but a maximum overlap assumption is used in the SG scheme.

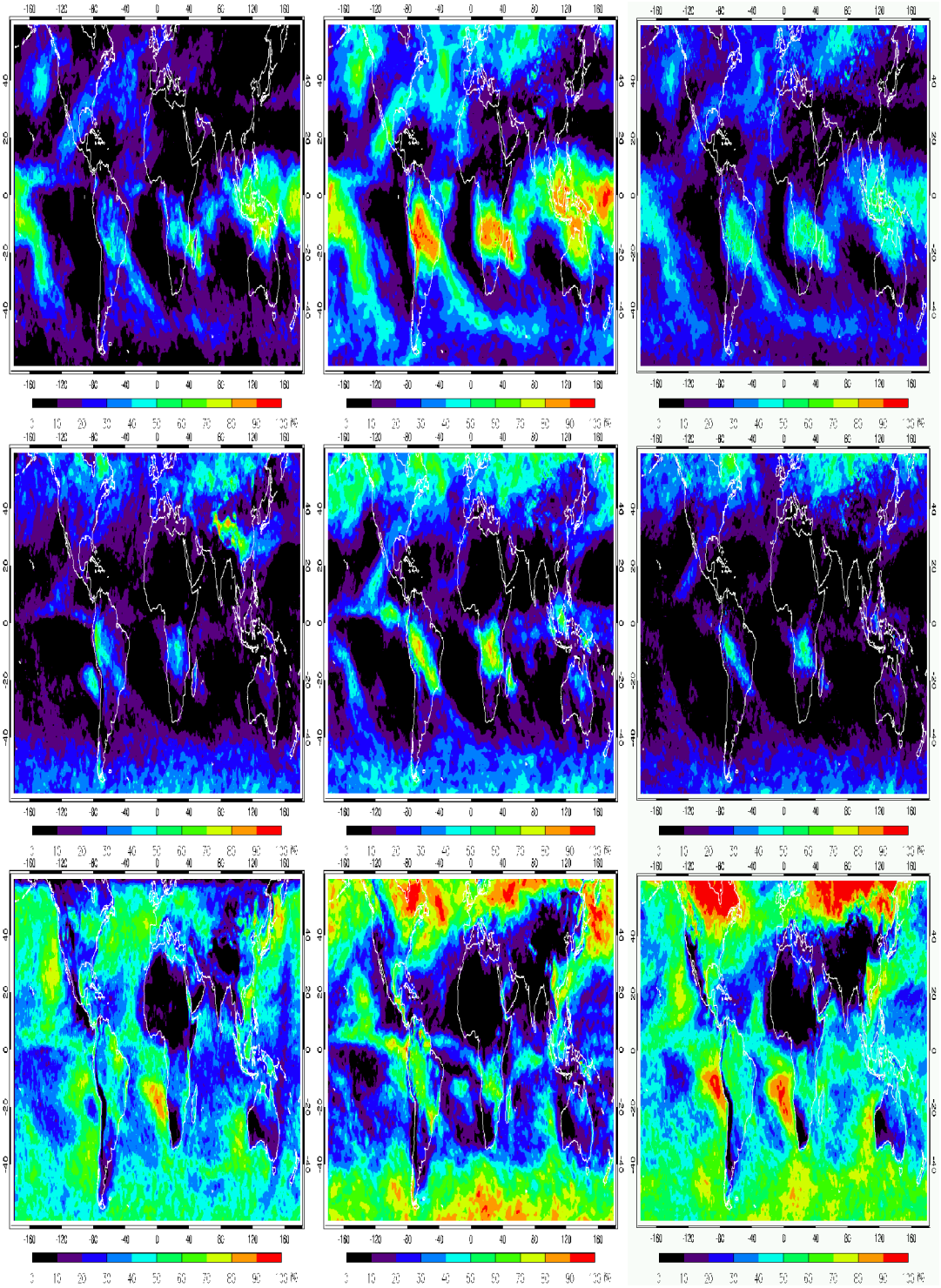

Figure 3.14. Geographic distributions of monthly mean cloud fractions from the C-L algorithm (left panels), the original GFS product (middle panels), and the results using the SG scheme (right panels) in January 2007. Top, middle, and bottom plots denote high, middle, and low clouds, respectively.

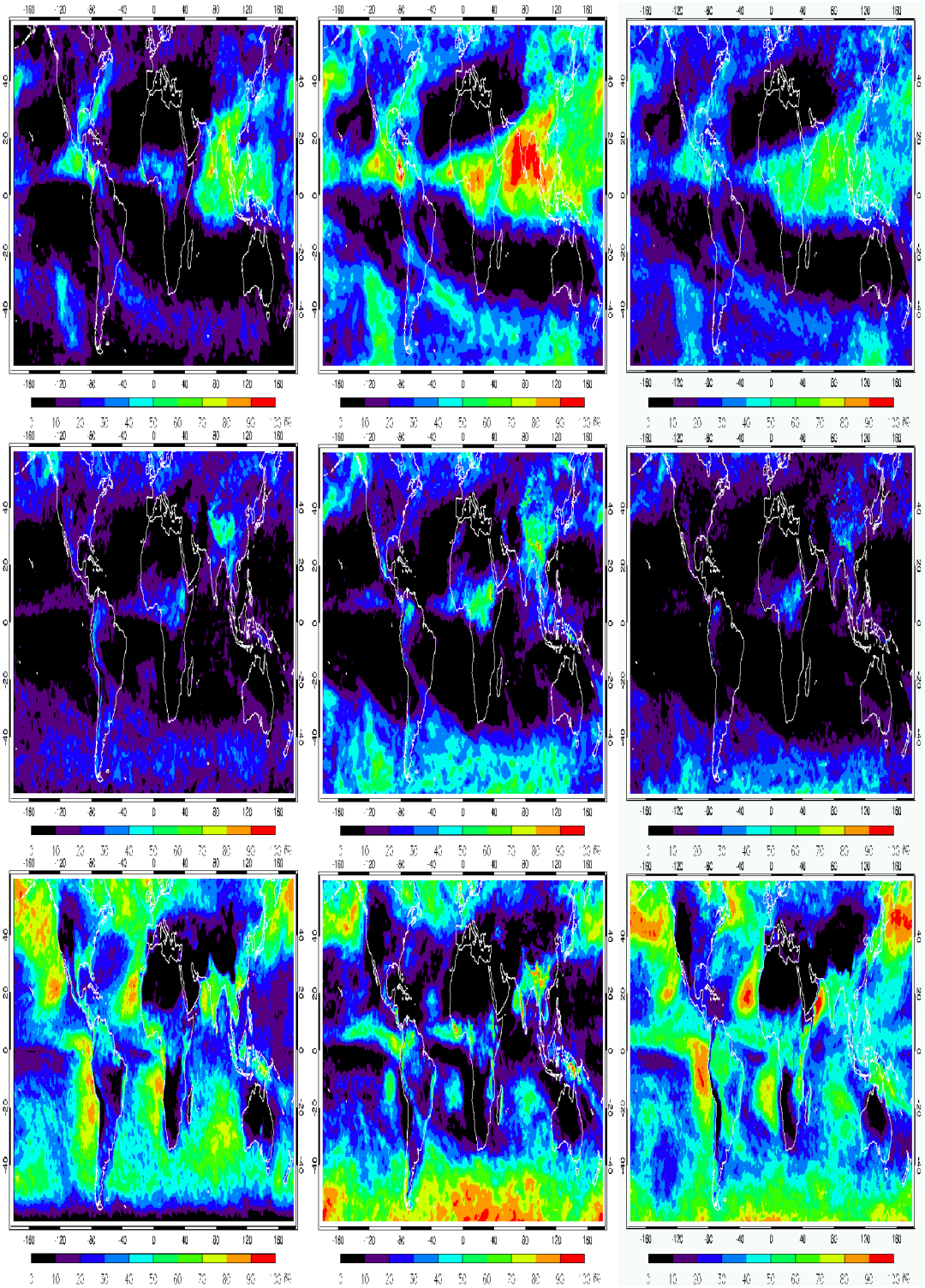

Figure 3.15. Same as Figure 3.14 except for July 2007.

Figure 3.16 compares three cloud fraction products at different vertical levels during January and July 2007. The products include the satellite retrievals based on the C-L algorithm (CL), the original GFS cloud products (GFS), and the product generated from the application of the SG cloud scheme to the GFS model (GFS_new). To better examine the global distribution patterns of clouds, all clouds are separated into ocean and land category. The CL, GFS, and GFS_new results are represented for blue, orange, and red color bars, respectively. Top (bottom) panels display a monthly mean cloud fraction from three different products during January (July) 2007.

Clearly, high cloud fractions of the original GFS products are significantly overestimated over both ocean and land while the GFS_new products have about 8% less than the original values. However, the two modeled high cloud fractions are still more than the observation. The global mean value of middle-level cloud fraction from the CL lies between the GFS and the GFS_new results over both ocean and land. The GFS model simulates too much middle-level cloud fractions, but the SG scheme produces less them. Low cloud fractions from the GFS_new are generated more than the GFS as a result of the recovery of a large quantity of marine stratocumulus clouds. Note that the low cloud fractions from the GFS_new are overestimated over both ocean and land during January, but they are comparable with the CL results during July. Possible causes may stem from a set of α or β values determining a transition point in Eq. 3.7 or from inaccurate pressure vertical velocity information. Presumably, it implies that the same value cannot be used for both

January and July. Further studies are needed to verify the reasons why low cloud fractions from the GFS_new during January are more generated than during July.

At the moment, based on the results outlined above only, one cannot say that where major flaws exist in cloud simulations of the GFS model from either cloud parameterization scheme or cloud overlapping assumption. However, it is learned that the SG cloud scheme can help form stratocumulus clouds which are destroyed by the original GFS cloud scheme. Consistent with the improvement in such stratocumulus clouds over the eastern tropical oceans, the global cloud fraction distributions at different vertical levels and reasonable magnitudes of cloud fraction are also improved with the SG cloud scheme.

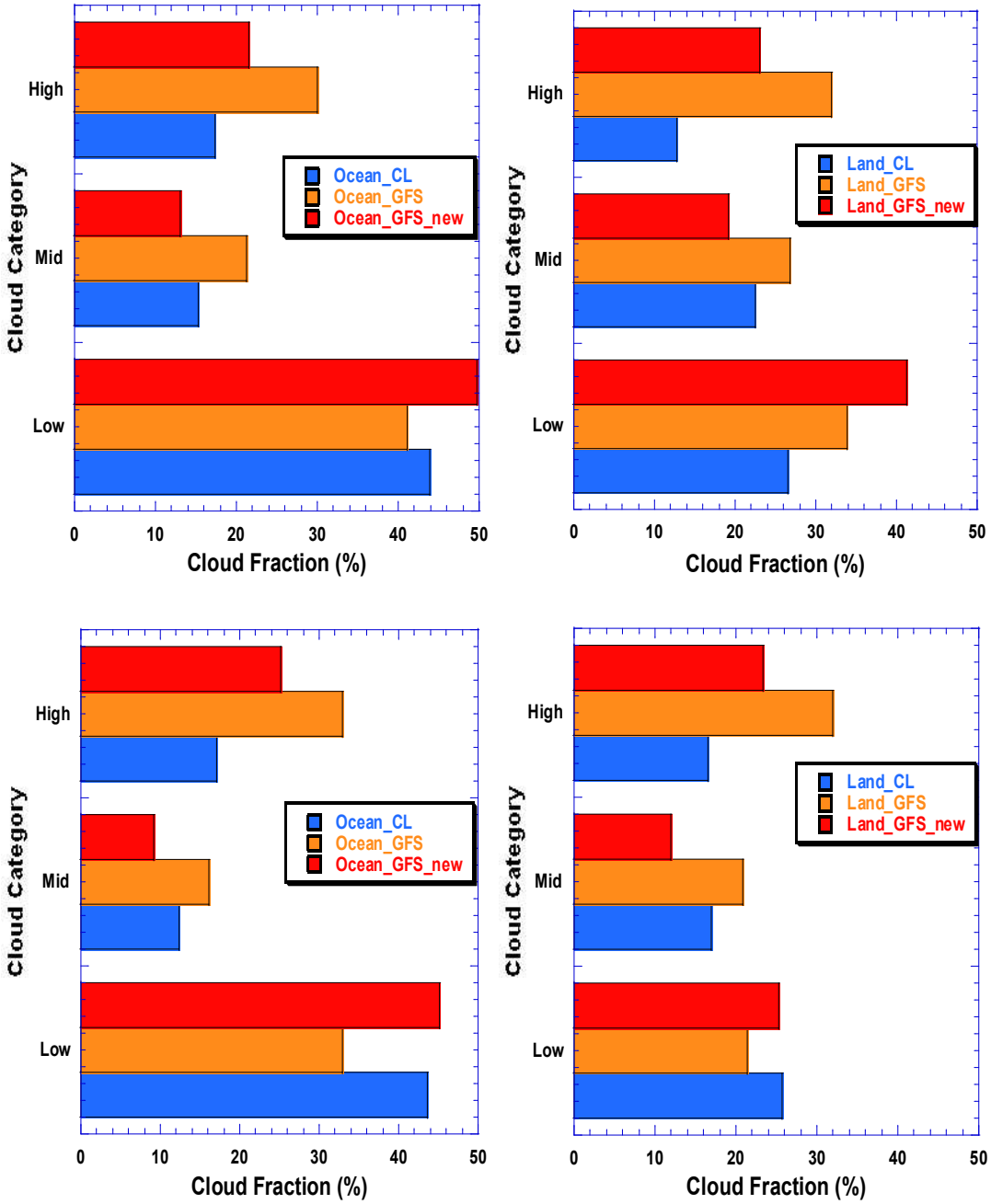

Figure 3.16. Comparisons of monthly mean cloud fraction from three different products: the C-L algorithm (CL), the original GFS cloud products (GFS), and the SG cloud products applied to the GFS model (GFS_new) over both ocean and land. The blue, orange, and red colors represent for the CL, the GFS, and the GFS_new results. Top (bottom) panels show the results during January (July) 2007.

3.4.3.2. Regional Analysis of the GFS cloud fraction calculated from the SG scheme

Figure 3.17 shows latitudinal variations of zonal-mean low cloud fraction from the three different products over the selected four regions as defined in the previous section. The global mean low cloud fraction during July 2008 increased from 31.57 % (the original GFS output) to 40.82 % (the GFS_new output). This amount is more comparable with the observed cloud fraction of 38.59 %. Note that the GFS_new products reveal more abundant low clouds than those produced by the original GFS scheme. More marine stratocumulus clouds are now generated in all four regions and variations in zonal-mean low cloud amounts agree well with patterns seen in satellite observations. Agreement is particularly remarkable for the Californian and Namibian regions.

These findings support that the SG cloud scheme can produce more reasonable cloud fractions associated with marine stratocumulus clouds for a global scale as well as mitigating the overestimated high and middle-level cloud fractions generated by the original GFS scheme.

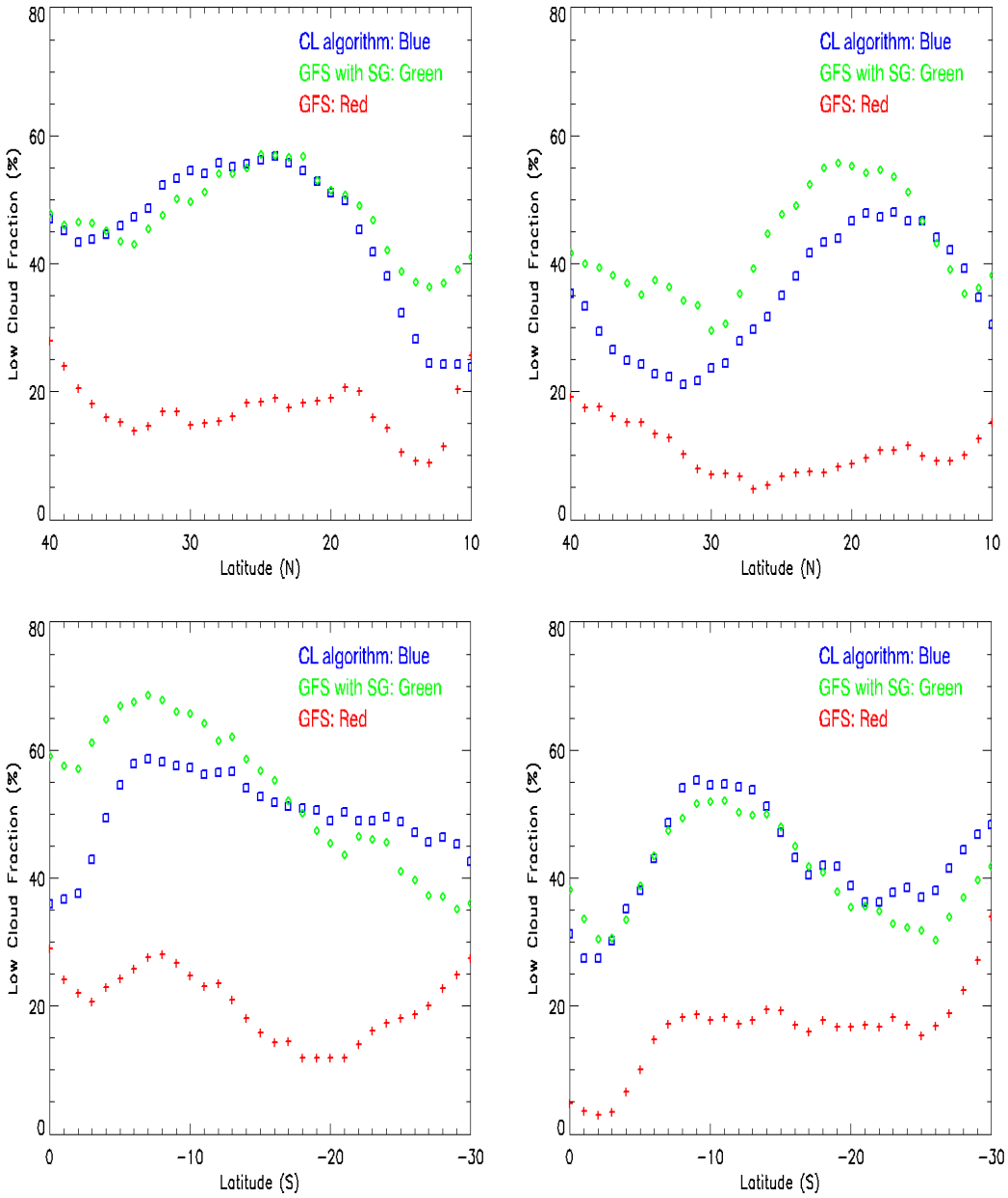

Figure 3.17. Latitudinal variations of zonal-mean low cloud fraction from three different cloud products for (clockwise, starting from the upper left plot) Californian, Canarian, Namibian, and Peruvian regions during July 2008. The blue square symbols, the green diamond symbols, and the red plus symbols represent results from the CL algorithm, the GFS model using the SG scheme, and the original GFS scheme, respectively.

3.4.3.3. Accuracy and Heidke Skill Score

To provide a suitable measure of performance, two of the common scores such as accuracy and Heidke Skill Score (HSS) are calculated. An accuracy is used to know what fraction of the forecasts are in the correct category and has a range of 0 to 1. This can be expressed as below

$$\text{Accuracy} = \frac{1}{N}\sum_{i=1}^{K} n(Fi, Oi), \tag{3.11}$$

where N is the total number and n(Fi,Oi) is the number of occurrences within the same category from both observations and forecasts.

The HSS is one of the generalized skill score and measures the fractional improvement of the forecast over the standard forecast. The 'standard forecast' usually means the number of forecasts in a random situation (Marzban 1998). A range of HSS is from -∞ to 1. A zero value indicates no skill and a perfect forecast of HSS is 1. The HSS is a popular score because it is simple and relatively easy to compute.

$$\text{HSS} = \frac{\frac{1}{N}\sum_{i=1}^{K} n(Fi, Oi) - \frac{1}{N^2}\sum_{i=1}^{K} N(Fi)N(Oi)}{1 - \frac{1}{N^2}\sum_{i=1}^{K} N(Fi)N(Oi)}, \tag{3.12}$$

where N(Fi) is the number of forecasts in a specific category and N(Oi) is the number of observations for that. The numbers of occurrence in multi-category for high, middle, and low clouds are given in Tables 3.3-8. For July, domain covering 55ºS - 60ºN is only considered for HSS and accuracy calculations since no satellite retrievals are made beyond 55ºS. It is learned from Table 3.9 that the GFS_new cloud fractions show more improved accuracy and HSS values in all categories for both January and July.

Table 3.3. Monthly mean high cloud fractions from the original GFS/the GFS with the SG scheme during January 2007.

		Observation					
	CFR (%)	0-20	20-40	40-60	60-80	80-100	Total
Forecast	0-20	13600/18580	220/1245	0/16	0/0	0/0	13820/19841
	20-40	13278/10343	3836/7086	92/1078	0/113	0/1	17206/18621
	40-60	2477/592	4223/1002	636/1301	21/820	0/7	7357/3722
	60-80	169/17	810/63	1362/83	534/44	1/0	2876/207
	80-100	53/0	310/3	400/12	427/5	7/0	1197/20
	Total	29577/29532	9399/9399	2490/2490	982/982	8/8	42456/42411

Table 3.4. As in Table 3.3, but for middle cloud fractions.

		Observation					
	CFR (%)	0-20	20-40	40-60	60-80	80-100	Total
Forecast	0-20	18028/23004	916/4187	183/240	60/84	6/14	19193/27529
	20-40	7181/2119	7618/7871	457/781	63/50	18/10	15337/10831
	40-60	980/102	4288/1218	891/693	23/16	6/6	6188/2035
	60-80	42/1	486/30	238/68	17/14	0/0	783/113
	80-100	3/0	16/0	29/0	2/0	0/0	50/0
	Total	26234/25226	13324/13306	1798/1782	165/164	30/30	41551/40508

Table 3.5. As in Table 3.3, but for low cloud fractions.

		Observation					
	CFR (%)	0-20	20-40	40-60	60-80	80-100	Total
Forecast	0-20	3110/2317	5275/1202	1848/279	271/18	30/0	10534/3816
	20-40	711/1127	6451/5431	4668/2648	796/322	62/5	12688/9533
	40-60	280/512	2200/6630	4987/9032	1191/1281	15/28	8673/17483
	60-80	475/302	1293/1448	5259/5558	1002/1634	11/23	8040/8965
	80-100	298/670	532/1030	1253/497	335/340	27/89	2445/2626
	Total	4874/4928	15751/15741	18015/18014	3595/3595	145/145	42380/42423

Table 3.6. Monthly mean high cloud fractions from the original GFS/the GFS with the SG scheme during July 2007.

		Observation					
	CFR (%)	0-20	20-40	40-60	60-80	80-100	Total
Forecast	0-20	11403/13831	71/482	1/37	0/0	0/0	11475/14320
	20-40	10786/10057	2456/6151	22/591	0/44	0/0	13264/16843
	40-60	2632/903	4922/2475	736/1831	34/637	0/13	8324/5859
	60-80	299/23	1589/149	1538/314	394/251	3/12	3823/749
	80-100	43/0	219/0	446/0	504/0	22/0	1234/0
	Total	25163/24814	9257/9257	2743/2743	932/932	25/25	38120/37771

Table 3.7. As in Table 3.6, but for middle cloud fractions.

		Observation					
	CFR (%)	0-20	20-40	40-60	60-80	80-100	Total
Forecast	0-20	20659/23947	850/4509	22/112	0/1	0/0	21531/28569
	20-40	6376/1665	5830/4289	120/342	1/8	0/0	12327/6304
	40-60	748/15	2184/185	330/75	9/1	0/0	3271/276
	60-80	13/0	142/8	58/7	0/0	0/0	213/15
	80-100	0/0	9/0	6/0	0/0	0/0	15/0
	Total	27796/25627	9015/8991	536/536	10/10	0/0	37357/35164

Table 3.8. As in Table 3.6, but for low cloud fractions.

		Observation					
	CFR (%)	0-20	20-40	40-60	60-80	80-100	Total
Forecast	0-20	5650/3223	7235/1442	2094/272	987/38	187/13	16153/4988
	20-40	480/2019	4454/6782	4642/4550	1624/532	156/12	11356/13895
	40-60	48/1044	1093/4469	3853/6091	2060/2204	211/47	7265/13855
	60-80	29/50	244/373	1530/1205	963/2128	127/424	2893/4180
	80-100	20/5	44/25	197/220	107/874	6/216	374/1340
	Total	6227/6341	13070/13091	12316/12338	5741/5776	1687/712	38041/38258

Table 3.9. HSS score and accuracy from the original GFS cloud fractions and the GFS_new cloud fractions for high, middle, and low clouds during two months.

		January		July	
		GFS	GFS_new	GFS	GFS_new
High	Accuracy	0.44	0.64	0.39	0.58
	HSS	0.16	0.36	0.13	0.34
Middle	Accuracy	0.64	0.78	0.72	0.81
	HSS	0.38	0.55	0.42	0.46
Low	Accuracy	0.37	0.44	0.39	0.48
	HSS	0.16	0.21	0.19	0.28

3.5. Summary

Understanding low cloud properties and their spatial-temporal variations is crucial for studying global climate change. One of the key issues for the impact of low clouds on the Earth's radiation budget is how to represent their sensitivity to the radiation field and quantify their effect on the cloud feedback in GCMs. Meteorological satellites make it possible to evaluate cloud parameterization schemes and validate model-simulated products by providing a wealth of information regarding the global distribution of cloud properties and atmospheric variables.

This Chapter examined low cloud fractions, the impact of clouds on the radiation field, meteorological variables, and the cloud parameterization scheme of the GFS model in comparison with satellite measurements and ground-based observations in July of 2008. The GFS model generated a reasonable distribution of low clouds but huge discrepancies in low cloud amounts are found over the eastern tropical oceans. The MODIS standard product (MYD06) and a new MODIS-based product retrieved by the CL algorithm show more marine stratus clouds than the GFS model simulations. An underestimation of such marine stratus clouds leads to more outgoing longwave radiation and less shortwave radiation at the TOA over those regions. To diagnose the causes of the bias in simulated cloud fractions, some key variables used in the cloud parameterization scheme are compared with satellite observations and in-situ measurements over the selected marine stratus cloud regimes. The GFS temperature field agrees well with AIRS observations at different

vertical levels, while the difference becomes somewhat larger close to the surface. The evaluation for GFS RH field is worse than that for temperature and the GFS RH simulations both in the lower and upper troposphere tend to be overestimated than satellite observations in all the regions.

The GFS cloud fractions and input variables are also examined by comparing ground-based measurements with a high temporal resolution. The simulated RH values have a wet bias in the lower atmosphere, but its temperature field shows a reasonable resemblance to the measurements in the entire vertical levels. These results imply that the deficiency in simulating condensed water vapor amount rather than temperature variable is a potential contributor to the discrepancies of low cloud fractions. The 2008 version of the GFS model in generating low clouds cannot match cloud fractions retrieved from satellites. Such findings are expected to help improve the inherent problems of the GFS cloud parameterization scheme, suggesting insights into the method in determining low cloud fractions.

To improve simulations of low-level clouds, an experiment is performed by using the GFS model's original atmospheric fields with the SG (based on Slingo (1987) and Gordon (1992)) cloud parameterization scheme. Application of the SG scheme to the GFS model generated a large quantity of marine stratocumulus clouds over the eastern tropical oceans, as well as low cloud amounts over other regions around the world. Latitudinal variations in zonal mean low cloud amounts agree well with the patterns seen in satellite observations. Such results are expected to help improve the inherent problems of the GFS cloud parameterization scheme and to gain insights into the method in determining low cloud fractions.

Chapter 4 : A test of the exponential random overlap scheme

4.1. Introduction

Cloud vertical structure plays a critically important role in the radiative energy budget (Morcrette and Fouquart 1986; Tian and Curry 1989; Rossow and Zhang 1995; Barker et al. 1999; Collins 2001) and has an impact on the vertical heating rate in general circulation models (GCMs) (Wang and Rossow 1998; Chen et al. 2000). For a given set of cloud amounts in model layers, the cloud fraction of the entire atmospheric column may differ substantially depending on cloud overlap assumption used in simulations (Morcrette and Jakob 2000; Collins 2001). GCMs generally parameterize cloud fraction in a given model grid since the horizontal resolution of GCMs is much coarser than the scale of clouds. Large uncertainties may be incurred in the calculations of radiaitve fluxes because of discrepancies in cloud fraction are determined independently at every vertical level in GCMs. Thus, climate changes simulated by GCMs are quite sensitive to the treatment of the cloud overlap assumption (Liang and Wang 1997; Liang and Wu 2005). Validation of several cloud overlap assumptions requires a good knowledge of cloud vertical structure as obtained from space using passive (Chang and Li 2005) and active (Dessler et al. 2006; Barker 2008; Mace et al. 2009) sensors, as well as ground (Clothiaux et al. 2000; Oreopoulos and Norris 2011) measurements.

In general, there are four different cloud overlap assumptions: maximum, random, maximum-random, and minimum overlap. Figure 4.1 (from Hogan and

Illingworth 2000) illustrates three different cloud overlap assumptions widely used in GCMs. Each overlap assumption can be described as follows. Maximum overlap describes the situation where cloud layers are overlapped as much as possible; whereas the opposite is the case for the minimum overlap. A random overlap assumes that horizontal cloud distributions from different vertical levels are independent.

A previous study showed the important effects of these different assumptions on global mean cloud fractions using the European Centre for Medium-Range Weather Forecasts (ECMWF) model (Morcrette and Jakob 2000). They found that the global mean cloud fraction is 71.4% when a random overlap is used. However, it would be 60.9% in the case of maximum overlap. Barker et al. (1999) reported large impacts of these assumptions on calculation of solar flux with instantaneous bias errors on the order of several hundred W/m^2.

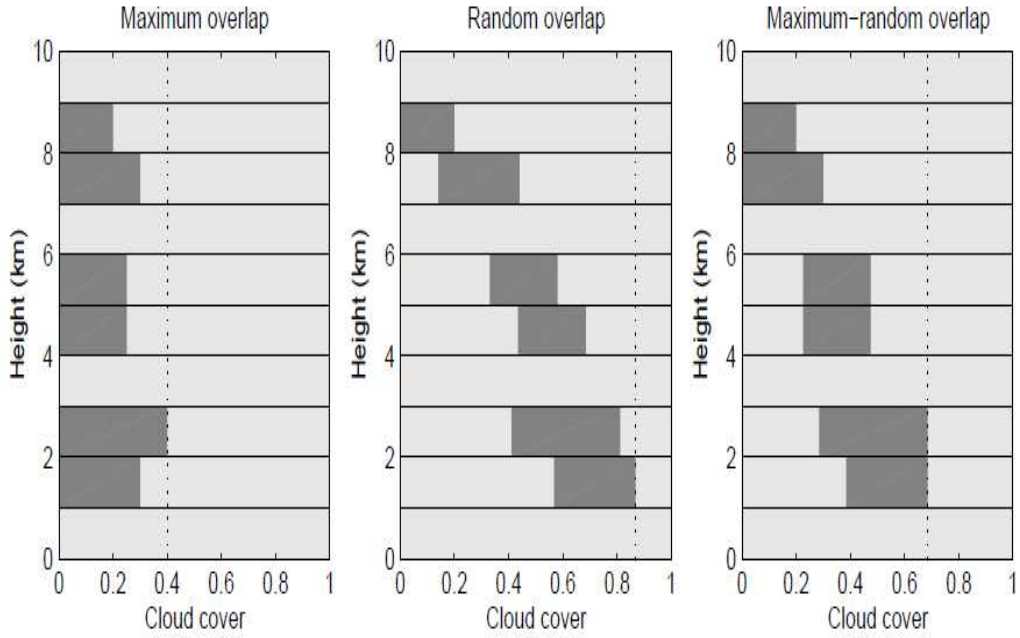

Figure 4.1. A schematic illustrating the three overlap assumptions that are commonly made in GCMs. The dotted vertical lines denote total cloud fraction (from Hogan and Illingworth 2000).

Numerous operational weather and climate models employ the maximum-random overlap (MRO) assumption (Barker et al. 2003). The MRO assumes that vertically continuous cloud layers are maximally overlapped while cloud layers separated by a clear layer are randomly overlapped (Geleyn and Hollingsworth 1979). A study by Tian and Curry (1989) quantitatively evaluated the MRO method with the 15-level U.S Air Force 3D Nephanalysis over the North Atlantic Ocean. They showed that the MRO assumption is reasonable in describing realistic characteristics of cloud vertical structure.

However, the MRO assumption has some limitations in explaining cloud overlap well because actual cloud overlap in the atmosphere is much more complex.

Hogan and Illingworth (2000) evaluated the MRO assumption against the time series of vertically-pointing millimeter-wave cloud radar profiles for three winter months at Chilbolton in the United Kingdom and found that clouds were overlapped randomly for cloud layers separated by at least one layer of clear air, but for vertically contiguous cloud layers, clouds were overlapped maximally only when the cloud layers were close to each other. In other words, the degree of correlation between cloud layers is determined by the vertical separation of the layers.

Hogan and Illingworth (2000) and Bergman and Rasch (2002) suggested that the MRO assumption include an overlap parameter, which is a weighted factor depending on the de-correlation length for overlapping clouds and layer altitudes. In this overlap assumption, the cloud overlap lies somewhere between maximum and random. It is called an 'exponential random overlap' (hereafter referred to as ERO). A vertically-projected cloud fraction of two layers (C_{true}) is defined as a linear combination of maximum and random overlap. Given

$$C_{max} = Max(C1,C2), \quad (4.1)$$

$$C_{ran} = C1 + C2 - C1*C2, \quad (4.2)$$

$$C_{min} = Min(1, C1 + C2), \quad (4.3)$$

, where C1 and C2 are cloud fractions in two layers at different altitudes,

$$C_{true} = \alpha C_{max} + (1 - \alpha)C_{ran.} \quad (4.4)$$

The value of α determines the degree of correlation between cloud layers. When α is zero, the overlap is random and when α is 1, a maximum overlap is implied. The value of α is defined as

$$\alpha = \exp(\frac{-\Delta z}{Lcf}) \tag{4.5}$$

and has a value between zero and one.

The overlap parameter is described in terms of a de-correlation length (Lcf) and the separation distance between the two layers (Δz). The value of Lcf is related to the vertical resolution and horizontal domain size and varies with season and latitude.

A number of studies have suggested values for the weighting factor (Bergman and Rasch 2002; Mace and Benson-Troth 2002; Oreopoulos and Khairoutdinov 2003; Pincus et al. 2005; Liang and Wu 2005; Naud et al. 2008; Barker 2008). Mace and Benson-Troth (2002) used millimeter radar data collected over multiple years from the four Atmospheric Radiation Measurement (ARM) Climate Research Facility (ACRF) sites and found that the value of Lcf varies with location and season. An increase in convective activities leads to more maximally-overlapped clouds with larger Lcf values. Cloud overlap results using the ERO assumption in cloud-resolving models also agreed well with observations (Oreopoulos and Khairoutdinov 2003).

Other studies have made considerable attempts at developing an improved parameterization of cloud overlap within models. Using a combination of cloud-resolving model simulations and ARM measurements with a mosaic approach,

Liang and Wu (2005) demonstrated that this approach can explain the characteristics of cloud overlap associated with different cloud regimes (i.e., convective, anvil, and stratiform clouds) and provided useful results to improve parameterizations for sub-grid cloud-radiation interactions. Pincus et al. (2005) used a month-long cloud-resolving model simulation and also found that overlap assumptions can be strongly affected by the presence of convection and wind shear. They showed that convective clouds are associated with large values of Lcf, while wind shear decreases the magnitude of Lcf.

Similarly, Naud et al. (2008) pointed out that atmospheric dynamics has a large impact on how cloud layers are overlapped, based upon the use of active remote sensing cloud layer (ARSCL) data in combination with reanalysis data from the National Centers for Environmental Prediction (NCEP). Vertical velocities derived from convective activities play a role in preserving maximum overlap for cloud layers with long separation distances.

It has been difficult to implement such findings into global models because the studies mentioned above only focused on a limited number of ground stations. Because the value of Lcf varies with location, season, and the background atmospheric environment, the most important task involves determining the optimum value of Lcf around the world. Thanks to space-borne cloud profiles observed from active sensors on the CloudSat and CALIPSO platforms, a closer view of clouds in the atmosphere on a global scale can be made. Barker (2008) performed a global study of cloud overlap properties using merged CloudSat and CALIPSO data. He found that cloud overlap is characterized by a vertically constant

value of Lcf and that the global median value of Lcf is about 2 km. Recently, Shonk et al. (2010) proposed a simple linear relationship between de-correlation lengths and latitudes based on the studies of Hogan and Illingworth (2000) and Mace and Benson-Troth (2002) (see Figure 4.2). They also compared such a linear fit with a series of Lcf values retrieved from CloudSat and CALIPSO. The linear fit is expressed as a relationship between Lcf in kilometers and the absolute latitude, Φ, in degrees (see equation 4.6). The Lcf values calculated from a smooth version of this simple equation were recently implemented into the ECMWF model.

$$Lcf = 2.899 - 0.02759 * \phi \tag{4.6}$$

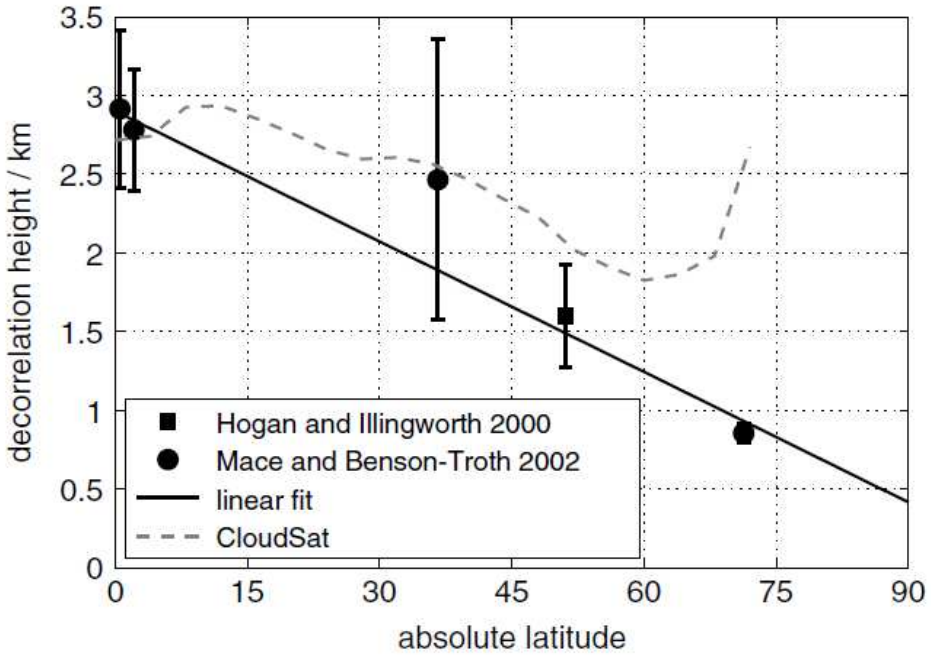

Figure 4.2. A simple linear fit of Lcf as a function of latitude based on the studies of Hogan and Illingworth (2000) and Mace and Benson-Troth (2002). The fitted line is shown as black solid, and the dashed line shows a series of de-correlation heights calculated using data from CloudSat and CALIPSO (from Shonk et al. 2010).

The primary purpose of this section is to test an application of this equation to the GFS model and to see how successfully this simple equation explains the characteristics of cloud vertical structure on the changes in cloud fraction at different vertical levels.

4.2. Data and methodology

Data collected from the 94-GHz cloud-profiling radar (CPR) onboard the CloudSat satellite and the dual-wavelength lidar onboard the CALIPSO satellite are used to illustrate global cloud overlap during July 2007. There are 37,081 profiles per orbit and the footprint is 1.4 km wide, 1.1 km along-track, and 0.24 km in the vertical. Here, some oversampling is encountered because the radar footprint is taken as 1-km along-track. The lowest 1 to 3 bins from the surface are not considered because the data near the surface may be contaminated by ground clutter. CPR cloud mask and radar reflectivity variables from the 2B-GEOPROF product and the cloud fraction field from the 2B-GEOPROF-LIDAR product are utilized in this study. Large CPR cloud mask field values indicate the likelihood of cloud, as summarized in Table 4.1.

Table 4.1. Description of CPR cloud mask values.

Value	Definition
-9	Missing data
5	Signal detected but likely ground clutter
6-10	Very weak signal echo
20	Weak detection found using along-track integration
30-40	Good to strong echo

For this study, values greater than 20 in the CPR cloud mask field are selected to reduce the probability of false detections. CPR radar reflectivities greater than -30 dBZ are considered because CloudSat's minimum detectable signal is -30 dBZ (Stephens et al. 2002). The data screening for cloud detection consists of a sequence of tests for three conditions. This approach is very similar to that described by Barker (2008). The tests are

$$\begin{aligned} &CPR\_cloud\_mask \geq 20 \\ &radar\_reflectivity \geq -30 dBZ \end{aligned}$$

Or

$$\begin{aligned} &CPR\_cloud\_mask < 20\_and\_cloud\_fraction \geq 99\% \\ &radar\_reflectivity \geq -30 \end{aligned} \quad (4.7),$$

.

If either set of criteria are satisfied, the bins are considered as cloudy.

A stochastic sub-grid scale cloudy column generator developed by Räisänen et al. (2004) was designed to enable GCMs to use the Monte Carlo Independent Column Approximation (McICA) (Pincus et al. 2003). The generator produces sub-grid-scale columns and generates synthetic cloud fields by utilizing profiles of cloud fraction derived from the corresponding observed ones. Here, it is used to compute a domain's cloud fractions corresponding to observation using 50,000 sub-columns. This tool is used for performing radiative transfer calculations in inhomogeneous clouds (Barker and Räisänen 2005). Here, the method to solve for Lcf is that described in Brent (1973), which is an effective tool when all values of the function are known and the roots are one-dimensional. The calculated Lcf values have a top limit of 20 km and a bottom limit of 0.05 km. All applications of the generator have a cross-section in length of 500 km because this length can provide adequate sampling for typical GCM grid size (Astin and Di Girolamo 1999). This method is a fast and efficient way to find Lcf values. The number of iterations for convergence is typically 4 to 8 then Lcf values are finally returned as total cloud fractions after stochastic fluctuations. Output files per each sample include one Lcf, the observed layer cloud fraction, the downward cumulative cloud fraction based on observations, the generated layer cloud fraction, and the generated accumulated cloud fraction.

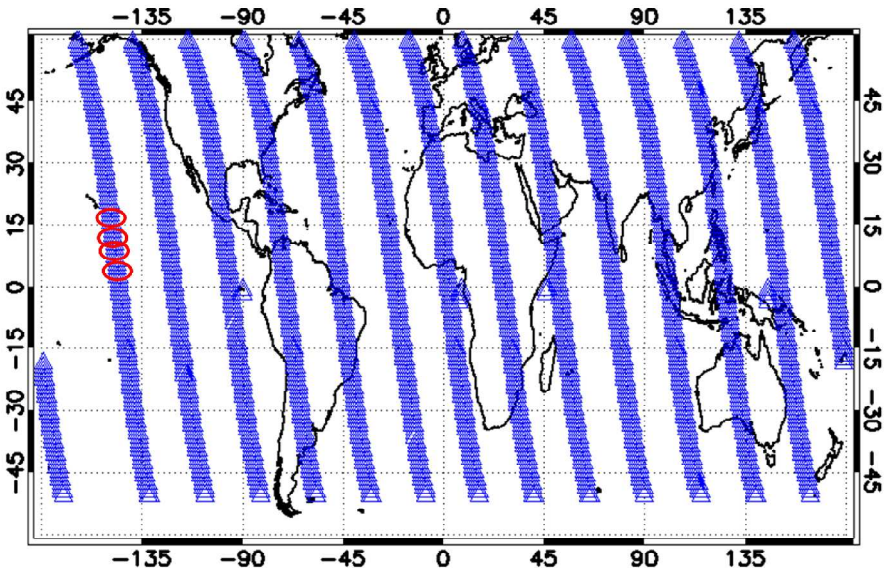

Figure 4.3. Blue triangles show CloudSat and CALIPSO day-time orbits. This study selects only day-time orbits during July 2007. Red circles represent each sample size of 500-km cross-sectional length.

4.3. Results

4.3.1. Characteristics of global cloud overlap

Figure 4.4 shows zonal mean and median values of Lcf for 500-km cross-sectional lengths. Mean Lcf can be influenced by a small number of large values, so median values of Lcf are also plotted. Superimposed on this figure is the simple linear function suggested by Shonk et al. (2010). Two features are seen. First, mean and median values of Lcf display almost identical patterns with respect to latitude of 10°N intervals and the mean values of Lcf are always greater than median values of Lcf with approximately 1-km differences except for around 60°S. Second, the simple linear fit has a maximum value of Lcf at 0°N which then monotonically

decreases toward high latitudes in both hemispheres. However, a series of Lcf calculated using the Brent (1973) method have a maximum value of Lcf at 10°N presumably due to the ITCZ; this is related to the movement of the Sun during summertime. These values decrease between 0° and 20°N but gradually increase toward high latitudes, showing a more maximally overlapped situation than that suggested by the simple linear fit. Such an offset pattern in subtropical regions is remarkable. The inclusion of precipitation in Lcf calculations may explain such a difference. Barker (2008) found that precipitation can cause an increase in Lcf by about 0.5 km. Lcf values derived from surface sites in previous studies did not include precipitation; in this study, we did not eliminate cases where precipitation was present.

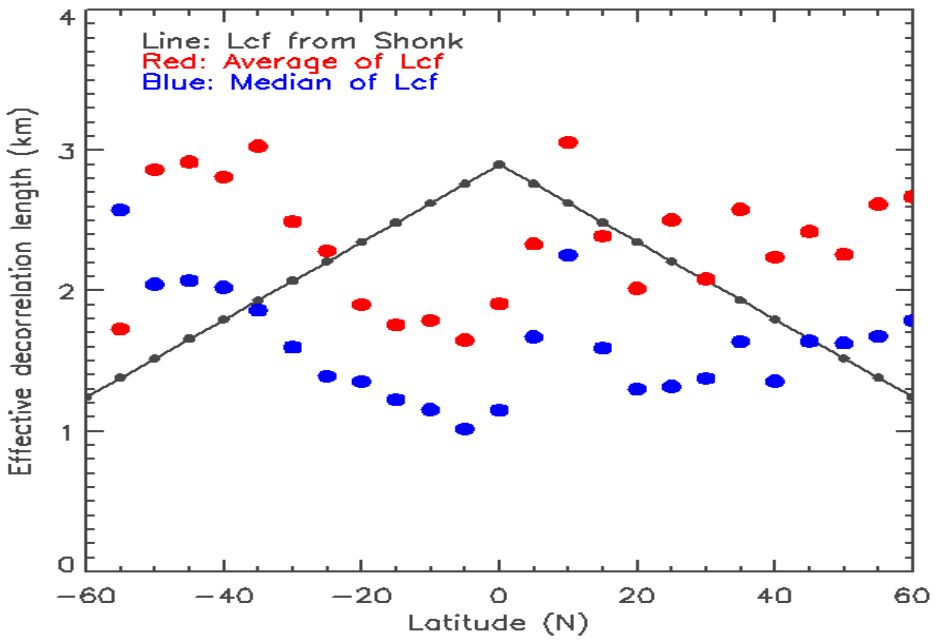

Figure 4.4. Effective Lcf values as a function of latitude for July 2007. The black solid line is a simple linear fit suggested by Shonk et al. (2010) and the red and blue dots show mean and median values of Lcf, respectively.

Figure 4.5 illustrates how median values of Lcf change as a function of total cloud fraction during July 2007. The smallest median values of Lcf seem to be associated with small total cloud fractions (~0.1), while the largest median values of Lcf tend to occur when the total cloud fraction is between 0.6-0.8. As total cloud fraction becomes larger, median values of Lcf similarly increase but then decrease before converging at 1.2 km-1.9 km.

Data used in this study are grouped into six zonal bands. Presumably, tropical regions have large Lcf values because deep convective clouds well-organized in vertically continuous layers are dominant over those regions. However, Figure 4.5 shows that median values of Lcf for extra-tropical areas are greater than those for tropical regions. We attribute this to the effect of multi-layered clouds. C-C satellites show that dual-layer clouds occur more frequently over the ITCZ, and relatively less frequently at middle or high latitudes (see Figure 2.2). Thin high clouds and low-level clouds are usually decoupled, which can result in smaller median values of Lcf in the Tropics.

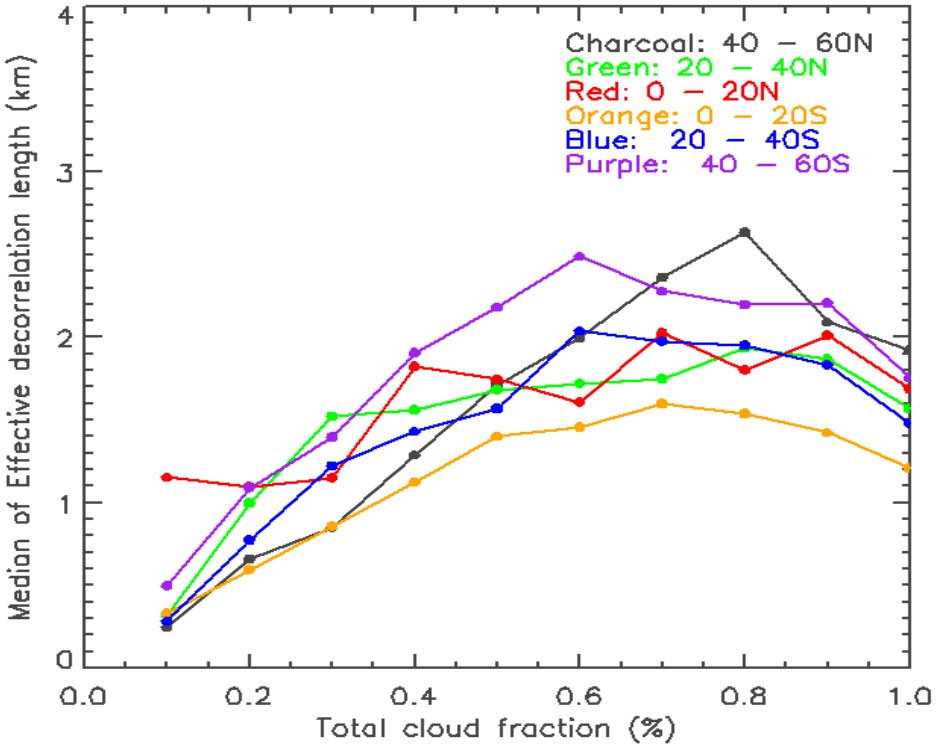

Figure 4.5. Median values of Lcf as a function of total cloud fraction for six zonal bands during July 2007.

Characteristics of the calculated median Lcf based on observed clouds vary widely depending on location, as shown in Figure 4.6. It does not appear to depend greatly on latitude. This finding is quite different from that suggested by Shonk et al. (2010). Their simple linear fit based on data from five sites does not take into account the presence of convection or atmospheric conditions. Figure 4.6 suggests that vertical motion such as convection and atmospheric state rather than latitude should be addressed to explain the variation in Lcf. However, it is not easy to differentiate between specific cloud types in observations. CloudSat provides cloud profiles consisting of 125 vertical bins, however, several different cloud types are

mixed within each profile. Our method determines only one value of Lcf for each 500-km cross-sectional sample and various cloud types can exist vertically and horizontally within each sample. In contrast, most models directly generate cloud fractions associated with different cloud regimes. This means that the cloud overlap in models can be applied separately to each cloud category. Further studies are required to elucidate the characteristics of Lcf and to develop applications for both satellite observational and modeling communities.

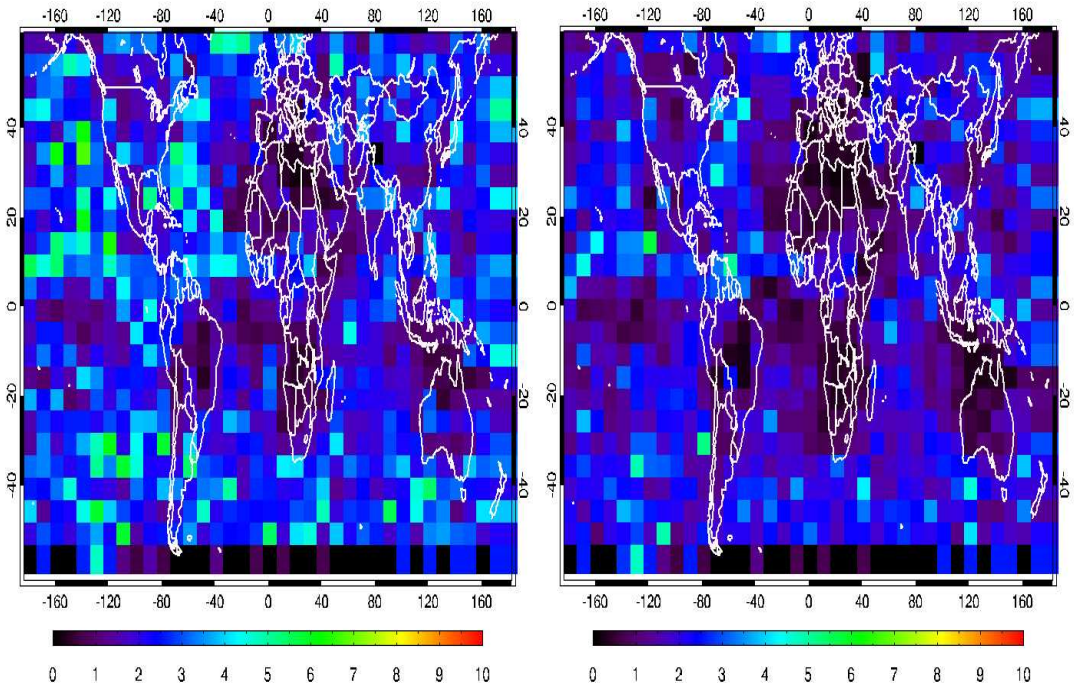

Figure 4.6. Geographic distributions of mean (left) and median (right) values of Lcf using a stochastic cloud generator from C-C data collected during July 2007.

4.3.2. Cloud fraction comparisons

Figure 4.7 shows the comparison of cloud fractions derived from different sources of Lcf. Overall, cloud fractions derived from a simple linear fit are slightly overestimated than those computed from Lcf values based on observations. Although the values of Lcf are quite different, cloud fractions derived from the two are remarkably correlated (R^2=0.98). Mean differences are calculated as cloud fractions derived from Lcf values based on observations minus those from a simple linear fit. For the high cloud category, cirrus and convective clouds are more pronounced in the upper part of the troposphere. Levels in the high zone are mostly occupied by clouds, which results in an increase in correlation length scale. So, when the high cloud fraction is computed from a grid box, estimates of Lcf do not have much effect on cloud fractions. However, this effect in the lower atmosphere is less sensitive to the strength of convection (Pincus et al. 2005). This is evident when two kinds of Lcf are separately applied to low-level cloud layers; points are then broadly scattered.

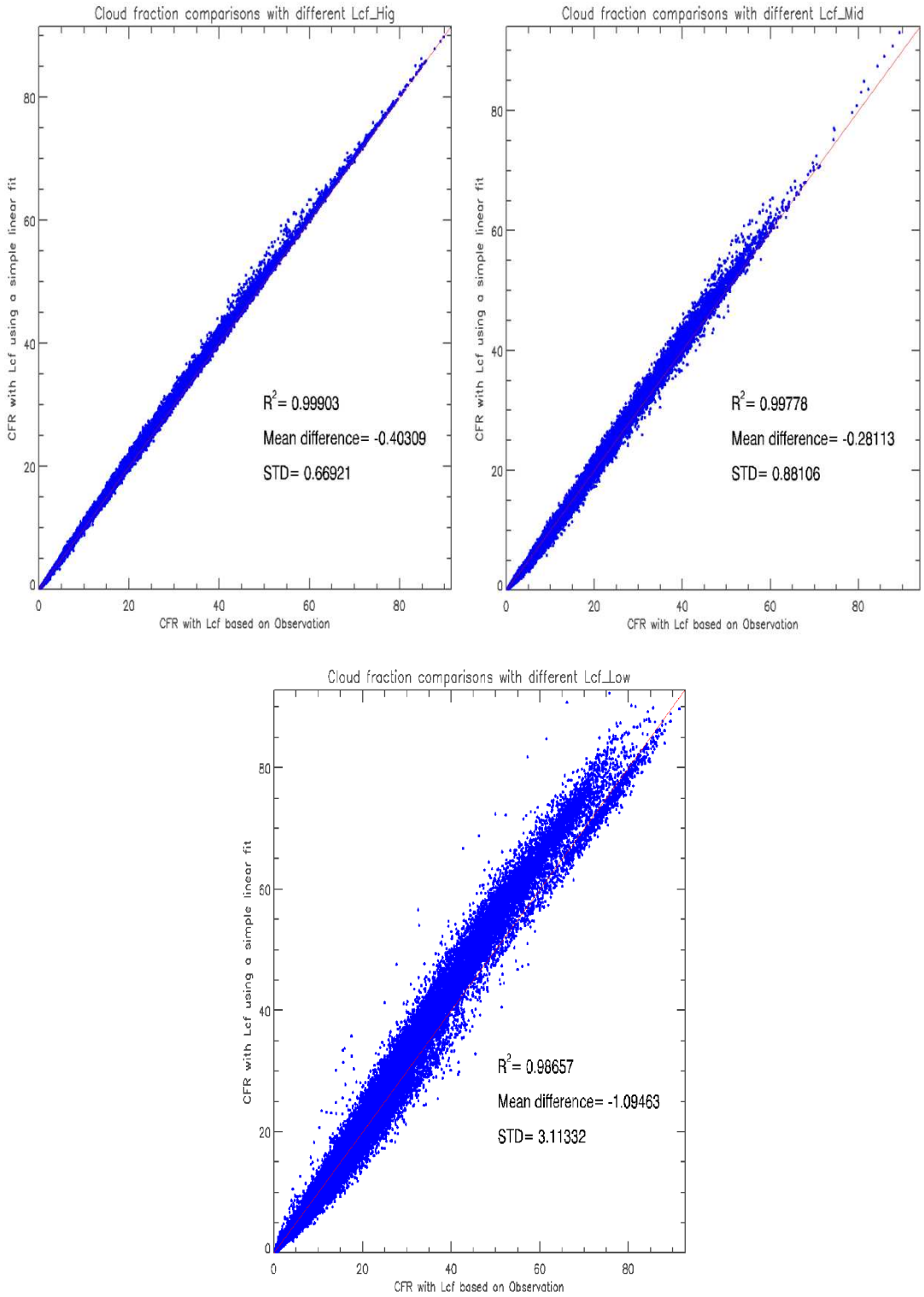

Figure 4.7. Comparison of cloud fractions derived from a simple linear fit against those with Lcf based on observations for high clouds (upper left), middle clouds (upper right), and low clouds (bottom center) during July 2007.

As mentioned earlier, a goal of this study is to diagnose cloud properties simulated by the GFS model and to suggest where improvements can be made. Testing the ERO assumption can be a tool used to generate more realistic cloud distributions. Figure 4.8 compares cloud fractions at different vertical levels from both the original GFS cloud product and through use of Lcf based on observations. High-level cloud fractions from the original GFS model are overestimated compared to observations, but those using Lcf mitigate such discrepancies. Middle-level cloud fractions are similar in terms of location and magnitude. For low-level clouds, the most significant deficiency is that the GFS model misses marine stratocumulus clouds over eastern tropical oceans and generates more boundary layer clouds over interior continents at high latitudes; this is not changed when using different overlap schemes. Using Lcf in computing cloud fractions makes cloud fractions smaller. We attribute this to different vertical resolutions. The original GFS model simulates cloud fractions at 64 vertical levels and outputs high, middle, and low-level cloud fractions after applying the MRO assumption. The ERO experiment is performed with model standard outputs at 21 vertical levels rather than implementing the ERO assumption into the GFS model. However, note that cloud fractions calculated from the SG cloud scheme showed quite better results and are well comparable with observational results despite a use of the same GFS model outputs used in the ERO analysis. Therefore, at this point, we conclude that discrepancies found in cloud fields arise mainly from an improper cloud parameterization scheme used in the GFS model.

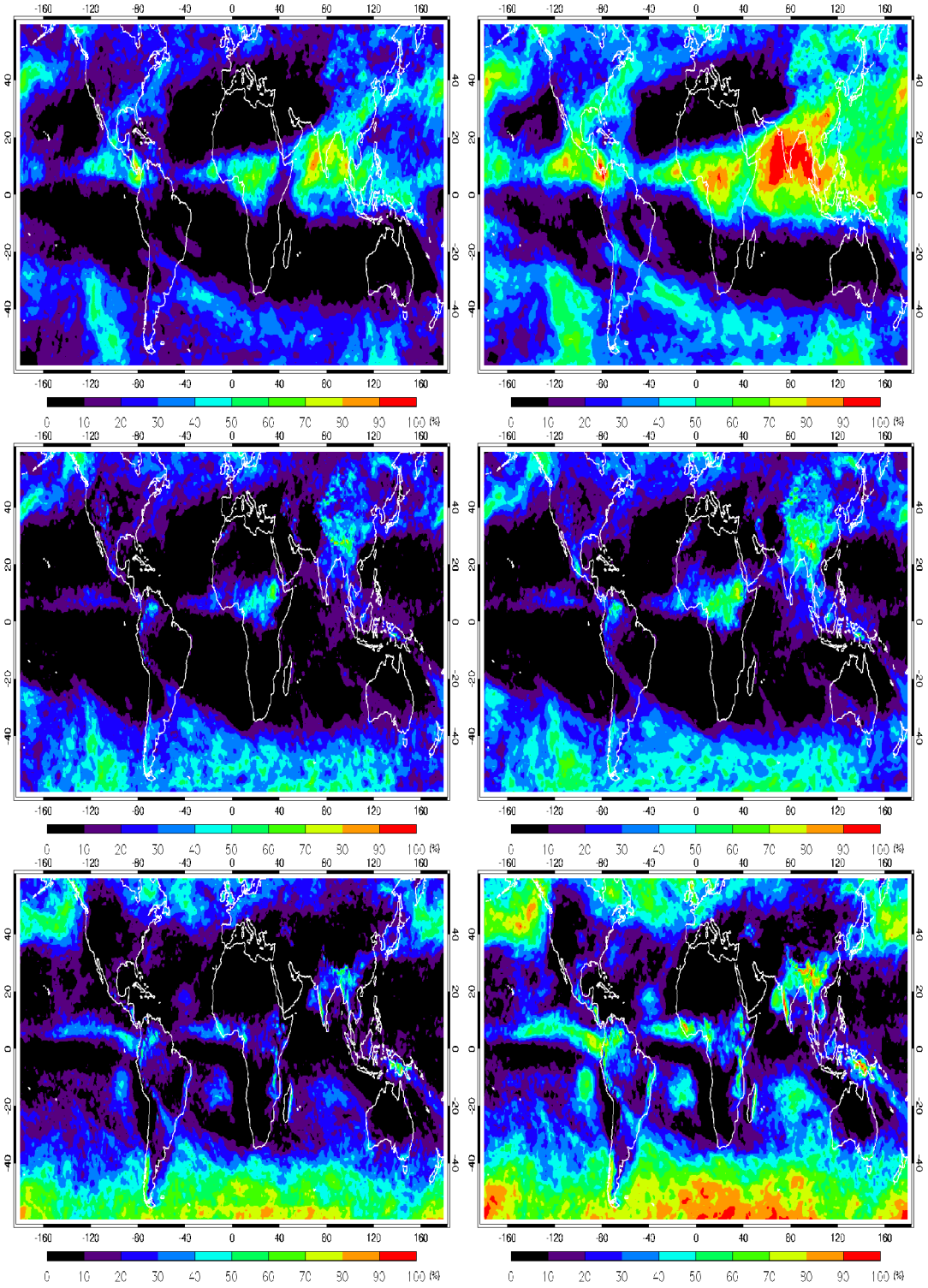

Figure 4.8. Comparison of cloud fractions derived from the original GFS model (right) and those with Lcf based on observations (left) for high clouds (upper panels), middle clouds (middle panels), and low clouds (bottom panels) during July 2007.

4.4. Summary

A consideration of cloud overlap assumptions in GCMs is critical and essential because cloud-scale dynamics are not fully resolved by models. Overlap assumptions determine column-integrated cloud fractions within a grid box, which provide the information needed to compute radiative fluxes and heating rates. Among typical cloud overlap assumptions, MRO assumption is widely employed by many weather forecasting and climate models. However, the MRO assumption has some limitations in describing a realistic cloud vertical structure well as pointed out by previous studies.

Hogan and Illingworth (2000) found that vertically continuous cloud layers are not generally maximally overlapped. Rather, cloud overlap tends to change from maximal overlap to random overlap as the vertical separation between cloud layers increases. This can be expressed as a linear combination of maximum and random overlap with an overlap parameter depending on vertical separation. One may use a fixed Lcf between every pair of cloud layers. However, radar observations at different locations around the world and cloud-resolving models with a ‘‘super-parameterization’’ (Räisänen et al. 2004) show that Lcf values vary with location, season, state of the atmosphere and in particular, cloud regime. This finding implies that cloud overlap needs to be parameterized because a unique overlap assumption does not work well.

Recently, a simple linear fit between Lcf and latitude derived from two previous studies was suggested by Shonk et al. (2010). This study tested a simple linear fit to the GFS model and evaluated the soundness of the relationship through

comparisons with Lcf values based on observations. Results show that the pattern of zonal Lcf values from a simple linear fit is quite different from that of Lcf values using the Brent (1973) method. The former has a maximum value of Lcf at 0°N then monotonically decreases toward high latitudes in both hemispheres while the latter decreases between 0° and 20°N but then gradually increases toward high latitudes, depicting a more maximally overlapped scenario. Such an offset pattern in subtropical regions is notable.

For median Lcf values as a function of total cloud fraction, as total cloud fraction becomes larger, median values of Lcf similarly increase then decrease to 1.2 km - 1.9 km. Median values of Lcf are most sensitive in mid-range of cloud fraction than in near-clear or overcast conditions. Unlike a simple linear fit suggested by Shonk et al. (2010), the distribution of median Lcf values calculated from observed clouds do not show much dependence on latitude. This suggests that other physics, such as convection and cloud formation mechanism rather than simply latitude, should be considered when explaining how Lcf behaves. Although Lcf values may differ between the two approaches, cloud fractions derived from these values agree remarkably well. High cloud fractions are not as sensitive to Lcf, but low cloud fractions are. This can be attributed to the effect of convection on de-correlation length scales. Convection is associated with greater vertical coherence and this generates larger Lcf values; this effect is weaker in the lower atmosphere.

Results shown here can help understand Lcf characteristics and its dependence on location and total cloud fraction. More consideration of the physical basis of clouds and of different cloud regimes should be taken into account when

addressing realistic cloud distributions within a model grid box. In addition, an accurate grid-mean cloud state profile such as cloud liquid, ice water and cloud fraction is required in order to represent an improved parameterization of the scale length in the context of a large-scale model.

Chapter 5 : Summary and Future Work

5.1. Summary of the thesis

Clouds are one of the most critical regulators in weather and climate systems. Their importance in controlling the Earth's radiative energy and global temperature has been recognized for a long time. However, the knowledge of clouds and cloud processes has not been fully understood because clouds interact with other atmospheric components in many ways. Clouds in weather forecasting and climate models are represented through cloud parameterization scheme and such processes result in large sources of uncertainty due to insufficient understanding of the vertical structure of clouds and cloud horizontal inhomogeneity. Numerous studies have made considerable efforts to improve the representation of clouds and to make progress on this issue. More reliable cloud observation and representation of clouds is still one of the active research issues to be resolved in both observation and model communities.

In this study, an evaluation of NCEP GFS cloud properties using a number of space-borne observational datasets is a main objective. The various cloud parameters and meteorological variables simulated by the GFS model are compared with a large array of cloud variables retrieved independently from different sensors. Synthetic analyses with regard to cloud products and the soundness of the cloud parameterization scheme were presented to eventually improve the performance of the GFS model. The frequencies of clouds in multi-layers, cloud fraction and thickness, cloud optical depth (COD), liquid water path (LWP), ice water path

(IWP), and cloud-top and base heights of the lowest cloud layers are retrieved from a suite of satellite sensors aboard the A-Train sensors, including cloud products from Moderate Resolution Imaging Spectroradiometer (MODIS), CloudSat, and CloudSat-the Cloud-Aerosol Lidar and Infrared Pathfinder Satellite Observations (CALIPSO), and the atmospheric profiles of temperature and relative humidity (RH) from the Atmospheric InfraRed Sounder (AIRS), longwave/shortwave fluxes at the top-of-the-atmosphere (TOA) from the Clouds and Earth's Radiant Energy System (CERES). In addition, ground-based measurements are also employed at the Southern Great Plains (SGP) site operated by the Atmospheric Radiation Measurement (ARM) program including the temperature and water vapor profiles from the Atmospheric Emitted Radiance Interferometer (AERI), cloud products from the combined millimeter wavelength cloud radar (MMCR)-micropulse lidar (MPL) observations. Two global cloud products are derived from the same MODIS data but using different algorithms in this study: 1) the MODIS standard/official algorithm, 2) the algorithm of Chang and Li (2005a). The latter algorithm can identify and retrieve individual cloud quantities for overlapped thin cirrus clouds over thick water clouds. As a result, 10 – 20 % more low clouds underneath high clouds in the tropical and mid-latitude storm track regions are identified when compared to the MODIS algorithm products (Chang and Li 2005b). The estimate of total low clouds retrieved from the C-L algorithm over the globe matches closely with space-borne lidar-based retrievals.

The GFS model captures well the spatial distributions of hydrometeors, which bear a reasonable distribution to those seen from satellite retrievals, although

large differences exist in magnitude in different layers. The GFS model tends to simulate more high, middle-level clouds, and interior continental low-level clouds but less low-level marine stratocumulus clouds, leading to an overall severe overestimation of high and mid-level clouds and an underestimation of low clouds. This results in large discrepancies in the global distributions of low clouds. Optically thick clouds in deep convective cloud regimes are overproduced whereas optically thin or intermediate clouds are underestimated by the GFS model. This finding shows a rather uniform distribution of clouds throughout the atmosphere and is clearly different from the distinct bi-modal distributions of cloud tops generated by the algorithm of Chang and Li. GFS-modeled LWP distributions are similar with satellite retrievals but the magnitudes are less. IWP distributions generated by the GFS model have a better agreement with observations.

To understand the causes for the large discrepancies in low cloud distributions between the model and observations, both input parameters and the model cloud parameterization scheme are investigated using satellite retrievals of temperature and humidity profiles. They are found to partially account for the poor simulation of low-level clouds. In addition, to investigate the causes of the discrepancies in marine stratocumulus cloud decks, four areas along the west coast of America and Africa are selected. Regional analyses reinforce the findings that the GFS model substantially underestimates the amount of stratocumulus clouds in all regions and this result causes less upward shortwave radiation and more outgoing longwave radiation than that measured by CERES at the TOA. As a result, net radiation at the TOA from CERES and the model has opposite signs, emphasizing

the impact of clouds on global net radiation.

The GFS temperature field mostly agrees well with AIRS observations and AERI measurements at different vertical levels but their differences become somewhat larger close to the surface. GFS RH simulations in the lower and upper troposphere tend to be overestimated against the AIRS retrievals and AERI measurements for both global scales and the selected four regions. The comparison reveals that condensed water vapor is not adequately generated near the surface even though the GFS model slightly overestimates the absolute amount of water vapor in the lower troposphere. Such problem is also found in a previous study and is attributed to the shallow convection scheme, which makes cloud condensate water vapor to be destroyed by increasing vertical diffusion in the cloud layers (Han and Pan 2011).

Therefore, it does not help resolve considerable discrepancies in low cloud amounts if cloud water mixing ratios are used as a primary predictor of cloudiness in the GFS cloud scheme. A diagnostic cloud parameterization scheme based on Slingo (1987) and Gordon (1992) (i.e., the SG scheme) is applied to the GFS model. This scheme is similar to the GFS cloud parameterization scheme in that cloudiness is determined by an empirical formulation, but a link with convective activity is also included. The areal cloud fraction in the scheme depends more on thermodynamical and dynamical variables.

The results of cloud fractions calculated from the SG scheme show considerable improvements showing much less high and middle-level clouds and more low clouds than the original GFS cloud products. The SG cloud scheme

generates a large quantity of marine stratocumulus clouds over the eastern tropical oceans, as well as low cloud amounts over other regions around the world.

With respect to cloud biases, an evaluation of the cloud overlapping assumption used in the GFS model and a test of exponential random overlap assumption are performed. Many weather forecasting and climate models employ a maximum-random overlap (MRO) assumption. However, the MRO assumption has some limitations in describing a realistic cloud vertical structure well. Hogan and Illingworth (2000) proposed an exponential random overlap (ERO) assumption in which cloud overlap tends to change from maximal overlap to random overlap as vertical separations are increased. The ERO assumption uses an overlap parameter, which is described by a decorrelation length (Lcf) and the separation distance of the two layers. The value of Lcf is related to the vertical resolution and horizontal domain size and varies with seasons and latitudes. Recently, a simple linear relationship between decorrelation lengths and the absolute latitudes is suggested by Shonk et al. (2010). Data collected from CloudSat and CALIPSO satellites are utilized to illustrate a global feature of cloud overlap using a stochastic cloud generator and Brent's method (Brent 1973).

The results show that the patterns of Lcf values from a simple linear fit are quite different from those retrieved from observations. Lcf values do not depend much on latitudes. This suggests that other physics such as convection and cloud formation mechanism rather than a latitudinal relationship should be considered to explain the characteristic of Lcf.

In conclusion, the inter-comparisons presented in this study reveal

considerable discrepancies in cloud fields which are related to misrepresentation of cloud water mixing ratios in the lower troposphere and overestimation of RH simulations as cloud input data. These shortcomings of the GFS model in simulating clouds can be fairly overcome by applying the SG cloud scheme. Such fundamental challenges emphasize the urgency of making more modifications in the simulation of cloud processes.

5.2. Suggestions for Future Work

In the previous sections, we discussed the evaluation of cloud properties simulated by the 2007 and 2008 operational version of the GFS model. A new physics package related to convection and shallow convection schemes is incorporated into the GFS model since July 2010. Based on advanced physical parameterizations of the shallow convective scheme, an overall improvement is found in the forecasts of vector wind, hurricane tracks, continental US precipitation, and more simulations of stratocumulus clouds over the eastern Pacific and Atlantic oceans. The new shallow convection scheme can represent the physical processes of shallow convection by using a bulk mass-flux parameterization and removing unrealistic diffusion of heat and moisture (Han and Pan 2011).

Modifications of the GFS cloud fraction in the updated GFS version are as follows: 1) the criterion for high clouds is changed from 350 hPa to 400 hPa; 2) low clouds are defined when pressure is greater than 650 hPa; 3) cloud fraction is

calculated from Xu and Randall (1996), but empirical coefficients of 0.25, 2000, and 0.25 are replaced with the values of 0.25, 100, and 0.49, respectively. The revision of the shallow convective and boundary layer parameterization schemes accompanies considerable changes in other parts of the model such as vertical diffusion, relative humidity, and cloud water mixing ratios.

Figure 5.1 compares the geographical distributions of cloud fraction in three layers among three products during January. The results from the C-L retrievals, the old GFS version, and the updated GFS version represent left, middle, and right panels, respectively. Note that a remarkable difference between the updated and old GFS versions is seen in marine stratocumulus clouds in the lower atmospheric layers. The updated GFS version shows much better improvements in simulating clouds over the eastern tropical oceans than the old GFS cloud products. However, results of the updated GFS version are significantly different from the C-L retrievals in the upper troposphere. This is especially the case in the Tropics and mid-latitude storm track regions where high clouds are abundant. For middle-level clouds, the updated GFS version generates reasonable cloud fractions. Table 5.1 presents a comparison of the global mean cloud fractions derived from the three products. The near-global (60ºS - 60ºN) averaging of high (< 400 hPa), middle (400-650 hPa), and low (> 650 hPa) cloud fractions from the C-L retrievals during January 2011 are 19.71 %, 14.06 %, and 41.50 %, respectively. The corresponding cloud fractions are 30.61 %, 22.79 %, and 39.24 % from the old GFS version during January 2007 and 35.99 %, 14.41 %, and 28.77 % from the updated GFS version during January 2011, respectively. Note that middle and low-level cloud fractions of the updated GFS

version are somewhat less whereas high-level cloud fraction of that is more about 5 % when compared to those from the old GFS version (see Table 5.1).

Table 5.1. Global monthly mean high-, mid-, and low-level cloud fractions obtained from the C-L algorithm during January 2011, the old GFS version during January 2007, the updated GFS version during January 2011.

	C-L	GFS_old	GFS_new
High	19.71 %	30.61 %	35.99 %
Middle	14.06 %	22.79 %	14.41 %
Low	41.50 %	39.24 %	28.77 %

For high clouds in the SG scheme, cloud fraction only depends on RH values and the RH threshold of cloudiness is 80 %. Based on preliminary results, frequencies with larger than the RH threshold in the updated GFS version are greater than those of the old GFS version (not shown). This leads to an increase in high cloud fraction. For marine stratocumulus clouds, vertical velocity and lapse rate are the main factors in determining cloud fraction. Similarly, values of the vertical velocity and lapse rate with larger than the threshold are more frequent in the updated GFS version for low-level clouds. The modified shallow convective scheme affects other dynamics and atmospheric state. This may thus be incurred in changes of input data used in the SG scheme, resulting in the change of the cloud distributions throughout the atmosphere. Further studies for the cloud parameterization of the GFS model are necessary in order to fully describe and understand physical processes taking place in modeled cloud systems.

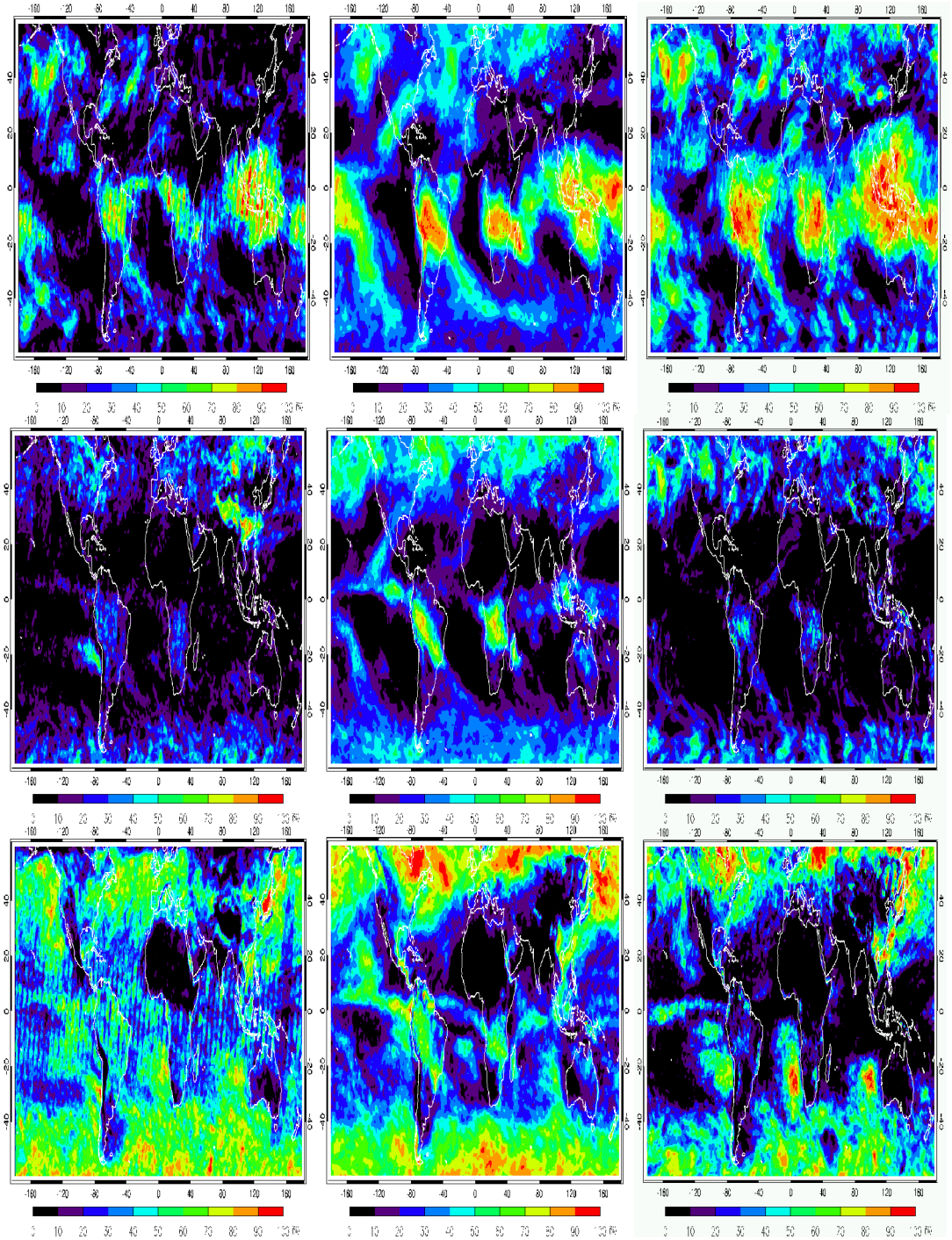

Figure 5.1. Geographic distributions of monthly mean cloud fractions from the C-L algorithm (left panels) during January 2011, the old GFS products (middle panels) during January 2007, and the updated GFS products (right panels) during January 2011. Top, middle, and bottom plots denote high, middle, and low clouds, respectively.

Glossary of acronyms

ACRF: Climate Research Facility

AERI: Atmospheric Emitted Radiance Interferometer

AGCM: Atmospheric General Circulation Model

AIRS: Atmospheric Infrared Sounder

AMSU-A: Advanced Microwave Sounding Unit

ARM: Atmospheric Radiation Measurement

ARSCL: Active Remote Sensing Cloud Layer

ASTEX: Atlantic Stratocumulus Transition Experiment

AVHRR: Advanced Very High Resolution Radiometer

CALIOP: Cloud-Aerosol Lidar with Orthogonal Polarization

CALIPSO: Cloud-Aerosol Lidar and Infrared Pathfinder Satellite Observations

CERES: Clouds and Earth's Radiant Energy System

CF: Cloud Fraction

COD : Cloud Optical Depth

CPR: Cloud Profiling Radar

ECMWF: European Center for Medium-range Forecasting

ERO: Exponential Random Overlap

GCM: General Circulation Model

GFDL: Geophysical Fluid Dynamics Laboratory

GFS: Global Forecast System

GLAS: Geoscience Laser Altimeter System

GMS: Geostationary Meteorological Satellites

GOES: Geostationary Operational Environmental Satellites

HIRS: High resolution Infrared Radiation Sounder

HSB: Humidity Sounder for Brazil

HSS: Heidke Skill Score

IR: Infrared

ISCCP: International Satellite Cloud Climatology Project

ITCZ: inter-tropical convergence zone

IWP: Ice Water Path

Lcf: de-correlation length

LW: longwave

LWP: Liquid Water Path

McICA: Monte Carlo Independent Column Approximation

METEOSAT: European Meteorological Satellites

MISR: Multiangle Imaging SpectroRadiometer

MMCR: millimeter wavelength cloud radar

MODIS: Moderate Resolution Imaging Spectroradiometer

MPL: micropulse lidar

MRO: Maximum-Random Overlap

MW: Microwave

NCEP: National Center for Environmental Prediction

NOAA: National Oceanic and Atmospheric Administration

OMI: Ozone Monitoring Instrument

PDF: Probability Distribution Functions

RAS: Relaxed Arakawa-Schubert

Re : Effective Radius

RH: Relative Humidity

RHe: environmental relative humidity

RMS: Root Mean Square

SGP: Southern Great Plains

SSF: Single Scanner Footprint

SW: shortwave

SZA: Solar Zenith Angle

TOA: top-of-atmosphere

WRF: Weather Research and Forecasting

Bibliography

Agee EM (1984) Observations from space and thermal convection: A historical perspective. *Bull. Amer. Meteor. Soc.,* **65,** 938-949.

Ackerman SA, Strabala KI, Menzel WP, Frey RA, Moeller CC, Gumley LE (1998) Discriminating clear-sky from clouds with MODIS. *J. Geophys. Res.,* **103**, 32,141-32,158.

Astin I, Di Girolamo L (1999) A general formalism for the distribution of the total length of a geophysical parameter along a finite transect. *IEEE Trans. Geosci. Remote Sens*., **37**, 508– 512.

Aumann HH et al (2003) AIRS/AMSU/HSB on the Aqua mission: design, science objectives, data products, and processing systems. *IEEE Trans. Geosci. Remote Sens*. **41**, 253-264.

Barker HW, Stephens GL, Fu Q (1999) The sensitivity of domain averaged solar fluxes to assumptions about cloud geometry. *Q. J. R. Meteorol. Soc.,* **125**, 2127– 2152.

Barker HW et al (2003) Assessing 1D atmospheric solar radiative transfer models: Interpretation and handling of unresolved clouds. *J. Clim.,* **16**, 2676– 2699.

Barker HW, Räisänen P (2005) Radiative sensitivities for cloud structural properties that are unresolved by conventional GCMs. *Q. J. R. Meteorol. Soc.,* **131**, 3103–3122.

Barker HW (2008) Overlap of fractional cloud for radiation calculations in GCMs: A global analysis using CloudSat and CALIPSO data. *J. Geophys. Res.,* **113**, D00A01, doi:10.1029/2007JD009677.

Barnes WL, Pagano TS, Salomonson VV (1998) Prelaunch characteristics of the Moderate Resolution Imaging Spectroradiometer (MODIS) on EOS-AM1. *IEEE Trans. Geosci. Remote Sens.,* **36,** 1088-1100.

Baum BA, Uttal T, Poellot M, Ackerman TP, Alvarez JM, Intrieri J, Starr DO'C, Titlow J, Tovinkere V, Clothiaux E (1995) Satellite remote sensing of multiple cloud layers. *J. Atmos. Sci.*, **52,** 4210-4230.

Baum BA, Spinhirne JD (2000) Remote Sensing of cloud properties using MODIS airborne simulator imagery during SUCCESS. 3. Cloud Overlap. *J. Geophys. Res.*, **105,** 11,793-11,804.

Bergman JW, Rasch PJ (2002) Parameterizing vertically coherent cloud distributions. *J. Atmos. Sci.*, **59**, 2165– 2182.

Bodas-Salcedo A, Webb MJ, Brooks ME, Ringer MA, William KD, Milton SF, Wilson DR (2008) Evaluating cloud systems in the Met Office global forecast model using simulated CloudSat radar reflectivities. *J. Geophys. Res.,* **113,** D00A13, doi:10.1029/2007JD009620.

Bony S, Dufresne JL, Treut HL, Morcrette JJ, Senior C (2004) On dynamic and thermodynamic components of cloud changes. *Clim. Dyn.,* **22(2/3),** 71–76.

Bony S, Dufresre JL (2005) Marine boundary layer clouds at the heart of tropical cloud feedback uncertainties in climate models. *Geophys. Res. Lett.,* **32**, L20806, doi:10.1029/2005GL023851.

Bony S et al (2006) How well do we understand and evaluate climate change feedback processes?. *J. Clim.* **19,** 3445–3482.

Brent RP (1973) Algorithms for Minimization without Derivatives. Chap. 4. pp. 61-167, Prentice-Hall, Englewood Cliffs, N.J.

Chahine MT et al (2006) The Atmospheric Infrared Sounder (AIRS): Improving weather forecasting and providing new data on greenhouse gases. *Bull. Amer. Meteor. Soc.,* **87**, 911–926, doi:10.1175/BAMS-87-7-911.

Cess RD et al (1990) Intercomparison and interpretation of climate feedback processes in 19 atmospheric general circulation models. *J. Geophys. Res.,* **95,** 16,601–16,615.

Chang FL, Li Z (2002) Estimating the vertical variation of cloud droplet effective radius using multispectral near-infrared satellite measurements. *J. Geophys. Res.,* **107,** 4257, doi:10.1029/2001JD000766.

Chang FL, Li Z (2003) Retrieving vertical profiles of water-cloud droplet effective radius: Algorithm modification and preliminary application. *J. Geophys. Res.,* **108,** 4763, doi:10.1029/2003JD003906.

Chang FL, Li Z (2005a) A new method for detection of cirrus-overlapping-low clouds and determination of their optical properties. *J. Atmos. Sci.*, **62,** 3993-4009.

Chang FL, Li Z (2005b) A near global climatology of single-layer and overlapped clouds and their optical properties retrieved from TERRA/MODIS data using a new algorithm. *J. Clim.,* **18,** 4752-4771.

Chen R, Chang FL, Li Z, Ferraro R, Weng F (2007) The impact of vertical variation of cloud droplet size on estimation of cloud liquid water path and detection of warm raining cloud. *J. Atmos. Sci.,* **64,** 3843-3853.

Chen T, Zhang YC, Rossow WB (2000) Sensitivity of atmospheric radiative heating rate profiles to variations of cloud layer overlap. *J. Clim.*, **13**, 2941-2959, doi:10.1175/1520-0442(2000)013<2941:SOARHR>2.0.CO;2.

Chepfer H, Bony S, Winker D, Cesana G, Dufresne JL, Minnis P, Stubenrauch CJ, Zeng S (2010) The GCM Oriented CALIPSO Cloud Product (CALIPSO-GOCCP). *J. Geophys. Res.*, **115**, D00H16, doi:10.1029/2009JD012251.

Chou MD, Suarez MJ, Ho CH, Yan HMM, Lee KT (1998) Parameterizations for cloud overlapping and shortwave single scattering properties for use in general circulation and cloud ensemble models. *J. Clim.,* **11,** 202-214.

Clothiaux EE, Ackerman TP, Mace GG, Moran KP, Marchand RT, Miller M, Martner BE (2000) Objective determination of cloud heights and radar reflectivities using a combination of active remote sensors at the ARM CART Sites. *J. Appl. Meteor.,* **39**, 645-665.

Collins WD (2001) Parameterization of generalized cloud overlap for radiative calculations in general circulation models. *J. Atmos. Sci.,* **58**, 3224 – 3242.

Dai A, Trenberth KE (2004) The diurnal cycle and its depiction in the community climate system model. *J. Clim.,* **17**, 930–951.

de Szoeke SP, Wang Y, Xie SP, Miyama T (2006) Effect of shallow cumulus convection on the eastern Pacific climate in a coupled model. *Geophys. Res. Lett*., **33**, L17713, doi:10.1029/2006GL026715.

Del Genio A, Wolf AB, Yao MS (2005) Evaluation of Regional Cloud Feedbacks using Single-Column Models. *J. Geophys. Res.*, **110**, D15S13, doi:10.1029/2004JD005011.

Dessler AE, Palm SP, Spinhirne JD (2006) Tropical cloud-top height distributions revealed by the Ice, Cloud, and Land Elevation Satellite (ICESat)/Geoscience Laser Altimeter System (GLAS). *J. Geophys. Res.,* **111**, D12215, doi:10.1029/2005JD006705.

Divakarla MG, Barnet CD, Goldberg MD, McMillin LM, Maddy E, Wolf W, Zhou L, Liu X (2006) Validation of Atmospheric Infrared Sounder temperature and water vapor retrievals with matched radiosonde measurements and forecasts. *J. Geophys. Res.*, **111**, D09S15, doi:10.1029/2005JD006116.

Dupont JC, Haeffelin M, Morille Y, Comstock JM, Flynn C, Long CN, Sivaraman C, Newson RK (2011) Cloud properties derived from two lidars over the ARM SGP site. *Geophys. Res. Lett.,* **38**, L08814, doi:10.1029/2010GL046274.

Geleyn JF, Hollingsworth A (1979) An economical analytical method for the computation of the interaction between scattering and line absorption of radiation. *Contrib. Atmos. Phys.*, **52**, 1–16.

Giese BS, Carton JA (1994) The seasonal cycle in a coupled ocean-atmosphere model. *J. Clim.,* **7**, 1208-1217.

Gordon CT (1992) Comparison of 30-day integrations with and without cloud-radiation interaction. *Mon. Wea. Rev.,* **120**, 1244-1277.

Haladay T, Stephens G (2009) Characteristics of tropical thin cirrus clouds deduced from joint CloudSat and CALIPSO observations. *J. Geophys. Res.,* **114,** D00A25, doi:10.1029/2008JD010675.

Han J, Pan HL (2011) Revision of Convection and Vertical Diffusion Schemes in the NCEP Global Forecast System. *Wea. Forecasting*, **26**, 520–533.

Hannay et al (2009) Evaluation of Forecasted Southeast Pacific Stratocumulus in the NCAR, GFDL, and ECMWF Models. *J. Clim.,* **22**, 2871–2889.

Harshvardhan RD, Randall DA, Corsetti TG, Dazlich DA (1989) Earth radiation budget and cloudiness simulations with a general circulation model. *J. Atmos. Sci.*, **46,** 1922-1942.

Hartmann DL et al (1992) The Effect of Cloud Type on Earths Energy-Balance - Global Analysis. *J. Clim.,* **5**, 1281-1304.

Heymsfield AJ, McFarquhar GM (1996) High Albedos of Cirrus in the Tropical Pacific Warm Pool: Microphysical Interpretations from CEPEX and from Kwajalein, Marshall Islands. *J. Atmos. Sci.,* **53,** 2424-2451.

Hogan RJ, Illingworth AJ (2000) Deriving cloud overlap statistics from radar. *Q. J. R. Meteor. Soc.*, **128**, 2903– 2909.

Holz RE, Ackerman SA, Nagle FW, Frey R, Dutcher S, Kuehn RE, Vaughan MA, Baum B (2008) Global Moderate Resolution Imaging Spectroradiometer (MODIS) cloud detection and height evaluation using CALIOP. *J. Geophys. Res.,* **113**, D00A19, doi:10.1029/2008JD009837.

Houghton JT et al (2001) Climate change: the Scientific Basis. Contributions of Working Group I to the Third Assessment Report of the Intergovernmental Panel on Climate Change. Cambridge Univ. Press.

Im E, Durden SL, Wu C (2006) Cloud profiling radar for the CloudSat mission. *IEEE Aerosp. Electron. Syst. Mag.,* **20,** 15-18.

Jin Y, Rossow WB, Wylie DP (1996) Comparison of the climatologies of high-level clouds from HIRS and ISCCP. *J. Clim.*, **9,** 2850-2879.

Kahn BH, Chahine MT, Stephens GL, Mace GG, Marchand RT, Wang Z, Barnet CD, Eldering A, Holz RE, Kuehn RE, Vane DG (2008) Cloud type comparisons of AIRS, CloudSat, and CALIPSO cloud height and amount. *Atmos. Chem. Phys.,* **8,** 1231-1248.

Katayama A (1972) A simplified scheme for computing radiative transfer in the troposphere. UCLA Tech. Rep. No.6, pp 77.

King MD et al (2003) Cloud and aerosol properties, precipitable water, and profiles of temperature and humidity from MODIS. *IEEE Trans. Geosci. Remote Sens.*, **41**, 442-458.

Klein SA, Hartmann DL (1993) The seasonal cycle of low stratiform clouds. *J. Clim.,* **6**, 1587-1606. doi:10.1175/1520-0442(1993)006<1587:TSCOLS>2.0.CO;2.

Kuettner JP (1971) Cloud bands in the earth's atmosphere. *Tellus,* **23,** 404-425.

Lazarus SM, Krueger SK, Frisch SA (1999) An evaluation of the Xu-Randall cloud fraction parameterization using ASTEX data. Preprints, 13th Symposium on Boundary Layers and Turbulence, Dallas, TX. *Amer. Meteor. Soc.,* 582–585.

Leon DC, Wang Z, Liu D (2008) Climatology of drizzle in marine boundary layer clouds based on 1 year of data from CloudSat and Cloud-Aerosol Lidar and Infrared Pathfinder Satellite Observations (CALIPSO). *J. Geophys. Res*., **113**, D00A14, doi:10.1029/2008JD009835.

Li Z, Leighton H (1991) Scene identification and its effect on cloud radiative forcing in the Arctic. *J. Geophys. Res.*, **96,** 9175-9188.

Liang XZ, Wang WC (1997) Cloud overlap effects on general circulation model climate simulations. *J. Geophys. Res.,* **102**, 11 039–11 047.

Liang XZ, Wu X (2005) Evaluation of a GCM subgrid cloudradiation interaction parameterization using cloud-resolving model simulations. *Geophys. Res. Lett*., **32**, L06801, doi:10.1029/2004GL022301.

Loeb NG et al (2007) Multi-instrument comparison of top-of-atmosphere reflected solar radiation. *J. Clim.,* **20**, No. 3, 575-591.

Ma CC, Mechoso CR, Robertson AW, Arakawa A (1996) Peruvian stratus clouds and the tropical Pacific circulation: A coupled ocean-atmosphere GCM study. *J. Clim.,* **9**, 1635-1645.

Mace GG, Benson-Troth S (2002) Cloud-layer overlap characteristics derived from long-term cloud radar data. *J. Clim.,* **15**, 2505–2515.

Mace GG, Zhang Q, Vaughn M, Marchand R, Stephens G, Trepte C, Winker D (2009) A description of hydrometeor layer occurrence statistics derived from the first year of merged Cloudsat and CALIPSO data. *J. Geophys. Res.,* **114**, D00A26, doi:10.1029/2007JD009755.

Marchand R, Mace GG, Ackerman T, Stephens G (2008) Hydrometeor detection using Cloudsat—An earth-orbiting 94-GHz cloud radar. *J. Atmos. Oceanic Technol.*, **25(4)**, 519– 533.

Marzban C (1998) Scalar measures of performance in rare-event situations. *Wea. Forecasting*, **13**, 753-763.

Mechoso CR et al (1995) The seasonal cycle over the tropical Pacific in coupled ocean-atmosphere general circulation models. *Mon. Wea. Rev.,* **123**, 2825-2838.

Menzel WP, Baum BA, Strabala KI, Frey RA (2002) Cloud top properties and cloud phase algorithm theoretical basis Doc. ATBD-MOD-04.

Ming Y, Ramaswamy V, Ginoux PA, Horowitz LH, Russell LM (2005) Geophysical Fluid Dynamics Laboratory general circulation model investigation of the indirect radiative effects of anthropogenic sulfate aerosol. *J. Geophys. Res.,* **101,** D22206, doi:10.1029/2005JD006161.

Ming Y, Ramaswamy V, Donner LJ, Phillips VT, Klein SA, Ginoux PA, Horowitz LW (2007) Modeling the interactions between aerosols and liquid water clouds with a self-consistent cloud scheme in a general circulation model. *J. Atmos. Sci.*, **64**, 1189–1209.

Morcrette JJ, Fouquart Y (1986) The overlapping of cloud layers in shortwave radiation parameterizations. *J. Atmos. Sci.*, **43**, 321– 328.

Morcrette JJ, Jakob C (2000) The response of the ECMWF model to changes in the cloud overlap assumption. *Mon. Wea. Rev.*, **128**, 1707 – 1732.

Nalli NR et al (2006) Ship-based measurements for infrared sensor validation during Aerosol and Ocean Science Expedition 2004. *J. Geophys. Res.,* **111**, D09S04, doi:10.1029/2005JD006385.

Naud CM, Del Genio A, Mace GG, Benson S, Clothiaux EE, Kollias P (2008) Impact of dynamics and atmospheric state on cloud vertical overlap. *J. Clim.,* **21**, 1758-1770, doi:10.1175/2007JCLI1828.1.

Nicholls S (1987) A model of drizzle growth in warm, turbulent stratiform clouds. *Q. J. R. Meteorol. Soc.,* **113**, 1141-1170.

Oreopoulos L, Khairoutdinov MF (2003) Overlap properties of clouds generated by a cloud-resolving model. *J. Geophys. Res.,* **108(D15)**, 4479, doi:10.1029/2002JD003329.

Oreopoulos L, Norris PM (2011) An analysis of cloud overlap at a midlatitude atmospheric observation facility. *Atmos. Chem. Phys. Discuss.,* **11**, 597-625, doi:10.5194/acpd-11-597-2011.

Otkin JA, Greenwald TJ (2008) Comparison of WRF model simulated and MODIS derived cloud data. *Mon. Wea. Rev.,* **136**, 1957-1970.

Ou SC, Liou KN, Baum BA (1996) Detection of multilayer cirrus cloud systems using AVHRR data: Verification based on FIRE-II IFO composite measurements. *J. Appl. Meteorol.*, **35,** 178-191.

Pagano TS, Auman HH, Hagan DE, Overoye K (2003) Prelaunch and in-flight radiometric calibration of the Atmospheric Infrared Sounder (AIRS). *IEEE Trans. Geosci. Remote Sens.*, **41**, 265-273.

Philander SGH, Gu D, Halpern D, Lambert G, Lau NC, Li T, Pacanowski RC (1996) The role of low-level stratus clouds in keeping the ITCZ mostly north of the equator. *J. Clim.,* **9**, 2958-2972.

Pierce DW, Barnett TP, Fetzer EJ, Gleckler PJ (2006) Three-dimensional tropospheric water vapor in coupled climate models compared with observations from the AIRS satellite system. *Geophys. Res. Lett.*, **33**, L21701, doi:10.1029/2006GL027060.

Pincus R, Barker HW, Morcrette JJ (2003) A fast, flexible, approximate technique for computing radiative transfer in inhomogeneous cloud fields. *J. Geophys. Res.,* **108(D13)**, 4376, doi:10.1029/2002JD003322.

Pincus R, Hannay C, Klein SA, Xu KM, Hemler R (2005) Overlap assumptions for assumed probability distribution function cloud schemes in large scale models. *J. Geophys. Res.*, **110**, D15S09. doi: 10.1029/2004JD005100.

Platnick S, King MD, Ackerman SA, Menzel WP, Baum BA, Riedi JC, Frey RA (2003) The MODIS cloud products: Algorithms and examples from Terra. *IEEE Trans. Geosci. Remote Sens.,* **41,** 459-473.

Platt CMR et al (1994) The Experimental Cloud Lidar Pilot Study (ECLIPS) for cloud–radiation research. *Bull. Amer. Meteor. Soc.,* **75**, 1635–1654.

Poore KD, Wang J, Rossow WB (1995) Cloud layer thicknesses from a combination of surface and upper-air observations. *J. Clim.*, **8**, 550-568.

Räisänen P, Barker HW, Khairoutdinov M, Li J, Randall DA (2004) Stochastic generation of subgrid-scale cloudy columns for largescale models. *Q. J. R. Meteorol. Soc.,* **130**, 2047–2067.

Randall DA, Krueger S, Bretherton C, Curry J, Duynkerke, Moncireff M, Ryan B, Starr D, Miller M, Rossow W, Tselioudis G, Wielicki B (2003) Confronting models with data: The GEWEX Cloud Systems Study. *Bull. Amer. Meteorol. Soc.*, **84**, 455-469, doi:10.1175/BAMS-84-4-455.

Randall DA et al (2007) Climate Models and Their Evaluation. In: Climate Change 2007: The Physical Science Basis. Contribution of Working Group I to the Fourth Assessment Report of the Intergovernmental Panel on Climate Change. Cambridge Univ. Press.

Rosenkranz PW (2003) Rapid radiative transfer model for AMSU/HSB channels. *IEEE Trans. Geosci. Remote Sens.*, **41**, 362-368, doi:10.1109/TGRS.2002.808323.

Rosenkranz PW (2006) Cloud liquid-water profile retrieval algorithm and validation. *J. Geophys. Res.*, **111**, D09S08, doi:10.1029/2005JD005832.

Rossow WB, Gardner LC, Lacis AA (1989) Global seasonal cloud variations from satellite radiance measurements. Part I: Sensitivity of analysis. *J. Clim.,* **2**, 419-458.

Rossow WB, Zhang YC (1995) Calculation of surface and top of atmosphere radiative fluxes from physical quantities based on ISCCP data sets, 2. Validation and first results. *J. Geophys. Res.*, **100**, 1167–1197.

Rossow WB, Schiffer RA (1999) Advances in understanding clouds from ISCCP. *Bull. Amer. Meteor. Soc.,* **80**, 2261-2287.

Sassen K, Wang Z (2008) Classifying clouds around the globe with the CloudSat radar: 1-year of results. *Geophys. Res. Lett.*, **35**, L04805, doi:10.1029/2007GL032591.

Sheu RS, Curry JA, Liu G (1997) Vertical stratification of tropical cloud properties as determined from satellite. *J. Geophys. Res.,* **102,** 4231-4245.

Shonk JKP, Hogan RJ, Edwards JM, Mace GG (2010) Effect of improving representation of horizontal and vertical cloud structure on the Earth's global radiation budget. Part I: Review and parametrization. *Q. J. R. Meteorol. Soc.*, **136**, 1191–1204. DOI:10.1002/qj.647.

Slingo JM (1987) The development and verification of a cloud prediction scheme for the ECMWF model. *Q. J. R. Meteorol. Soc.,* **113**, 899-927, doi:10.1002/qj.49711347710.

Starr DO'C, Cox SK (1985) Cirrus clouds. Part II: Numerical experiments on the formation and maintenance of cirrus. *J. Atmos. Sci.*, **42,** 2682-2694.

Stephens GL (1990) On the relationship between water vapor over the oceans and sea surface temperature. *J. Clim.*, **3**, 634-645.

Stephens GL, Vane DG, Boain RJ, Mace GG, Sassen K, Wang Z, Illingworth AJ, O'Connor EJ, Rossow WB, Durden SL, Miller SD, Austin RT, Benedetti A, Mitrescu C (2002) The Cloudsat Mission And The A-Train. *Bull. Amer. Meteor. Soc.,* **83,** 1771-1790.

Stephens GL (2005) Cloud feedbacks in the climate system: A critical review. *J. Clim.,* **18,** 237-273.

Stockdale T, Latif M, Burgers G, Wolff JO (1994) Some sensitivities of a coupled ocean-atmosphere GCM. *Tellus,* **46A**, 367-380.

Stowe LL, Yeh HYM, Eck TF, Wellemeyer CG, Kyle HL, the Nimbus-7 Cloud Data Processing Team (1989) Nimbus-7 global cloud climatology. Part II: First year results. *J. Clim.,* **2**, 671-709.

Sun R, Moorthi S, Xiao H, Mechoso CR (2010) Simulation of low clouds in the Southeast Pacific by the NCEP GFS: sensitivity to vertical mixing. *Atmos. Chem. Phys.,* **10**, 12261-12272, doi:10.5194/acp-10-12261-2010.

Susskind J, Barnet CD, Blaisdell JM (2003) Retrieval of atmospheric and surface parameters from AIRS/AMSU/HSB data in the presence of clouds. *IEEE Trans. Geosci. Remote Sens.*, **41**, 390-409.

Susskind J, Barnet C, Blaisdell J, Iredell L, Keita F, Kouvaris L, Molnar G, Chahine M (2006) Accuracy of geophysical parameters derived from Atmospheric Infrared Sounder/Advanced Microwave Sounding Unit as a function of fractional cloud cover. *J. Geophys. Res.,* **111**, D09S17, doi:10.1029/2005JD006272.

Tian L, Curry JA (1989) Cloud overlap statistics. *J. Geophys. Res*., **94**, 9925– 9935.

Tiedtke M (1993) Representation of clouds in large-scale models. *Mon. Wea. Rev.,* **212,** 3040–3061.

Tobin DC et al (2006) Atmospheric Radiation Measurement site atmospheric state best estimates for Atmospheric Infrared Sounder temperature and water vapor retrieval validation. *J. Geophys. Res.,* **111**, D09S14, doi:10.1029/2005JD006103.

Tselioudis G, Jakob C (2002) Evaluation of midlatitude cloud properties in a weather and a climate model: Dependence on dynamic regime and spatial resolution. *J. Geophys. Res.,* **107(D24),** 4781, doi:10.1029/2002JD002259, 2002.

Walden VP, Roth WL, Stone RS, Halter B (2006) Radiometric validation of the Atmospheric Infrared Sounder over the Antarctic Plateau. *J. Geophys. Res.*, **111**, D09S03, doi:10.1029/2005JD006357.

Wang J, Rossow WB (1998) Effects of cloud vertical structure on atmospheric circulation in the GISS GCM. *J. Clim.*, **11**, 3010–3029.

Wang J, Rossow WB, Zhang Y (2000) Cloud vertical structure and its variations from a 20yr global rawinsonde dataset. *J. Clim*., **13**, 3041-3056.

Wang Z, Sassen K (2004) An improved cloud classification algorithm based on the SGP CART site observations. The Fourteenth ARM Science Team Meeting, March 22 to 26, 2004, Albuquerque, New Mexico, http://www.arm/gov/publications/proceedings.stm.

Warren SG, Hahn CJ, London J (1985) Simultaneous occurrence of different cloud types. *J. Climate Appl. Meteor.,* **24**, 658–667.

Weare BC, AMIP Modeling Groups (1996) Evaluation of the vertical structure of zonally averaged cloudiness and its variability in the Atmospheric Model Intercomparison Project. *J. Clim.,* **9,** 3419 –3431.

Webb M, Senior C, Bony S, Morcrette JJ (2001) Combining ERBE and ISCCP data to assess clouds in the Hadley Centre, ECMWF and LMD atmospheric climate models. *Clim. Dyn.*, **17**, 905-922.

Weisz E,Li J, Menzel WP, Heidinger AK, Kahn BH, Liu CY (2007) Comparison of AIRS, MODIS, CloudSat and CALIPSO cloud top height retrievals. *Geophys. Res. Lett.*, **34**, L17811,doi:10.1029/2007GL030676.

Wielicki BA, Cess RD, King MD, Randall DA, Harrison EF (1995) Mission to planet Earth: Role of clouds and radiation in climate. *Bull. Amer. Meteor. Soc.,* **76**, 2125–2153.

Williams KD, Tselioudis G (2007) GCM intercomparison of global cloud regimes: Present-day evaluation and climate change response. *Clim. Dynam.*, **29**, 231-250, doi:10.1007/s00382-007-0232-2.

Winker DM, Hunt WH, McGill MJ (2007) Initial performance assessment of CALIOP. *Geophys. Res. Lett.,* **34,** L19803, doi:10.1029/2007GL030135.

Wu DL et al. (2009) Vertical distributions and relationships of cloud occurrence frequency as observed by MISR, AIRS, MODIS, OMI, CALIPSO, and CloudSat. *Geophys. Res. Lett.*, **36,** L09821, doi:10.1029/2009GL037464.

Wyant MC, Bretherton CS, Bacmeister JT, Kiehl JT, Held IM, Zhao M, Klein SA, Soden BJ (2006) A comparison of low-latitude cloud properties and their response to climate change in three AGCMs sorted into regimes using mid-tropospheric vertical velocity. *Climate Dyn.,* **27,** 261–279, doi:10.1007/s00382-006-0138-4.

Wylie D, Eloranta E, Spinhirne JD, Palm SP (2007) A Comparison of Cloud Cover Statistics from the GLAS Lidar with HIRS. *J. Clim.,* **20,** 4968–4981, doi: 10.1175/JCLI4269.1.

Xi B, Dong X, Minnis P, Khaiyer MM (2010) A 10 year climatology of cloud fraction and vertical distribution derived from both surface and GOES observations over the DOE ARM SGP site. *J. Geophys. Res.,* **115,** D12124, doi:10.1029/2009JD012800.

Xie SP et al (2007) A regional ocean–atmosphere model for eastern Pacific climate: Toward reducing tropical biases. *J. Clim.*, **20**, 1504–1522.

Xu KM, Randall DA (1996) A semiempirical cloudiness parameterization for use in climate models. *J. Atmos. Sci.,* **53,** 3084-3102.

Yang F, Pan HL, Krueger SK, Moorthi S, Lord SJ (2006) Evaluation of the NCEP Global Forecast System at the ARM SGP site. *Mon. Wea. Rev.,* **134**, 3668–3690.

Zhang MH et al (2005) Comparing clouds and their seasonal variations in 10 atmospheric general circulation models with satellite measurements. *J. Geophys. Res.,* **110,** D15S02, doi:10.1029/2004JD005021.

Zhang YH, Zhang SD, Yi F, Chen ZY (2011) Statistics of lower tropospheric inversions over the continental United States. *Ann. Geophys*., **29,** 401–410.

Zuidema P (1998) The 600-800 mb minimum in tropical cloudiness observed during TOGA COARE. *J. Atmos. Sci.,* **55,** 2220-2228.